

AN IMPLICIT ONE-LINE NUMERICAL MODEL ON LONGSHORE
SEDIMENT TRANSPORT

A THESIS SUBMITTED TO
THE GRADUATE SCHOOL OF NATURAL AND APPLIED SCIENCES
OF
MIDDLE EAST TECHNICAL UNIVERSITY

BY

MUSTAFA ESEN

IN PARTIAL FULFILLMENT OF THE REQUIREMENTS
FOR
THE DEGREE OF MASTER OF SCIENCE
IN
CIVIL ENGINEERING

JULY 2007

Approval of the Graduate School of Natural and Applied Sciences

Prof.Dr. Canan Özgen
Director

I certify that this thesis satisfies all the requirements as a thesis for the degree of Master of Science.

Prof.Dr. Güney Özcebe
Head of Department

This is to certify that we have read this thesis and that in our opinion it is fully adequate, in scope and quality, as a thesis for the degree of Master of Science.

Dr. Işıkhan Güler
Co-Supervisor

Prof.Dr. Ayşen Ergin
Supervisor

Examining Committee Members:

Prof.Dr. Yalçın Yüksel	(YTU, CE)	_____
Prof.Dr. Ayşen Ergin (Supervisor)	(METU, CE)	_____
Prof.Dr. Halil Önder	(METU, CE)	_____
Dr. Işıkhan Güler (Co-Supervisor)	(METU, CE)	_____
Assoc.Prof.Dr. Ahmet Cevdet Yalçiner	(METU, CE)	_____

I hereby declare that all information in this document has been obtained and presented in accordance with academic rules and ethical conduct. I also declare that, as required by these rules and conduct, I have fully cited and referenced all material and results that are not original to this work.

Name, Last Name: Mustafa ESEN

Signature :

ABSTRACT

AN IMPLICIT ONE-LINE NUMERICAL MODEL ON LONGSHORE SEDIMENT TRANSPORT

ESEN, Mustafa

M.S., Department of Civil Engineering

Supervisor: Prof. Dr. Ayşen Ergin

Co-Supervisor: Dr. Işıkhan Güler

July 2007, 108 Pages

In this study, a numerical model “Modified Coast-Structure Interaction Numerical Model” (CSIM) is developed with an implicit approach to determine the shoreline changes due to wind wave induced longshore sediment transport under the presence of groins, T-groins and offshore breakwaters by making modifications on the explicit numerical model “Coast-Structure Interaction Numerical Model” (CSI). Using representative wave data transformed to a chosen reference depth from deep water, numerical model (CSIM) simulates the shoreline changes considering structure interference. Breaking and diffraction within the sheltered zones of coastal structures defined for offshore breakwaters by using vectorial summation of the diffraction coefficients and as for T-groins shore-perpendicular part forms a boundary to define the shoreline changes separately at two sides of the structure. Numerical model, CSIM is tested with a case study by applying in Bafra Delta, Kızılırmak river mouth at Black sea coast of Turkey. Numerical model simulations show that model results are in good agreement qualitatively with field measurements.

Key Words: Longshore Sediment Transport, One-line Theory, Shoreline Change, Representative Wave Data, Coastal Structures

ÖZ

KIYI BOYU KATI MADDE TAŞINIMI ÜZERİNE ÖRTÜLÜ YÖNTEMLE YAPILAN VE TEK ÇİZGİ TEOREMİNE DAYANAN SAYISAL MODEL

ESEN, Mustafa

Yüksek Lisans, İnşaat Mühendisliği Bölümü

Tez Yöneticisi: Prof. Dr. Ayşen Ergin

Ortak Tez Yöneticisi: Dr. Işıkhan Güler

Temmuz 2007, 108 Sayfa

Bu çalışmada, açık yöntemle geliştirilmiş “Kıyı-Yapı Etkileşimi” (CSI) sayısal modelinde değişiklikler yapılarak, mahmuzların, T-mahmuzların ve açık deniz dalgakıranlarının varlığında, rüzgar dalgaları sonucu oluşan kıyı boyu katı madde taşınımının neden olduğu kıyı çizgisi değişimlerini belirleyen, örtülü yöntem yaklaşımının kullanıldığı “Uyarlanmış Kıyı-Yapı Etkileşimi” (CSIM) sayısal modeli geliştirilmiştir. Sayısal modelde, dalga verisinin derin denizden belirlenmiş bir referans derinliğine dönüştürülmesiyle elde edilen temsili dalga verisinin kullanılmasıyla yapı etkisi altında kıyı çizgisi değişimleri hesaplanmaktadır. Kıyı yapılarının korunumlu bölgelerindeki kırılma ve sapma olayları, açık deniz dalgakıranları için sapma katsayılarının vektörel olarak toplanmasıyla, T-mahmuzlar içinse T-mahmuzun kıyıya dik kısmının sınır olarak tanımlanması sonucu yapının her iki tarafındaki kıyı çizgisi değişimlerinin ayrı ayrı tanımlanmasıyla açıklanmıştır. Sayısal model (CSIM), Kızılırmak nehir ağzının Karadeniz’e döküldüğü yer olan Bafra Deltası’na uygulanan örnek bir çalışmayla test edilmiştir. Sayısal model benzetimleri model sonuçlarının saha ölçümleriyle nitelik olarak uyumlu olduğunu göstermiştir.

Anahtar Kelimeler: Kıyı boyu katı madde taşınımı, Tek çizgi teoremi, Kıyı çizgisi değişimi, Temsili dalga verisi, Kıyı yapıları

*To My Family
and
To My Friends*

ACKNOWLEDGEMENTS

I would like to thank my supervisor Prof.Dr. Ayşen Ergin and my co-supervisor Dr. Işıkhan Güler not only for their guidance throughout this study but also for teaching me in coastal engineering profession, for making me a part of the dynamic and warm atmosphere Coastal Engineering Laboratory preserves and for showing how to join intense work with joy in a very busy academic life. I would like to extend my thanks to Assoc.Prof.Dr. Ahmet Cevdet Yalçın for his close interest in my thesis and his support throughout this study.

I would like to express my appreciations for the studies and works of contributors which enlighten my path and widen my knowledge.

I would like to thank my dear friends Mr Ilgar Şafak and Mr Salih Artagan for their suggestions and support which provided me with extremely worthy information.

My special thanks is for my dear friend Mr Cüneyt Baykal for his enormous support and efficacious suggestions and for turning this study into a joyful odyssey that we share within our office room in Coastal Engineering Laboratory.

This thesis would be a really unbearable and long study without the support of my lovely friends Ms Hülya Karakuş and Ms Ceren Özer.

I would like to thank the assistants and technicians of Coastal Engineering Laboratory for their close interests in my study and for their precious helps.

Words are insufficient to express my love and gratitude to my family to whom I owe everything I own.

TABLE OF CONTENTS

PLAGIARISM.....	iii
ABSTRACT.....	iv
ÖZ	v
ACKNOWLEDGEMENTS.....	viii
TABLE OF CONTENTS.....	ix
LIST OF FIGURES.....	xii
LIST OF TABLES.....	xv
LIST OF SYMBOLS.....	xvi
CHAPTER	
1. INTRODUCTION.....	1
2. LITERATURE REVIEW.....	6
2.1 Coastal Structures.....	7
2.1.1 Groins.....	7
2.1.2 Offshore Breakwaters.....	10
2.1.3 Seawalls.....	10
2.2 Historical Background of Numerical Models.....	11
3. ONE-LINE THEORY AND COAST-STRUCTURE	
INTERACTION NUMERICAL MODEL, CSI.....	16
3.1 One-Line Theory.....	16
3.1.1 Basic assumptions and limitations.....	16
3.1.2 Fundamental equations.....	17
3.1.3 Beach profile.....	19
3.1.4 Effective breaking wave angle.....	22
3.1.5 Longshore sediment transport rate.....	23
3.1.6 Boundary conditions.....	27
3.2 Coast-Structure Interaction Numerical Model, CSI.....	28
3.2.1 Explicit solution of sediment continuity equation.....	29

3.2.2	Stability.....	30
3.2.3	Wave breaking.....	31
3.2.4	Wave diffraction.....	34
3.2.5	Combined refraction-diffraction.....	36
4.	MODIFIED COAST-STRUCTURE INTERACTION	
	NUMERICAL MODEL, CSIM.....	38
4.1	Implicit Solution of Sediment Continuity Equation.....	38
4.2	Stability.....	41
4.3	Reference Depth.....	45
4.4	Wave Diffraction and Combined Refraction-Diffraction.....	45
4.4.1	Wave Diffraction Calculations for a Groin.....	49
4.4.2	Wave Diffraction Calculations for an Offshore Breakwater.....	51
4.5	Longshore Sediment Transport Rate, CERC Formula.....	55
4.6	Structures.....	56
4.6.1	Groins.....	56
4.6.1.1	Bypassing.....	57
4.6.1.2	Permeability.....	61
4.6.1.3	Combined Effect of Bypassing and Permeability.....	63
4.6.2	T-Groins.....	64
4.6.3	Offshore Breakwaters.....	67
5.	CASE STUDY.....	69
5.1	Problem at Case Study Area.....	69
5.2	Wave Hindcasting.....	71
5.3	Model Wave Data.....	74
5.4	Case Study Simulation Results and Discussions.....	78
6.	CONCLUSION.....	85
	REFERENCES.....	89
	APPENDICES.....	96
	A : FLOWCHART OF THE DEVELOPED NUMERICAL MODEL.....	96
	B : SHORELINE AND WAVE DATA OF CASE STUDY	

SIMULATIONS.....	97
C : INPUTS AND OUTPUTS OF CASE STUDY AND SAMPLE SIMULATIONS.....	102

LIST OF FIGURES

FIGURES

Figure 2.1	Layout of a single groin.....	8
Figure 2.2	Shoreline evolution in case of a single groin and a groin field.....	9
Figure 3.1	Depth of closure.....	16
Figure 3.2	Sand continuity equation sketch.....	18
Figure 3.3	Dean Profile.....	20
Figure 3.4	Comparison of influence of median grain size on sediment scale parameter ($0.1 \leq D_{50} \leq 1$ mm).....	21
Figure 3.5	Effective breaking wave angle.....	22
Figure 3.6	Grid system.....	28
Figure 3.7	Longshore transport rates in and out of a calculation cell...	30
Figure 3.8	Wave diffraction.....	34
Figure 4.1	Execution times for CSI and CSIM with various time increments	42
Figure 4.2	Stability ratio comparisons between CSI and CSIM.....	43
Figure 4.3	Execution time comparisons between CSI and CSIM	44
Figure 4.4	Breaking wave heights for each iteration	46
Figure 4.5	Diffraction coefficients (K_d) in case of a single groin.....	48
Figure 4.6	Diffraction coefficients (K_d) in case of an offshore breakwater.....	49
Figure 4.7	Diffraction of waves at the sheltered zone of a groin (Kamphuis, 2000).....	51
Figure 4.8	Schematic representations of K_{d1} and K_{d2} (Artagan, 2006)..	52

Figure 4.9	Schematic figure of proposed method in CSIM for wave diffraction calculations.....	53
Figure 4.10	Vectorial summation of diffraction coefficients.....	54
Figure 4.11	Ground plan of bypassing around a groin.....	57
Figure 4.12	Bypassing approach in the developed numerical model.....	60
Figure 4.13	Bypassing around an impermeable groin at an initially straight shoreline.....	61
Figure 4.14	Permeability of a single groin.....	62
Figure 4.15	Types of groins that can be simulated with the methodology used for T-Groins.....	65
Figure 4.16	Diffraction condition behind a T-Groin.....	66
Figure 4.17	Shoreline evolution in case of a single T-groin	67
Figure 4.18	Shoreline evolution of an initially straight shoreline in case of an offshore breakwater.....	68
Figure 5.1	Location of Bafra Delta, Black Sea, Turkey.....	70
Figure 5.2	Initial layout of groins and measured shoreline coordinates in 1999 at Bafra Delta (April, 1999)	70
Figure 5.3	Layout of groins and measured shoreline coordinates in 1999, 2003 and 2007 at Bafra Delta (February, 2007)....	71
Figure 5.4	Fetch distances for Bafra Region.....	72
Figure 5.5	Probability distributions of deep water significant wave height for directions, W to N.....	73
Figure 5.6	Probability distributions of deep water significant wave height for directions, NNE to ESE.....	74
Figure 5.7	4 year simulation results of shoreline evolution under annual and seasonal wave data input methods (Input 1 and Input 2).....	79
Figure 5.8	4 year simulation results of shoreline evolution under annual and seasonal wave data input methods	

	(Input 3 and Input 4).....	79
Figure 5.9	4 year simulation results of shoreline evolution under wave data input methods of deep water and reference depth (Input 1 and Input 3).....	80
Figure 5.10	4 year simulation results of shoreline evolution under deep water and reference depth wave data input methods (Input 2 and Input 4).....	81
Figure 5.11	4 year simulation results of shoreline evolution under all wave data input methods.....	82
Figure 5.12	4 year simulation results of shoreline evolution of CSI and CSIM with Input 1.....	83
Figure A.1	Flowchart of the developed numerical model	96
Figure C.1	4 year case study simulation results of shoreline evolution under annual deep water wave data input	105
Figure C.2	4 year case study simulation results of shoreline evolution under seasonal deep water wave data input.....	105
Figure C.3	4 year case study simulation results of shoreline evolution under annual reference depth wave data input....	106
Figure C.4	4 year case study simulation results of shoreline evolution under seasonal reference depth wave data input..	106
Figure C.5	Sample simulation 1	107
Figure C.6	Sample simulation 2	108
Figure C.7	Sample simulation 3	108

LIST OF TABLES

TABLES

Table 5.1	Effective fetch distances and probability equations for effective wave directions.....	73
Table 5.2	Average annual deep water wave heights, corresponding periods and annual exceeding frequencies at Bafra Delta...	75
Table 5.3	Average annual reference depth wave heights, corresponding periods and annual exceeding frequencies at Bafra Delta.....	76
Table 5.4	Average annual reference depth wave heights, corresponding periods and annual exceeding frequencies for representative waves at Bafra	77
Table 5.5	Applied wave data input methods at the case study for Bafra Delta.....	78
Table B.1	Annual deep water representative wave data of case study simulations.....	97
Table B.2	Annual representative wave data of case study simulations at reference depth	97
Table B.3	Seasonal deep water representative wave data of case study simulations.....	98
Table B.4	Seasonal representative wave data of case study simulations at reference depth	99
Table B.5	Initial shoreline data of case study simulations.....	101
Table C.1	Annual deep water representative wave data of sample simulations.....	107

LIST OF SYMBOLS

a_1	empirical longshore sediment transport coefficient
a_2	empirical longshore sediment transport coefficient
A	a parameter for defining wave and beach characteristics
A_p	beach profile scale parameter
B	longshore transport parameter
BB	modified longshore transport parameter
BYP	bypassing factor
$C_{g,o}$	deep water group velocity
C_{gb}	breaking wave group velocity
C_o	deep water wave celerity
CSI	coast-structure interaction numerical model
CSIM	modified coast-structure interaction numerical model
d	water depth
D_{50}	median grain size (median grain size diameter)
d_b	depth of breaking
D_B	average berm height above mean water level
D_C	depth of closure
D_g	water depth at the seaward tip of a groin
D_{LT}	limiting depth of long-shore transport
dt	time increment
dx	longshore increment
d_y	water depth at y distance from shoreline
E	double-sweep parameter
EE	double sweep recurrence coefficient
E_w	wave energy
F	double-sweep parameter
FF	double sweep recurrence coefficient

f_r	representative frequency
g	gravitational acceleration
H	wave height at a particular location
H_b	breaking wave height
H_{bd}	diffracted breaking wave height
H_d	diffracted wave height at a point in the lee of the structure
H_i	incoming wave height at the tip of the structure
H_o	significant deep water wave height
H_r	representative wave height
H_{rms}	root-mean-square wave height
H_S	significant wave height
$H_{S,12}$	wave height that occurs 12 hours in a year
H_{sb}	significant breaking wave height
I_l	longshore immersed-weight transport rate
K	dimensionless empirical proportionality coefficient
K_1	longshore transport calibration parameter
K_2	longshore transport calibration parameter
K_d	diffraction coefficient
K_{dP}	modified diffraction coefficient
L	wave length
L_b	breaking wave length
L_e	effective length of groin
L_g	length of groin from the shoreline
l_{gb}	distance between tip of the groin to the breaker line
L_o	deep water wave length
m_b	bottom slope at breaking location
p	in-place sediment porosity
P	occurrence probability of waves with height of H
PB	factor showing the combined effect of bypassing and permeability
$PERM$	permeability ratio of a groin
P_l	potential longshore sediment transport rate
q	source and/or sink along the coast

Q	longshore sediment transport rate
Q_{in}	longshore sediment transport rate into a beach
Q_l	volumetric sediment transport rate
Q_L	longshore sediment transport rate from left direction
Q_{out}	longshore sediment transport rate out of a beach
Q_{NET}	net longshore sediment transport rate
Q_R	longshore sediment transport rate from right direction
Q_T	total longshore sediment transport rate
R_s	stability ratio
t	time
T	significant wave period
T_r	representative wave period
$\tan \beta$	average bottom slope from the shoreline to the limiting depth of longshore transport
V	total volume of the beach profile per unit length
x	longshore coordinate of shoreline
X_g	spacing between groins
y	shoreline position
y_{acc}	distance of accumulated sediment from shoreline at the updrift side of a groin
y_c	shoreline position halfway between shoreline positions at current and next time steps
y_p	perpendicular offshore distance from shoreline
Y_g	offshore distance of groin from the shoreline
y_{LT}	offshore distance of limiting depth of longshore sediment transport
ρ	mass density of water
ρ_s	mass density of sediment particles
α_b	breaking wave angle
α_{bd}	diffracted breaking wave angle
α_{bs}	effective breaking wave angle (angle of wave crests to shoreline)
α_{dP}	modified breaking wave angle
α_i	incident wave angle at the tip of the structure

α_o	deep water approach angle of waves
α_s	angle of shoreline to x-axis
ξ_o	surf similarity parameter
γ_b	wave breaker index
Ω_b	breaker height index
θ	angle between a point at the lee of a structure and the extension of incident wave direction
Δt	time increment
Δx	shoreline increment

CHAPTER 1

INTRODUCTION

*For look! Within my hollow hand,
While round the earth careens,
I hold a single grain of sand
And wonder what it means.
Ah! If I had the eyes to see,
And brain to understand,
I think Life's mystery might be
Solved in this grain of sand.*

Robert W. Service

Coasts have always been an attraction for humanity from the beginning of the civilization for the benefits, opportunities and facilities offered as economic potentials. After the realization of opportunities offered by coastal regions, migration to these areas increased even more in recent years. As a result, coastal regions have become the most populated and developed regions of the world. However, with the new inventions of the inevitable rise of civilizations, coastal structures such as ports, harbors, quays, etc. were constructed for several needs and uses without much understanding or caring for the consequences and response of coastal systems and processes to these structures.

For a long time, the priority of interest was far more for the construction of coastal structures for various purposes rather than protecting the natural beauties of coastal areas. However, currently this blindness and never-ending interference of mankind with nature which resulted in brutal and undesirable impacts of erroneously or inadequately designed and constructed coastal structures has created a new understanding towards the conservation and protection. As an emerging need, dynamics of waves and coastal systems studied more intensively. Under the light of nearshore processes, field measurements, laboratory

experiments and numerical models became the vital input together with other parameters such as locations of structures, wave and wind climate of the region, interaction of waves and structures at planning, design and construction stages of coastal structures.

Nearshore processes play one of the crucial roles in these stages as they cause several of the leading effects on coastal dynamics. Waves, currents, tides and sediment transportation are the most critical parameters that govern the nearshore processes. As coastal sediment transportation severely determines the nearshore bathymetry characteristics and coastal topography significantly affects these processes, it has always been one of the main concerns of coastal engineers. Wind wave induced sediment transportation occurs in two ways one of which is longshore sediment transportation which is the transportation parallel to the shoreline and the other is cross-shore sediment transportation which is observed vertical to the shoreline. Longshore sediment transportation is mainly caused by breaking of wind induced waves approaching to shore from a certain direction with an angle to the shoreline or the nearshore currents which are caused by wind induced waves. In most of the cases, longshore sediment transportation is the governing and influential factor that defines the long-term shoreline changes.

Importance of understanding the parameters that govern the sediment transportation processes is vital in order to overcome the problems which occur after the construction of structures. Without a proper grasp of these processes, outcomes of coastal structures may not be anticipated accurately. On the other hand, as erosion and accretion problems are commonly observed for most of the coastal regions where no coastal structure exists, construction of coastal structures is inevitable. Most of these structures such as groins, seawalls and offshore breakwaters are called hard structures as they occupy a massive volume and important amount of surface area. Hard structures are the most common measures that coastal engineers come up with. However, they are not the only recipe to coastal sedimentation problems. As concern about nature-friendly projects increase, soft measures such as sediment nourishment to eroded shores are

becoming popular. During the procedure to find the optimum solution to coastal engineering problems, before the decision of constructing hard structures, more attention and care should be given as these structures unavoidably cause the adjacent beaches to be affected. Furthermore, a detailed comparison of hard and soft solution alternatives should be performed with adequate consideration of natural processes in the region as well as local fauna, flora and scenery. Especially, for the case of constructing hard structures, it is almost impossible and extremely unnecessary and wasteful to move the structure to another location or completely remove it. No matter which solution is chosen, each alternative should be examined thoroughly with great concern on nature and without allowing any further damage to the shore after the construction.

Therefore, in order to predict the shoreline changes due to wind wave induced sediment transportation, the basis on which sediment transportation stands should be examined carefully. In parallel with the arising need for accurate prediction of shoreline evolution and for the aim of understanding the long term response of wind waves to coastal structures in terms of shoreline changes, new theories, studies and researches have been introduced into coastal engineering including the computer based one-line and n-line numerical models. The purpose of these models is to simulate shoreline changes occurring over a month to years due to wave action (wave induced sediment transport) and to observe the longterm shoreline changes mathematically. Moreover, as physical model studies and costs are hardly bearable for most of the institutions, not applicable for some cases and as they have long execution times, it is easier and practical to simulate the same conditions with a numerical model with comparably lower costs and shorter execution times. The common properties of these models are that they give quantitative results as well as visual outcomes showing shoreline changes which help in the planning stage. On the other hand, not all of them are user-friendly, applicable to different types of shores under all types of structures or give accurate shoreline change estimations. This is briefly due to non-linear distribution of coastal bathymetry and complex wave-structure interaction considering the non-linear coastal bathymetry. As a result, on the contrary to these numerical models,

still remain several uncertainties that are hard to define in a numerical model. Consequently, instead of working with currently used numerical models or programs in the market, it is realized that the best way is to implement a new user-friendly numerical model with acceptable assumptions and necessary improvements on unsolved problems. Building on an existing numerical model which is “Coast-Structure Interaction Numerical Model “CSI” is seemed to be proper because of its easy grasp, assumptions and equations it involves. Additionally, as a thorough and detailed study will be performed during the development of this numerical model, it would help deeper comprehension of nearshore processes which would be the first step of achieving a new, simpler and hopefully better n-line numerical model in the future.

In Chapter 2, literature review and historical background of coastal sedimentation studies are given together with contributions to coastal sedimentation numerical models and brief information about coastal structures.

In Chapter 3, principles and assumptions of one-line theory are specified together with the basis of the explicit numerical model, CSI.

In Chapter 4, the details of the fundamentals of the developed numerical model, CSIM are illustrated along with modifications on diffraction coefficient calculations behind structures, reference depth concept, implicit solution of sediment continuity equation and implementation of longshore transport rate equation (CERC equation) into the developed numerical model. Stability and execution time comparisons between CSI and CSIM are performed and the results are discussed. Moreover, boundary conditions of groins and offshore breakwaters and several sample applications for groins and offshore breakwaters are presented.

In Chapter 5, for verification of the developed numerical model, a case study is performed at Bafra Delta, Black Sea coast of Turkey with the developed numerical model. Case study simulations are performed concerning various input methods whose derivations are illustrated. Besides, case study simulation results

that are performed with all of these methods are given and discussions over the case study simulation results and comparisons of numerical model results with measured field data are illustrated.

In the last chapter, Chapter 6, the conclusion, a brief summary of results and recommendations for future studies is presented.

CHAPTER 2

LITERATURE REVIEW

Sediment transportation processes may cause erosion or accretion at coastal areas. Erosion is simply called the retreat of shoreline towards land and accretion is simply the opposite of erosion which is the land movement into the sea as a result of accumulation of sediment particles. Most of the sandy shores all around the world suffer shoreline changes either as erosion or accretion, but mostly affected by erosion. Only in United States, 33000 km of shoreline is eroding and 4300 km of shoreline is critically eroding which caused the U.S. Army Corps of Engineers to consider erosion as a serious threat to national economy (Phillips and Jones, 2005). For the purpose of preventing adverse effects of erosion or decreasing its magnitude, measures should be taken. Before the decision of which measures to exterminate, the main causes of erosion should be identified. These causes may be classified as (SOPAC, 1991):

- Natural causes:
 - Changes in wave climate
 - Reduction in the amount of sediment delivered to the coast
 - Rising sea level

- Human-induced causes:
 - Sand extraction from beaches
 - Coral mining and other mining activities
 - Insertion of structures such as seawalls and groins
 - Construction of causeways that alter tidal circulation and wave processes around islands and change sediment transport patterns
 - Removal of mangroves

- Dredging of channels which increases water depths at the shoreline and changes wave energy

Loss of sediment supply from rivers, increase in incident wave magnitudes and according to Kamphuis (2000), comminution which is the uncontrolled decrease in sediment size at the beach may be listed as other major causes of erosion.

Among the shoreline change problems due to coastal structures, erosion is the most often encountered cause and the hardest one to take precautions against. In fact, erosion may sometimes lead to severe problems causing damages on highways, buildings and other properties as well as economical losses when its magnitude increases significantly. Even though it is widely thought that erosion is the main problem to be dealt with, accretion may also result in vital outcomes. Construction of a coastal structure not only affects the downdrift beach but also results in shoreline changes at the updrift side. As an example, the insufficient design of a groin at some kilometers distance from the downdrift side of a harbor entrance may accrete sediment at the updrift side of groin therefore, causing the sediment to close the harbor entrance and making the navigation harder.

2.1 Coastal Structures

2.1.1 Groins

Groins are narrow structures, usually straight and perpendicular to the pre-project shoreline that are built to stabilize a stretch of natural or artificially nourished beach against erosion that is primarily due to a net longshore loss of beach material (Figure 2.1) (CEM, 2003).

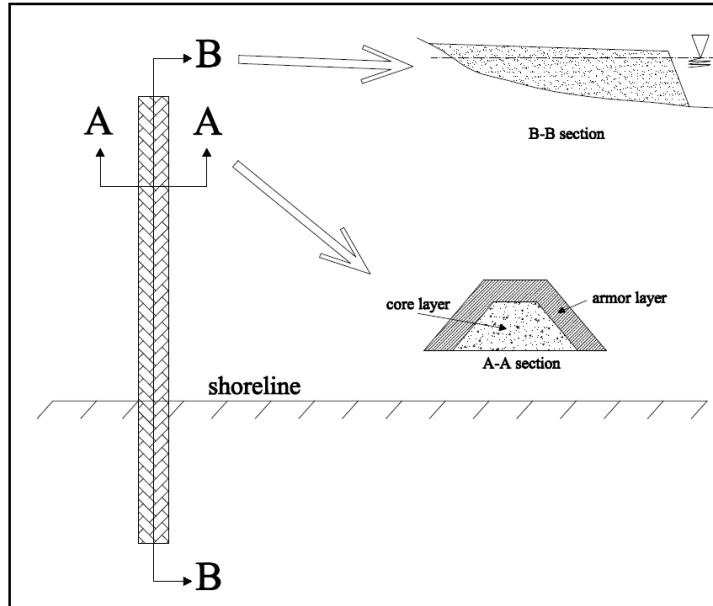


Figure 2.1 Layout of a Single Groin

Groins are only functional when longshore transport is dominant in shore profile changes throughout the projected beach. While a single groin accumulates sediment on its updrift side, shoreline retreats at its downdrift side. This outcome is the same for every groin of a groin field unless the spacing between two consecutive groins is long enough for proper behavior of groins (Figure 2.2). There is a very important relation that relates spacing between groins and length of groins for proper functioning of a groin field as;

$$2.0 \leq X_g / Y_g \leq 3.0 \quad 2.1$$

where X_g is the spacing between groins and Y_g is the offshore distance of groin from the shoreline. In a successfully designed and applied groin field, shoreline takes a shape of a saw in long-term. On the other hand, too closely constructed groins may cause bypassing of sediment through the groin intervals and groins that are constructed too far away from each other cause erosion of beach between

groins. Therefore, in order to prevent undesired conditions, an optimum design is obligatory for groins.

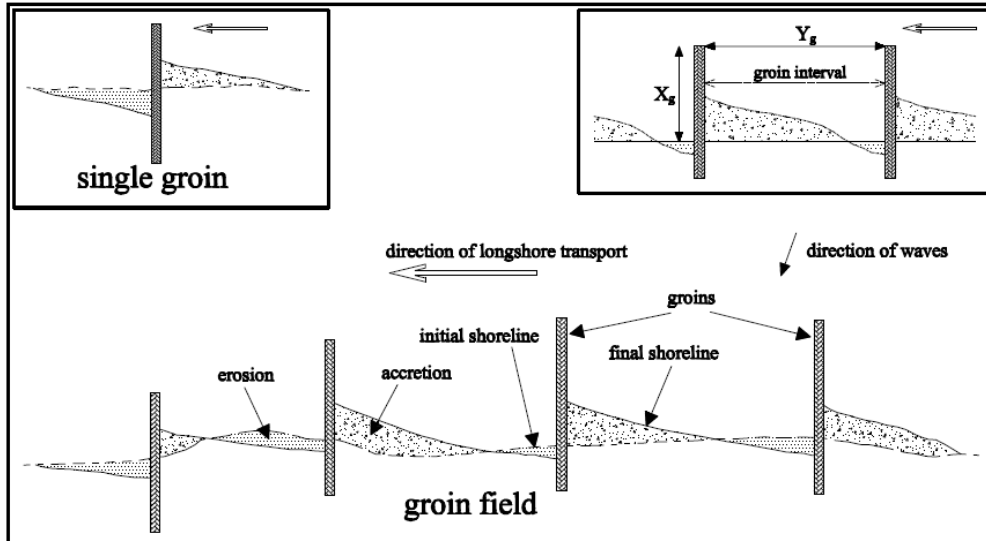


Figure 2.2 Shoreline Evolution in case of a Single Groin and a Groin Field

Groins may create very complex current and wave patterns especially at their downdrift side. However, well-designed groins slow down the longshore transport rate and provide protection for some portion of the coastline. Moreover, groins are very useful measures for protection of artificially nourished beaches. Another important point about groins is that landward end of the groin must extend to a point in order to avoid scouring that would occur due to sea level rise during severe storms. The extension of seaward end of the groins is as important as the landward end. For most of the cases, groins are designed as short groins, meaning that the groin does not exceed beyond surf zone whereas long groins exceed the surf zone limit. Additionally, in some situations, it may be beneficial to allow sediment transport through groins for better distribution of the shoreline. This type of groins are called permeable groins.

Design and site selection of groins are vital procedures because groins may not create the aimed situation for the beach due to poor designs and improper site selections of groins even though they are constructed perfectly. On the other hand, sometimes, several mistakes during construction phase may yield insufficient performance of groins and as a result unsuccessful solutions as well.

2.1.2. Offshore Breakwaters

Offshore breakwaters (nearshore breakwaters) are detached, generally shore-parallel structures that reduce the amount of wave energy reaching a protected area and thus slowing down the littoral drift, causing sediment deposition behind its body (CEM, 2003). Additionally, they do not hinder the longshore transport totally which is the case in groins, but they only reduce the littoral transport to a certain value resulting in sediment accumulation at its sheltered zone. However, as accumulation occurs at the sheltered area, a single breakwater may also cause erosion of some part of the beach by the accumulation area. However, this situation may be compensated by designing a series of offshore breakwaters that are necessary for precaution. Despite this adverse effect, a breakwater may offer many advantages such as on account of a breakwater, only offshore transportation is blocked at its lee not the longshore transportation like in a groin. Another advantage of a breakwater is the slowdown of the effect of longshore currents and prevention of current movement or offshore deflection of currents and sediment transport in the offshore direction and hence the sand loss due to cross-shore motion.

2.1.3. Seawalls

In cases of extensive or chronic erosion due to storm waves or water intrusion in a coastal region which can not be eliminated, buildings, roads and other resources at the coast are in great danger due to recession of the shoreline. If as a remedy to this undesired condition, artificial beach nourishment or construction of structures such as groins or breakwaters do not work properly or non-structural measures are

not feasible, a better, feasible and more lasting measure should be taken at the corresponding area. Seawall, whose main construction aim is to prevent inundation and beach erosion control, is a good measure against this problem among with bulkheads and coastal dikes. Even though it is specified that seawalls avoid shoreline retreat beyond a certain line which is the seawall location, at the two edges of the seawall, a certain amount of erosion is unavoidable. Therefore, before the decision of constructing seawalls, a detailed study should be performed taking into account all aspects of the current situation.

2.2. Historical Background of Numerical Models

For the purpose of understanding the consequences of coastal structures and their footprints on shore profile, it is necessary to use either a physical model or a numerical model to simulate shoreline changes depending on the situations. These situations strongly depends on how stable is the shoreline after construction of a structure, assuming that the structure's configuration will not change in the future. If the trend of shoreline change is stable enough for easy prediction of future shoreline evolution, without the help of models, shoreline changes can be forecast, but even in these situations, there remains several parameters as a mystery. On the other hand, if the fluctuations of conditions in control of shoreline and shore profile are unpredictable or conditions are complex, a simulation model is necessary for shoreline evolution predictions (Hanson, 1987). Therefore, a successful implementation of a numerical model to a particular beach confirms that model's applicability and validity on other beaches at regions where different wave climate and structures are observed. Numerical models possess considerable advantages over physical models when costs, execution times, applicability and scaling problems are concerned. Numerical models have low costs, shorter execution times, may be applicable to various sites and have no scaling problems. Therefore, with the aim of understanding the sophisticated phenomenon defining the shape of shores, models which simulate shoreline changes have been tried to develop for a very long time.

During severe storms, due to variations in incident wave characteristics, sand moves onshore and offshore changing the nearshore bottom topography dramatically. However, otherwise, after a short time, beach profile regains its pre-storm shape under similar cross-shore sediment transportation mechanisms. Therefore, changes in beach profile are strongly correlated to seasonal wave climate rather than conditions which occur during severe storms (Hanson, 1987).

As an outcome of aforementioned reason, dramatic changes and fluctuations in longshore sediment transportation result in gradual and permanent changes in both bottom and shoreline profiles. Based on these observations, Pelnard-Considere (1956) formulated an equation, which is the first major work that one-line theory is built on, by combining the linearized longshore sediment transport equation and conservation of mass equation to provide the diffusion equation in terms of shoreline coordinates, y ;

$$\frac{\partial y}{\partial t} = A \frac{\partial^2 y}{\partial x^2} \tag{2.2}$$

where A incorporates the wave and beach characteristics.

Bruun (1954) and Dean (1977) came up with an equilibrium beach profile concept which is the milestone at development of n-line and multi-line models. This concept mentions that a specific beach, depending on sediment properties and regardless of variations in wave climate, has a characteristic profile.

Kraus and Harikai (1983) proved that at beaches where short-term fluctuations are smaller than long-term fluctuations one-line theory based models give accurate shoreline evolutions in the vicinity of structures for a study at Oarai Beach, Japan. Furthermore, Kriebel and Dean (1985) studied shoreline changes at beaches where short-term changes are more significant than long-term changes, contributing useful information and assistance to one-line models. Hulsbergen et. al. (1976) verified one-line theory by comparing analytical solutions with results of

laboratory experiments concerning groins. Besides, several contributors such as Larson, Hanson and Kraus (1987) and Hanson and Larson (1987) compared analytical solutions with numerical solutions.

Even though one-line theory is first introduced in 1956, the first successful implementation of one-line theory is performed in 1973 by Price, Tomlinson and Willis (1973). Following this study, many new additional studies have been introduced. Some of these important studies include Willis's (1977) work which involved introduction of wave refraction over irregular bottom and representation of a new expression instead of CERC expression, Perlin's (1979) study for detached breakwaters, Le Mehaute and Soldate's (1980) work on presentation of an implicit model and comparison of its results with field data and Mimura, Shimizu and Horikawa's (1983) study on comparison of computer simulations of their program with laboratory data. Despite these studies, none of them offer one-line models as an engineering tool except Kraus, Hanson and Harikai (1985), Kraus et al. (1986) and Hanson and Kraus (1986).

Bakker (1969) extended the one-line theory to include two-lines, one of which represents shoreline and the other represents offshore contour. Inclusion of another contour in y-axis yields understanding of cross-shore motion between two contours because of non-equilibrium beach slope (Bakker et al., 1970). This step together with aforementioned work of Bruun (1954) and Dean (1977) is the introduction of cross-shore motion into one-line motion which would lead to development of n-line models. Bakker (1969) not only extended one-line theory but also conducted several trials along a beach under the existence of single and multiple groin systems and showed that accretion at updrift side of a groin continues up to a beach slope where no more accretion occurs due to steepness of the slope and as a result, sand is bypassed around the top of the groin to its downdrift side.

Hanson (1987) gathered all the previous works and built up a one-line numerical model called GENESIS. GENESIS is an implicit one-line model that evaluates

longterm shoreline changes at a beach where several coastal structures exist for various shore and wave climate data using CERC equation. Dabees (2000) developed another one-line numerical model called ONELINE and added new features and improved the coast-structure interaction processes.

Şafak (2006), Artagan (2006) and Baykal (2006) contributed to this area by developing an explicit one-line model called CSI as the abbreviation of “Coast-Structure Interaction Numerical Model” in which Kamphuis’s formula is utilized. Besides, new concepts especially in combined refraction-diffraction calculations, which were first deduced by Kamphuis (2000), are introduced along with diffraction calculations behind structures. An alternative that CSI offers is that as most of the one-line models currently in use are based on an implicit approach, as an explicit model, CSI, provides a fine alternative. Another advantage of CSI over implicit models is its short execution time and simple input data options for most of the cases. CSI is also verified by comparison of simulations with field data by studying the model at a specific site.

Unlike one-line models, n-line models or beach profile models take cross-shore sediment transportation into account as one of the decision makers at the shoreline change processes. As shoreline changes due to cross-shore motion is observed during severe storms, these changes are temporary. However, in several situations, shore profile may not regain its previous shape. In these cases, inclusion of cross-shore sediment transportation parameters is vital for accurate estimations of shoreline changes. Roelvink and Bakker (1993) discussed some of these theories in detail.

Dabees (2000) developed an n-line model called NLINE, which simulates the shore profile changes in 3-D concerning the complicated beach and structure conditions. However, not all of the researches agree with the concept that the more complex the model is, the better result it gives such as Thieler et. al (2000). Cooper and Pilkey (2004) denote that numerical models can not be specified as only solutions for predicting the behavior of a certain beach where a structure is

constructed. Instead of using these models, they believe that in order to understand the wave-structure interaction, it is better to install several low cost materials that may act like the proposed structure and observe beach behavior and changes in shoreline. By this method, the procedure time increases, but the possible future errors are omitted and unnecessary waste of investment is prevented.

Within the light of these studies, it is quite easily understood that one-line models remain as a popular tool for engineers to apply at beaches where longshore transportation dominates the shoreline changes. Moreover, as many discussions are still made over the applicability and effectiveness of these models, it seems like a promising field of coastal engineering and many new studies, theories and improvements may be appended to these models in the way of creating a better model or a more sophisticated n-line model.

CHAPTER 3

ONE-LINE THEORY AND COAST-STRUCTURE INTERACTION NUMERICAL MODEL, CSI

3.1. One-Line Theory

3.1.1. Basic Assumptions and Limitations

The basic assumption of one-line theory is that beach profile is in equilibrium and stable in long-term and only longshore component of wave induced sediment transportation determines the shore profile and longshore sediment transportation rate is strongly related to incident wave angle (Hanson, 1987). Second major assumption is that sediment movement is observed up to a depth beyond which no more bottom profile changes can be observed due to sediment transportation. This depth is designated as depth of closure, D_C (Figure 3.1).

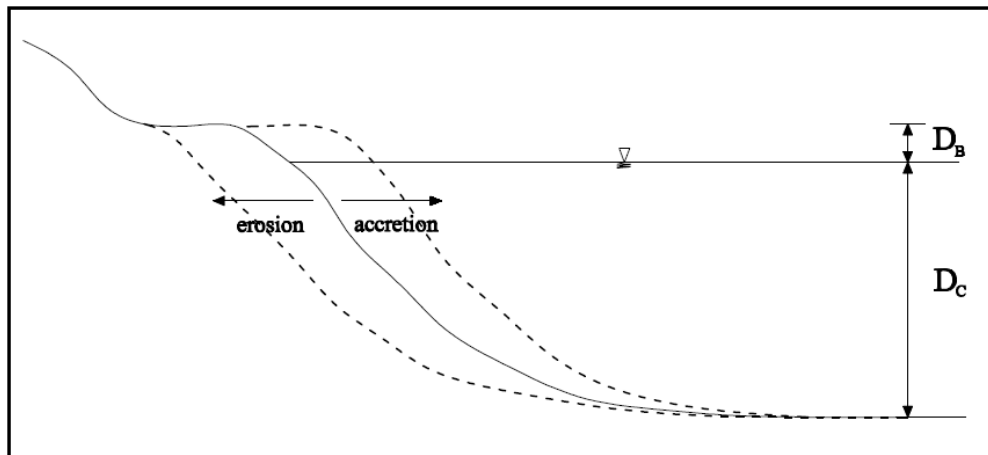


Figure 3.1 Depth of Closure

Even though wave induced longshore sediment movement is mentioned as the main cause of nearshore bottom profile changes, nearshore circulation is another pattern that governs shoreline changes. However, it is ignored in the one-line theory except the effect of longshore variations in breaking wave height, which influences the shoreline evolution near structures according to Kraus and Harikai (1983) and Kraus (1983).

3.1.2. Fundamental Equations

Sand continuity equation, which depends on the assumption that in a controlled volume, the amount of sediment entering a portion of beach, cell, should be equal to the total amount of sand remained in the cell and sand left the cell, is the fundamental equation of one-line theory (Figure 3.2);

$$\frac{\partial y}{\partial t} + \frac{1}{(D_C + D_B)} \left(\frac{\partial Q}{\partial x} + q \right) = 0 \quad 3.1$$

where

y : shoreline position

t : time

D_C : depth of closure

D_B : average berm height above mean water level

Q : longshore sediment transport rate

x : longshore coordinate of shoreline

q : source and/or sink along the coast

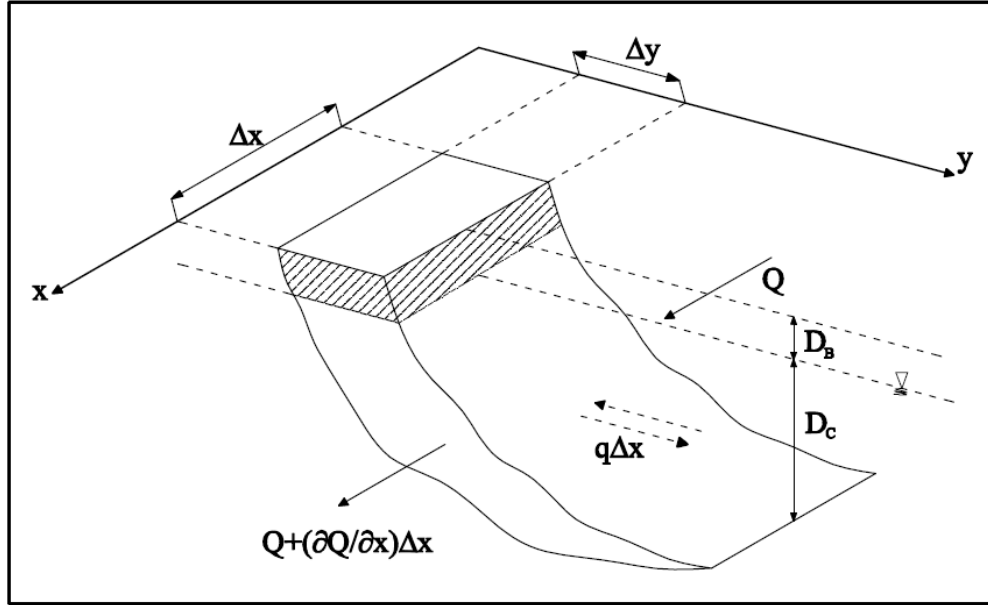


Figure 3.2 Sand Continuity Equation Sketch

Depth of closure, D_c , is also an important parameter defining the sediment motion boundaries as mentioned above. Several assumptions and measurements have been proposed suggesting that depth of closure is approximately twice the annual significant wave height until Hallermeier (1978) came up with a formula which relates depth of closure with $H_{s,12}$, wave height that occurs 12 hours in a year;

$$D_c = 2.28H_{s,12} - \frac{68.5(H_{s,12})^2}{gT^2} \quad 3.2$$

where g is the gravitational acceleration and T is the significant wave period.

Even though Hallermeier (1978) formula gives accurate results of limiting depth of sediment movement, as longshore sediment transport is the main parameter in shoreline changes in a one-line theory based models, use of $H_{s,12}$ within the formula overestimates the limiting depth of longshore sediment transport because this relation is assumed to be valid only for short-term calculations such as in

hours. Hanson (1987) modified this relation by using H_s , significant wave height, instead of $H_{s,12}$ as;

$$D_{LT} = 2.28H_s - \frac{10.9(H_s)^2}{L} \quad 3.3$$

where D_{LT} is the limiting depth of longshore sediment transport.

In the developed numerical model, as in CSI, a modified version of Hallermeier (1978) expression is used for limiting depth of longshore transport expression. Instead of using significant wave height, H_s , or $H_{s,12}$, breaking wave height, H_b , is used as wave breaking is the significant process in longshore sediment transportation as follows;

$$D_{LT} = 2.28H_b - \frac{68.5(H_b)^2}{gT^2} \quad 3.4$$

3.1.3. Beach Profile

As previously mentioned, equilibrium beach profile concept plays a significant role in one-line models. Equilibrium beach profile is sometimes called Dean Profile on account of a relation introduced by Dean (1977). Based on observations, Dean (1977) showed that this characteristic profile takes the shape of a concave and may be presented as;

$$d_y = A_p y_p^{2/3} \quad 3.5$$

where d_y is the water depth at y distance from shoreline, A_p is the beach profile scale parameter and y_p is the perpendicular offshore distance from shoreline (Figure 3.3).

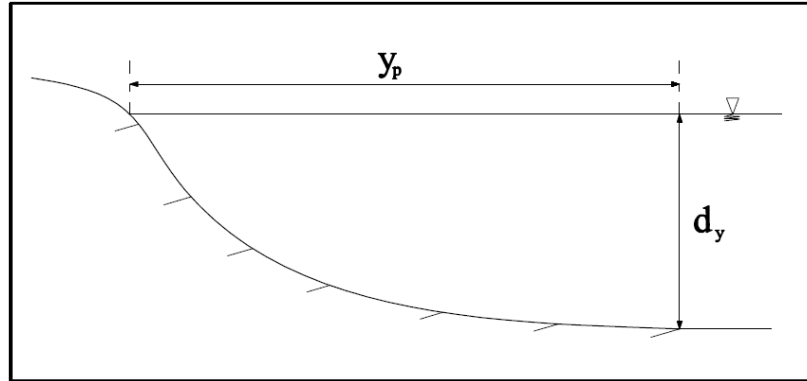


Figure 3.3 Dean Profile

The bottom slope at breaking location, m_b may be found according to:

$$m_b = \frac{2}{3} A_p^{1.5} d_b^{-0.5} \quad 3.6$$

where d_b is the depth of breaking.

Hanson and Kraus (1989) approximated Moore's curve by mentioning that for different ranges of D_{50} , there exists a different relation for A_p as in equations:

$$A_p = 0.41 D_{50}^{0.94} \quad \text{for } D_{50} < 0.4 \text{ mm} \quad 3.7(a)$$

$$A_p = 0.23 D_{50}^{0.32} \quad \text{for } 0.4 \text{ mm} \leq D_{50} < 1 \text{ cm} \quad 3.7(b)$$

$$A_p = 0.23 D_{50}^{0.28} \quad \text{for } 1 \text{ cm} \leq D_{50} < 4 \text{ cm} \quad 3.7(c)$$

$$A_p = 0.46 D_{50}^{0.11} \quad \text{for } D_{50} \geq 4 \text{ cm} \quad 3.7(d)$$

Kamphuis (2000) came up with an equation that relates beach scale profile, A_p , to median grain size diameter, D_{50} , which is given as;

$$A_p = [1.04 + 0.086 \ln D_{50}]^2 \quad 3.8$$

However, this equation is only valid for a certain range of D_{50} ($0.0001 \leq D_{50} \leq 0.001$ meters). Therefore, beaches composed of large sediment particles remain unrepresented when Eqn. 3.8 is utilized. Thus, for a wider representation and implementation of various coasts, Hanson and Kraus's (1989) relation (Eqn. 3.7) is appropriate to be used in the numerical model. Moreover, a comparison is performed between Hanson and Kraus's approach and Kamphuis's relation for sediment sizes between 0.1 mm and 1 mm, in order to understand the influence of median grain size on sediment scale parameters and the results are presented in Figure 3.4.

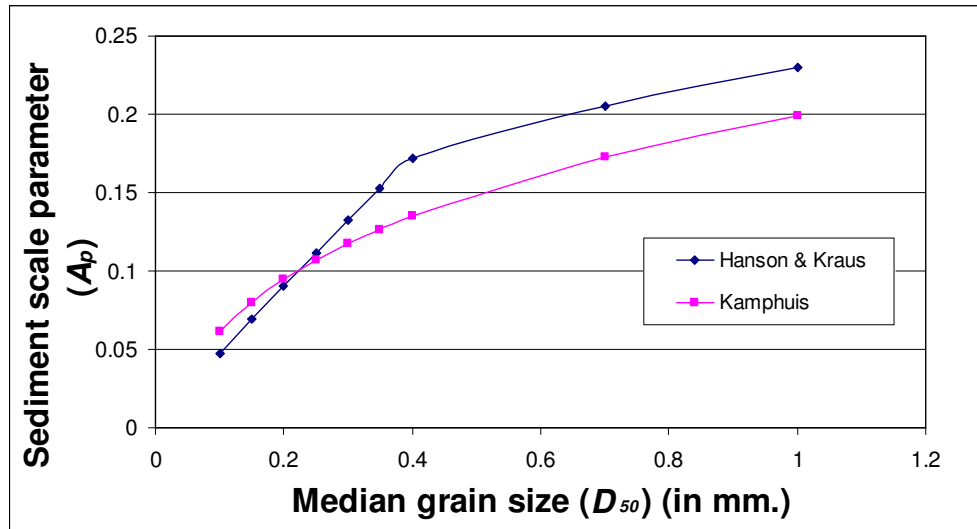


Figure 3.4 Comparison of influence of median grain size on sediment scale parameter ($0.1 \leq D_{50} \leq 1$ mm)

In between the stated ranges of median grain size, both approaches conclude close sediment scale parameter results. On the other hand, Kamphuis's approach reveals a smoother curve than Hanson & Kraus's approach since Hanson and Kraus offers different formulas for grain sizes smaller and larger than 0.4 millimeters. This is

mainly due Hanson and Kraus (1989) approximated Moore's curves by defining different formulas for each grain size interval. Even though there is a little difference between these approaches, it seems appropriate to use Hanson and Kraus's (1989) approach.

3.1.4. Effective Breaking Wave Angle

One-line models take into account the incident wave angle variations along the changing shoreline at each location (Hanson and Kraus, 1993) (Figure 3.5).

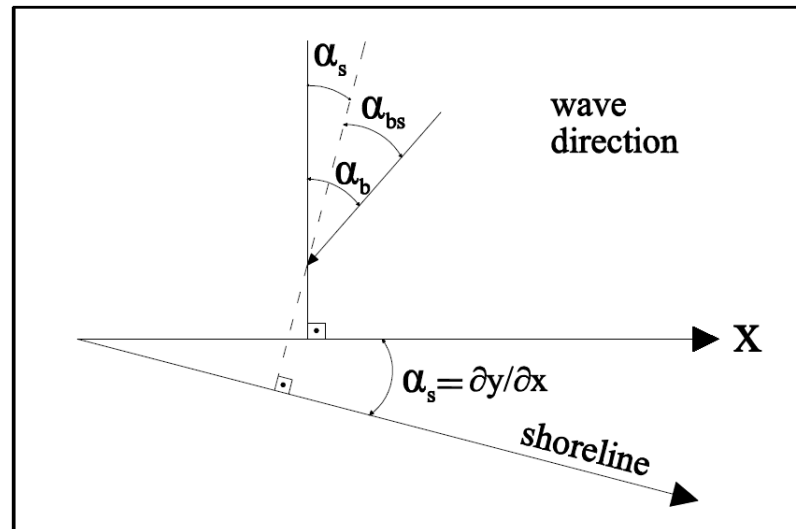


Figure 3.5 Effective Breaking Wave Angle

Effective breaking wave angle is a very important component of longshore sediment transport rate formula. Therefore, modification of breaking wave angle (α_b) that results in calculation of effective breaking wave angle, α_{bs} , is obligatory in one-line models as;

$$\alpha_{bs} = \alpha_b - \alpha_s \quad 3.9$$

where α_s is the angle of shoreline to x-axis as in;

$$\alpha_s = \tan^{-1} \frac{\partial y}{\partial x} \quad 3.10$$

3.1.5. Longshore Sediment Transport Rate

Breaking waves approaching the shore with an angle together with nearshore currents created by wave action compose the basics that littoral sediment transportation is built on (CEM, 2003). As currents due to nearshore circulation result in only local rearrangements of sand, currents generated by breaking wave height changes along the shore due to coastal structures affect only the downdrift side of the structure by creating an upwave motion. On the other hand, breaking waves influence a very significant part of the shore.

The decision about whether erosion or accretion will occur at a particular region of the shore is in control of longshore sediment transportation rates in and out of that region irrespective of the magnitude of the longshore sediment transport. In applications and calculations of littoral transport, the longshore sediment transport rate in right direction, Q_R , is assumed as positive transport whereas the transport rate in the opposite direction, Q_L , is denominated as negative transport. The decision step in beach evolution is the net longshore sediment transport rate, Q_{NET} , which is the difference between Q_R and Q_L ;

$$Q_{NET} = Q_R + Q_L \quad 3.11$$

Total longshore sediment transport rate, Q_T , gives hints about the significance of exposure of a particular shore or a portion of that shore to wave action;

$$Q_T = Q_R + |Q_L| \quad 3.12$$

In numerical model developments, utilizable and friendly longshore sediment transportation rate expressions are necessary such as Kamphuis's (1991) formula;

$$Q = 7.3H_{sb}^2 T^{1.5} m_b^{0.75} D_{50}^{-0.25} \sin^{0.6}(2\alpha_{bs}) \quad 3.13$$

where H_{sb} is the significant breaking wave height in meters, T is the significant wave period in seconds, m_b is the bottom slope at breaking location, D_{50} is the median grain size diameter in meters and α_{bs} is the effective breaking wave angle.

Another option for longshore sediment transportation is CERC formula (Eqn. 3.14) (SPM, 1984). CERC equation which has been utilized in several one-line models such as Hanson's GENESIS, is based on energy flux method that is introduced by Komar (1977).

$$I_l = KP_l \quad 3.14$$

I_l is the longshore immersed-weight transport rate, K is the dimensionless empirical proportionality coefficient and P_l is the potential longshore sediment transport rate that may be written as;

$$P_l = \left(\frac{\rho g^{1.5}}{16\gamma_b^{0.5}} \right) H_b^{2.5} \sin(2\alpha_{bs}) \quad 3.15$$

where

ρ : mass density of water (Ns^2/m^4)

γ_b : wave breaker index (=0.78)

H_b : breaking wave height (m)

α_{bs} : angle of wave crests to shoreline

If the longshore sediment transport rate is transformed into a volumetric sediment transport rate, Q_l , Eqn. 3.14 becomes;

$$Q_l = K \left(\frac{\rho \sqrt{g}}{16\gamma_b^{0.5} (\rho_s - \rho)(1-p)(1.426)^{2.5}} \right) H_b^{2.5} \sin(2\alpha_b) \quad 3.16$$

where ρ_s is the mass density of sediment particles in kg/m^3 and p is the in-place sediment porosity.

CERC equation includes only the longshore transport rate due to obliquely incident waves. Hanson (1987) included a new concept that was introduced by Ozasa and Brampton (1980) which accounts for the littoral transport rate which is the result of variations in breaking wave height, $(\partial H_b / \partial x)$, in longshore direction;

$$Q_l = H_b^2 C_{gb} (a_1 \sin 2\alpha_{bs} - a_2 \cos \alpha_{bs} \frac{\partial H_b}{\partial x}) \quad 3.17$$

where C_{gb} is the breaking wave group velocity and a_1 and a_2 are the empirical longshore sediment transport coefficients treated as calibration parameters and formulated as;

$$a_1 = \frac{K_1}{16(\rho_s / \rho - 1)(1-p)(1.416)^{2.5}} \quad 3.18(a)$$

$$a_2 = \frac{K_2}{8(\rho_s / \rho - 1)(1-p)(\tan \beta)(1.416)^{3.5}} \quad 3.18(b)$$

where K_1 and K_2 are the longshore transport calibration parameters and $\tan \beta$ is the average bottom slope from the shoreline to the limiting depth of longshore transport. As easily observed, Eqns. 3.18(a) and (b) include the terms, $(1.416)^{2.5}$ and $(1.416)^{3.5}$ in the divider part. These terms are used to convert from root-mean square wave height, H_{rms} which is a statistical wave height to significant wave weight, H_s .

Additionally, another argument appears in the decision of which equation for K_I is most suitable to implement in the numerical models. Komar and Inman (1970) determined a value of 0.77 for K_I based on their experiments using root-mean-square wave height, H_{rms} in the calculations. A further decrease to 0.58 is recommended for K_I by Kraus et al. (1982) on the basis of their experiments. However, as the basic assumption for one-line theory based approaches is that breaking waves dominate the longshore sediment transport concept and most investigators have concluded that the longshore sediment transport rate should decrease as grain size increases, a relation that relates median grain size, D_{50} to K_I is seemed necessary in a numerical model.

In the literature, several attempts have been made to modify the K_I coefficient to improve the CERC formula and this has frequently involved relating K_I to the grain size. Swart (1976) used a different form of the CERC relationship which is valid between $0.1 \text{ mm} < D_{50} < 1.0 \text{ mm}$;

$$K_{(rms)} = 1.15 \log_{10} (0.00146/D_{50}) \quad 3.19$$

Komar (1988) examined most of the available field data, and concluded that existing data, most of which were for sand-size beaches, showed little relationship between K_I and grain size. However, theory and data showed a trend of decreasing K_I with increasing grain size so Komar stressed that K_I should depend on sediment grain size, and the absence of such a trend in his analysis resulted from the imperfect quality of his data. An empirically based relationship for K_I , which shows decreasing K_I values with larger grain sizes, is developed by del Valle et al. (1993);

$$K_{(rms)} = 1.4e^{(-2.5D_{50})} \quad 3.20$$

where D_{50} is in millimeters. However, this equation is developed based on field data obtained from coasts that are composed of larger median grain sizes ($0.44 \leq D_{50} \leq 1.5$ mm).

King (2005) discussed these expressions and developed scatters that show the trend of the K_I term to median grain size (D_{50}). Even though the extension of the data is wide, there is a clear trend of decreasing transport with increasing grain size. Thus, it is derived that the trend in the data suggests a relationship of the form;

$$K_1 = 0.0001/D_{50} \quad 3.21$$

where D_{50} is in meters.

Artagan (2006) provides good discussions and detailed information about other longshore sediment formulas that are utilized in one-line models.

3.1.6. Boundary Conditions

In the structure of one-line models, there is a control cell having a specific volume and these cells constitute a control volume for the simulated shore. The boundaries of this control volume are specified differently in each one-line model. Another concept is that the shoreline position in the next time step for a location at the beach is calculated using the longshore transport rates entering and leaving that cell as in Figure 3.6.

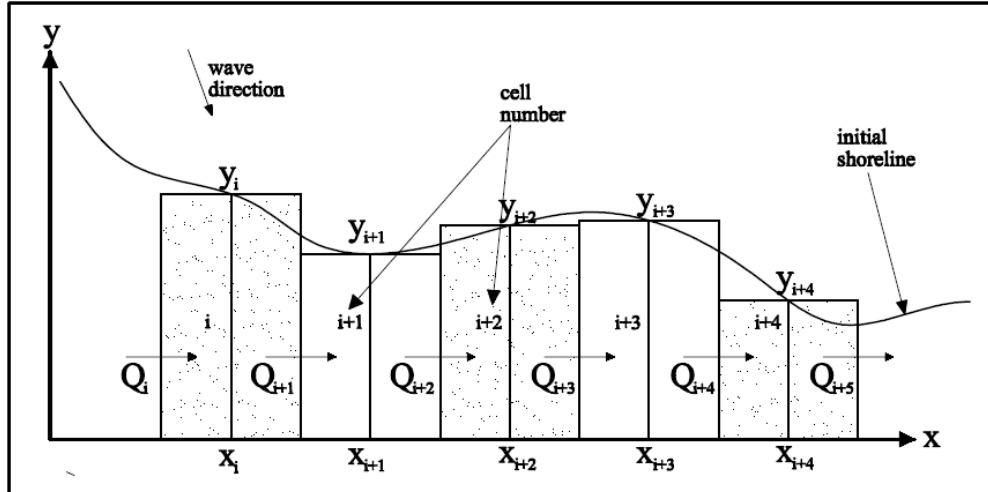


Figure 3.6 Grid System

As seen in Figure 3.6, for a number of i cells, $i+1$ number of Q 's should be defined. Therefore, identification of boundary conditions at the edges of control volume such as in the implemented numerical model, $Q_1=Q_2$ and $Q_N=Q_{N+1}$, is essential. Coastal structures which are usually called constraints bring out their own boundaries differently. Boundary conditions for the developed numerical model will be discussed in detail for each structure in Chapter 4.

3.2. Coast-Structure Interaction Numerical Model, CSI

“Coast-Structure Interaction” numerical model which is shortly called CSI is developed by Şafak (2006), Artagan (2006) and Baykal (2006) to contribute to shoreline evolution and simulation numerical models whose origins are longshore sediment transport. CSI is an explicit one-line numerical model in which Kamphuis’s formula is utilized. This choice is mainly due to the fact that Kamphuis relation involves median grain size, D_{50} along with the beach slope at breaking location (Şafak, 2006).

3.2.1. Explicit Solution of Sediment Continuity Equation

CSI is an explicit model and just like all coastal sediment one-line numerical models, it satisfies conservation of mass equations. Based on combination of sediment continuity equation and conservation of mass equation;

$$\frac{\partial V}{\partial t} + \frac{\partial Q}{\partial x} = 0 \quad 3.22$$

where V represents the total volume of the beach profile per unit length, a straightforward relation is approached;

$$\frac{\partial Q_i}{\partial x} = \frac{Q_{i+1} - Q_i}{\Delta x} \quad 3.23$$

where subscripts, i and $i+1$ designate the alongshore calculation steps. Eqn. 3.23 shows the explicit solution of one-line theory in terms of longshore sediment transport rates.

When Eqn. 3.23 is combined with a relation that gives shoreline position changes which is as;

$$\Delta y = (Q_i - Q_{i+1}) \frac{\Delta t}{\Delta x (D_B + D_C)} \quad 3.24$$

where Q_i and Q_{i+1} (Figure 3.7) are the longshore transport rates in and out of the beach or a certain portion of the beach, respectively, Δx is the shoreline increment, Δt is the time increment and D_B and D_C are average beach berm height and depth of closure respectively as in Figure 2.1, a new relation for calculation of shoreline position at next time step for i th cell is obtained;

$$y'_i = y_i + \frac{\Delta t}{(D_C + D_B)\Delta x} (Q_i - Q_{i+1} + q\Delta x) \quad 3.25$$

where (') denotes the next time step, y'_i and y_i are shoreline positions at next and current time steps at i th longshore step, respectively.

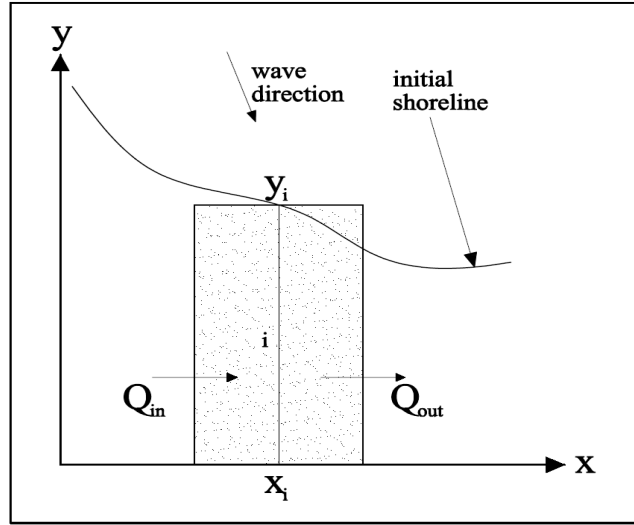


Figure 3.7 Longshore Transport Rates in and out of a Calculation Cell

A detailed description of explicit solution of sediment continuity equation and related formulas are given and discussed in Perlin and Dean (1978), Dean and Yoo (1992) and Şafak (2006).

3.2.2. Stability

In one-line numerical models, stability is an important phase, as y'_i depends on Q_i and Q_{i+1} , at each calculation step it must be calculated. Stability ratio in a model determines the numerical accuracy of the model not the physical accuracy. Thus, numerical accuracy should be distinguished from physical accuracy. Numerical accuracy is a measure of how well a finite difference scheme reproduces the

solution of a differential equation and physical accuracy is a measure of how well the differential equation or the numerical solution describes the process of interest (Hanson and Kraus, 1986). In CSI, stability calculations are performed according to a stability ratio (R_s) to understand the numerical accuracy of the model. Stability ratio is defined as;

$$R_s = \frac{Q}{\alpha_b(D_C + D_B)} \frac{\Delta t}{(\Delta x)^2} \quad 3.26$$

This condition is generally called Courant condition and has to be met at every calculation grid point along the shoreline (Hanson, 1987). As stability parameter strongly depends on Δt and Δx , and as for greater stability numbers shoreline evolutions are becoming less accurate and questionable, during the decision of which values to give great attention is needed. Therefore, in order to find reasonable and meaningful shoreline evolution results, stability number should be equal or less than 0.5 (Crank, 1975). If stability ratio takes a value greater than 0.5, calculations become unstable and the margin of error for calculated shoreline position increases causing the model results unreliable.

3.2.3. Wave Breaking

Waves are created in deep water mostly by wind action and start to propagate with a certain amount of energy towards land. On their journey, after deep water limit, they start to change in energy, height, length and direction. One of the most serious changes during these processes happens in surf zone. As a wave approaches a beach, its length L , decreases and its height, H , increases, causing the wave steepness H/L to increase. At a certain limiting point, the wave no longer carries its own state and loses its shape by releasing some of its energy. This limit is called limiting steepness which is a function of the relative depth, d/L and the beach slope, $\tan \beta$ (Munk, 1949);

$$\left(\frac{H}{L}\right)_{\max} = \frac{1}{7} \tanh\left(\frac{2\pi d}{L}\right) \quad 3.27$$

where d is the water depth and H/L is the wave steepness at a point on the path of a wave.

Breaking is the most critical situation in one-line numerical models as longshore sediment transport rate equations include effective breaking wave angle and in some longshore transport rate formulas variations in effective breaking wave heights are included. Moreover, breaking types have strong influence on the energy that is released during breaking and so the sediment motion within the control volume. What differs the types of breaking waves is the surf similarity parameter, ξ_o , which is a function of beach slope ($\tan \beta$), significant deep water wave height (H_o) and deep water wave length (L_o). For instance, spilling breakers generate less turbulence near the bottom and thus tend to be less effective in suspending sediment than plunging or collapsing breakers. However, the most intense local fluid motions are produced by a plunging breaker. As it breaks, the crest of the plunging wave acts as a free-falling jet that may scour a trough into the bottom (CEM, 2003).

Many studies have been performed to develop relationships to predict the wave height at incipient breaking, H_b . There are mainly two relationships for prediction of wave heights at incipient breaking, one of which is wave breaker index, γ_b ;

$$\gamma_b = H_b / d_b \quad 3.28$$

where d_b is the water depth at breaking location and the other is breaker height index, Ω_b ;

$$\Omega_b = H_b / H_o \quad 3.29$$

where H_o is the significant deep water wave height.

Together with many observations and measurements, for most of the cases, breaker index, γ_b , theoretically gets a value very close to 0.78 which is mentioned by Munk (1949) as an upper limit. Artagan (2006) reviews a detailed historical study on development procedure and relations of breaker indexes.

Throughout the odyssey of coastal engineering, several theories have been brought in about breaking wave height. Among these theories, following relation (CEM, 2003) is used in CSI;

$$H_b = H_o^{0.8} (C_{g,o} \cos \alpha_o)^{0.4} \left(\frac{g}{\gamma_b} - \frac{H_b g^2 \sin^2 \alpha_o}{\gamma_b^2 C_o^2} \right)^{-0.2} \quad 3.30$$

where α_o is the deep water approach angle of waves, $C_{g,o}$ is the deep water group velocity as;

$$C_{g,o} = 0.5 \frac{L_o}{T} \quad 3.31$$

C_o is the deep water wave celerity as;

$$C_o = \frac{L_o}{T} \quad 3.32$$

Moreover, the breaking wave angle, α_b , is determined by Snell's Law as a refraction equation as follows;

$$\frac{\sin \alpha_b}{\sin \alpha_o} = \frac{L_b}{L_o} \quad 3.33$$

where L_b is the breaking wave length which is determined by using Gravity Wave Table in SPM (1984) as;

$$L_b = L_0 \tanh\left(\frac{2\pi}{L} d_b\right) \quad 3.34$$

3.2.4. Wave Diffraction

As waves propagate towards land, there will be a lateral transfer of wave energy along the crest perpendicular to the direction of wave propagation. The energy transfer will be from points of greater to lesser wave heights. This process is known as wave diffraction (CEM, 2003). Wave diffraction is a natural result of pivoting of waves about the edge of an surface-piercing obstacle, either natural or artificial, such as a breakwater or an island, and penetration of waves into the shadow zone of the same obstacle (Goda, 1985). Due to diffraction, significant changes in orientations of waves and wave heights are observed (Figure 3.8).

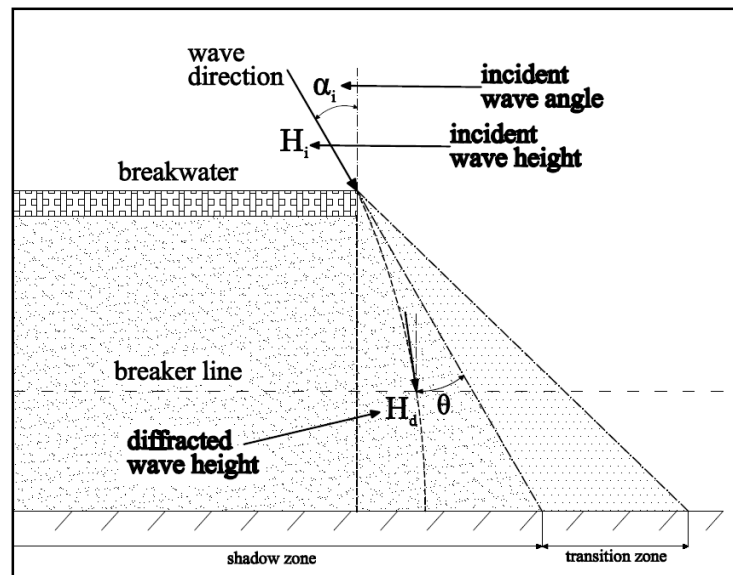


Figure 3.8 Wave Diffraction

In Figure 3.8, it is observed that two areas are defined within the sheltered zone of the structure. Shadow zone is the area that lays between the extension of incident wave directions at both edges of the structure and transition zone is the area between the extension of incident wave direction and the shoreline location where diffraction coefficients theoretically gets the value 1.0.

A coefficient called diffraction coefficient, K_d determines the relation about how much energy is lost due to diffraction;

$$K_d = \frac{H_d}{H_i} \quad 3.35$$

where H_d is the diffracted wave height at a point in the lee of the structure and H_i is the incoming wave height at the tip of the structure. In CSI, incoming wave height or in other words, incident wave height at the tip of the structure is assumed as the undiffracted wave height at the breaker line (Baykal, 2006).

Furthermore, Baykal (2006) gives brief discussions on regular and irregular wave diffractions and diffraction coefficient equations in which diffraction coefficients are defined in terms of several parameters for both regular and irregular waves. Even though up to this point, regular waves are mentioned as natural sea waves, in reality, sea waves are composed of many component waves from various directions. Hence, a superposition of all of the monochromatic waves is obligatory in order to include total effect of all of the waves. The proposed method in CSI is built on Kamphuis's (2000) method with a little modification. Firstly, diffraction coefficient at a point, radially θ degrees (Figure 3.8) away from the extension of incident wave direction is calculated for a contour using one of Kamphuis's equations;

$$K_d = 0.71 + 0.0093\theta + 0.000025\theta^2 \quad \text{for } -90 \leq \theta \leq 0 \quad 3.36(a)$$

$$K_d = 0.71 + 0.37 \sin \theta \quad \text{for } 0 \geq \theta \geq 40 \quad 3.36(b)$$

$$K_d = 0.83 + 0.17 \sin \theta \quad \text{for } 40 \geq \theta \geq 90 \quad 3.36(c)$$

For a point in transition zone, diffraction coefficient is linearly extended up to 1.0 beyond sheltered zone according to the trend of diffraction coefficient in shadow zone. In the applications, θ is assumed as negative (-) in shadow zone and positive (+) in transition zone.

Diffraction coefficient calculations both in shadow and transition zones are the key steps in determination of breaking wave heights in the sheltered zone which is the combined area including shadow and transition zones;

$$H_{bd} = K_d H_b \quad 3.37$$

where H_{bd} is the diffracted breaking wave height. Combined effects of coastal structures are also very important in determination of diffraction coefficient calculations within their sheltered zones.

3.2.5. Combined Refraction-Diffraction

If the depth between the breaker line and the tip of the structure is relatively very close to each other, diffraction methodologies that are discussed previously in wave diffraction part is adequate (Baykal, 2006). If otherwise, due to shoaling effects, changes in wave amplitudes are observed. Additionally, due to the difference in orientation between wave crest lines and the bottom contours, waves are exposed to refraction (CEM, 2003).

Combined refraction-diffraction concept has been utilized in numerical models which are mentioned in CEM (2003) and Baykal (2006). Dabees (2000) denotes that linear wave theory which is developed for constant water depth takes no refraction and shoaling effects and only pure diffraction is taken into account.

However, shoaling and refraction significantly affects the wave patterns behind structures. In order to include combined effect of refraction and diffraction in the shadow and transition zones, breaking wave angles are reduced in these zones.

Baykal (2006) takes Kamphuis's (2000) approach into account and compares these methods in detail together with figures showing the difference in diffraction coefficients between these methods. As a result of this comparison, Kamphuis's (2000) method which is relatively simpler than Hanson's (1987) method is used in CSI (Baykal, 2006).

CHAPTER 4

MODIFIED COAST-STRUCTURE INTERACTION NUMERICAL MODEL, CSIM

With the development of CSI, a new and user-friendly one-line model which contains new assumptions is being introduced for practical applications. However, it is believed that CSI must be upgraded by implementing an implicit scheme, adding a new longshore transport rate equation which is CERC equation, and performing several modifications on diffraction calculations at the sheltered zones of structures. Hence, in order to achieve this aim, “Modified Coast-Structure Interaction” numerical model, CSIM, whose base is CSI, is developed concerning various approaches and suggesting new propositions which will be mentioned within the scope of the following sections.

4.1. Implicit Solution of Sediment Continuity Equation

In CSIM, Hanson’s implicit methodology which constitutes the basis of GENESIS is taken as the primary source and several other approaches on diffraction and combined refraction-diffraction studies are treated as the second source. In the following two consecutive sections, these methods and approaches will be established and their implementations into CSIM will be illustrated.

One of the basic differences of implicit method from explicit method is that the longshore sediment transport rate at a cell of the simulated beach is related to the current longshore transport rates entering and leaving that cell and longshore transport rates entering and leaving that cell in the next time step as in;

$$\frac{\partial Q}{\partial x} = \frac{1}{2} \left[\frac{Q'_{i+1} - Q'_i}{\Delta x} - \frac{Q_{i+1} - Q_i}{\Delta x} \right] \quad 4.1$$

The other basic difference of implicit scheme from explicit scheme is that the shoreline position in next time step depends on both longshore transport rates at next time step and longshore transport rates in current time step as;

$$y'_i = B(Q'_i - Q'_{i+1}) + y_{c_i} \quad 4.2$$

where superscript (') denotes the next time step, B is the longshore transport parameter as;

$$B = \frac{\Delta t}{2(D_B + D_C)\Delta x} \quad 4.3$$

and y_{c_i} is the shoreline position halfway between shoreline positions at current and next time steps;

$$y_{c_i} = B(Q_i - Q_{i+1}) + B\Delta x(q'_i - q_i) + y_i \quad 4.4$$

where q_i is the source or sink at i th cell.

One of the complexities of implicit method is that longshore sediment transport rates and so the shoreline positions are calculated in the positive x-direction but only for the initial time step. In the following time steps, calculation of these parameters is performed in the opposite direction that is in negative x-direction. In the literature this is called double-sweep algorithm. Iterative solution of Eqn. 4.2 for every time step gives the shoreline evolutions after each time step. This procedure firstly introduced by Le Mehaute and Soldate (1978).

Perlin and Dean (1979) proposed a computationally faster method for shoreline calculations and this method is later expanded by Kraus and Harikai (1983) by expressing Q (Eqn. 3.17) in terms of y using trigonometric expressions and expanding the Eqns. 3.18(a) and 3.18(b) to first order, y' (Hanson,1987). Thus, Q'_i is presented as;

$$Q'_i = E_i(y'_{i+1} - y'_i) + F_i \quad 4.5$$

where E_i and F_i are double-sweep parameters (m^2/s) as;

$$E_i = \frac{(H_b^2 C_{gb})_i \left(2a_1 \cos 2\alpha_b \cos^2 \alpha_s + a_2 \frac{\partial H_b}{\partial x} \sin \alpha_b \cos \alpha_s \right)_i}{\Delta x} \quad 4.6$$

$$F_i = \frac{(H_b^2 C_{gb})_i \left(a_1 \sin 2\alpha_b (2 \cos^2 \alpha_s - 1) - a_2 \frac{\partial H_b}{\partial x} \cos \alpha_b \cos \alpha_s \right)_i}{\Delta x} \quad 4.7$$

As the number of unknowns is more than the number of equations in the equations above, they can not be solved without defining boundary conditions. Hence, in order to obtain equal number of unknowns and equations, the best way is to give boundary conditions at two boundaries of studied beach ($i=1$ and $i=n+1$). Then, Eqn. 4.5 can be solved by using the aforementioned double-sweep algorithm.

However, in the developed numerical model, a different version of Eqn. 4.5 is utilized which is achieved through rewriting Eqn. 4.5 as;

$$Q'_i = EE_i Q'_{i+1} + FF_i \quad 4.8$$

where EE_i and FF_i are double sweep recurrence coefficients as;

$$EE_i = \frac{BB_i}{1 + BB_i(2 - EE_{i-1})} \quad 4.9$$

$$FF_i = \frac{F_i + E_i(y_{c_{i-1}} - y_{c_i}) + BB_i FF_{i-1}}{1 + BB_i(2 - EE_{i-1})} \quad 4.10$$

where BB_i is the longshore transport parameter modified by E_i as;

$$BB_i = B E_i \quad 4.11$$

In this implicit method, Q' values are calculated in descending order and EE_i and FF_i values are calculated in ascending order. Therefore, solution procedure may be summarized as:

- i. Defining boundary conditions at $i=1$ and $i=n+1$ locations in terms of EE_i and FF_i .
- ii. Solving Eqns. 4.9 and 4.10 from $i=2$ to n for all calculation cells. This is the first sweep throughout whole shoreline.
- iii. Solving Eqn. 4.8 from $i=n$ to $i=1$ for all calculation cells. This is the second sweep procedure.
- iv. Finally, calculation of y_{c_i} values using Eqn. 4.4 and solving Eqn. 4.2 to obtain y'_i values.

4.2. Stability

In the developed implicit numerical model, just like in the explicit version, CSI, same stability ratio relation (R_s) (Eqn. 3.26) is used. The main difference in stability computations is that unlike in the explicit scheme, even though the stability ratios exceed 0.5 in the implicit model, stability of the model is not affected seriously and still calculates reliable values. Kraus and Harikai (1983) showed that an implicit model with a 6-hr time step is comparable in accuracy and

execution time to an explicit model with the same time step. Thus, regardless of how high the stability ratio increases, shoreline changes that an implicit model computes are accurate enough. However, to be on the safe side, by taking smaller time steps for a given space step, stability ratios below the necessary value in explicit model, 0.5, may be achieved for an implicit model. On the other hand, this would increase the execution time. The increase in execution time due to a decrease in time increment (Δt) in the developed numerical model is presented in Figure 4.1.

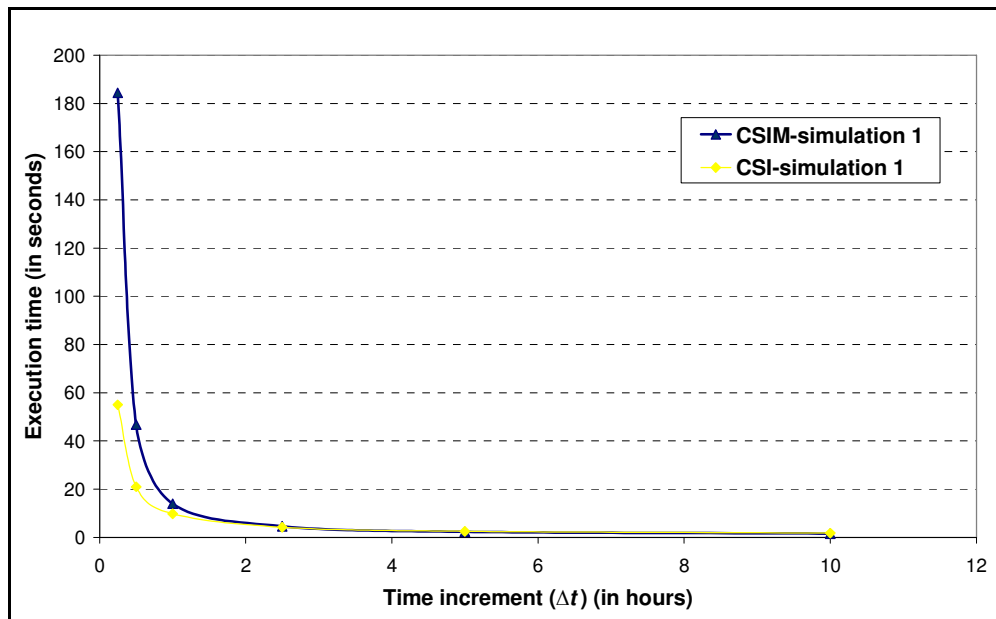


Figure 4.1 Execution Times for CSI and CSIM with Various Time Increments

All the sample simulations in CSI and CSIM are performed concerning the same shoreline, structure and wave data. As seen in Figure 4.1, implementing smaller time increments (Δt) in both CSI and CSIM increases the execution times and the observed increase is extremely drastic for very small time increments ($\Delta t < 1$). For time increments that are higher than 2 seconds, both numerical models, CSI and CSIM give close execution times. As mentioned before, Kraus and Harikai (1983)

showed that if the time increment, Δt , is given high, the explicit and implicit numerical models result in very close accuracy and execution times. Kraus and Harikai (1983) achieved this condition with very high time increments which is 6 hours. However, the same situation is achieved with 2.5 hour time increment with CSI and CSIM. On the other hand, execution time also depends on processor speed of computers and thus the capacity of the computer where simulations are performed.

Additionally, in order to observe and compare execution time and stability ratios for implicit and explicit numerical models, several comparisons have been performed between CSI and CSIM. As previously mentioned CSI is based on Kamphuis's (2000) longshore transport rate formula. In order to perform a realistic comparison, an option is added to CSI by implementing CERC equation into the numerical model. For comparison, two figures related to stability ratios and execution times are obtained and are presented in Figure 4.2 and Figure 4.3.

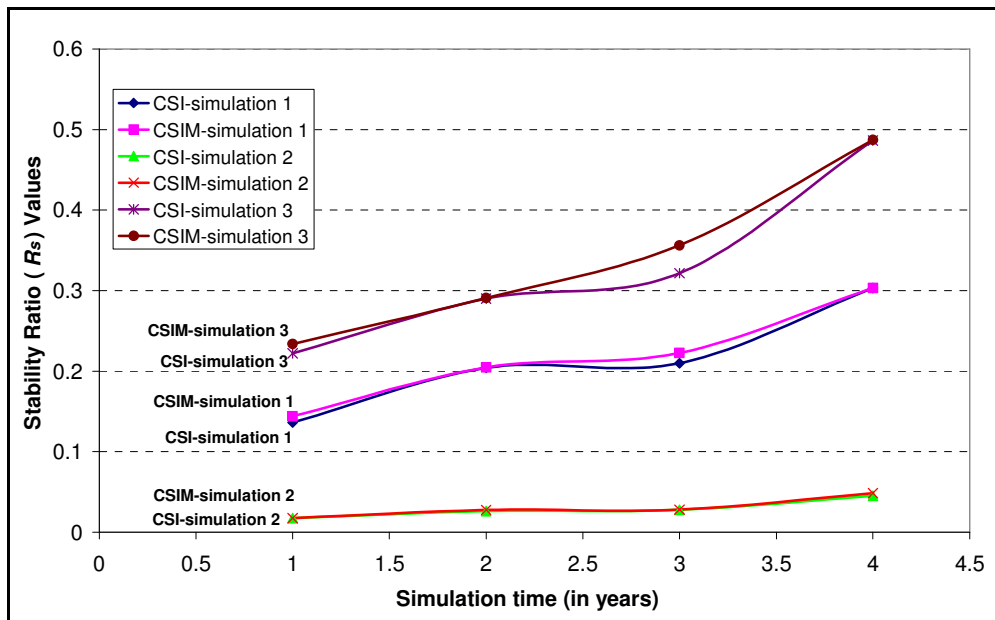


Figure 4.2 Stability Ratio Comparisons between CSI and CSIM

While obtaining Figure 4.2, all the sample simulations in both numerical models, CSI and CSIM are performed using the same wave and shoreline data. The x axis and y axis represent the number of repetitions of the numerical model and the stability ratios (Eqn 3.26) at each repetition of sample simulations, respectively. It is understood from Figure 4.2 that implicit and explicit numerical models give almost the same stability ratios. However, nearly for all sample simulations, implicit numerical model, CSIM, gives a little bit higher stability ratio which is an expected situation.

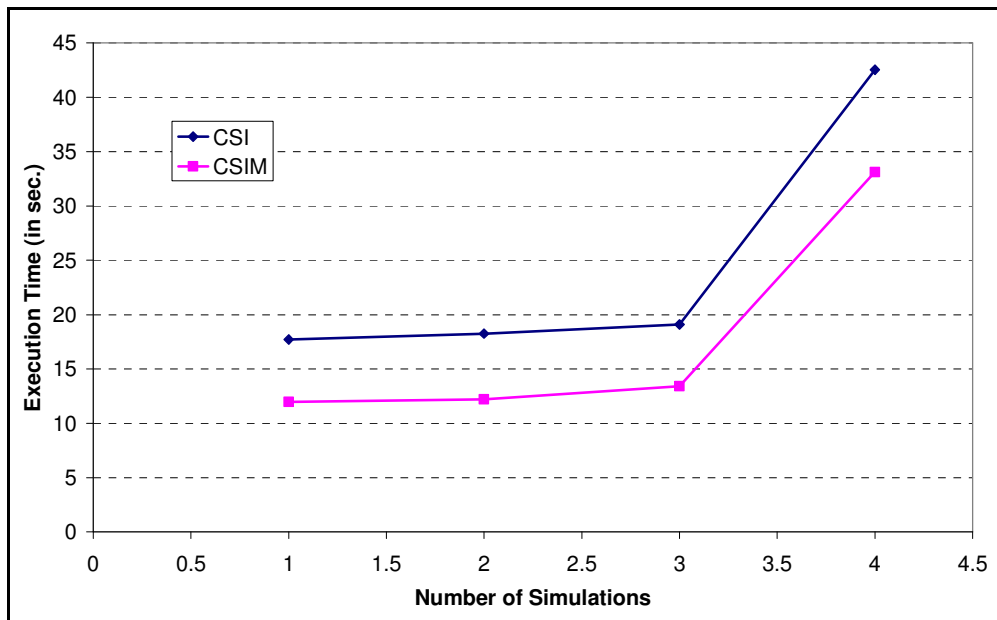


Figure 4.3 Execution Time Comparisons between CSI and CSIM

During the process of achieving Figure 4.3, all the sample simulations in both numerical models, CSI and CSIM are performed using the same wave and climate data just like the procedure of obtaining Figure 4.3. The x axis and y axis represent the number of trials or number of sample simulations made with the numerical models and the execution times of these sample simulations,

respectively. It is derived from Figure 4.3 that implicit numerical model is faster than explicit numerical model which is a little different from the information attained during literature survey. This may be due to capacity and speed of the computer or the simplicity of the developed numerical model.

4.3. Reference Depth

In the developed numerical model, CSIM, wave data input which contains deep water wave characteristics of the study area may be organized according to wave characteristics that are obtained for a reference depth which is smaller than deep water limit and closer to the shoreline. This is achieved by transforming deep water wave characteristics to a reference depth by performing shoaling, refraction analysis and if needed diffraction effects of natural obstacles such as headlands. The reference depth is determined according to the water depth at which structures are constructed. This means that the water depth where structures are constructed should not exceed the reference depth in order not to include the diffraction effects of coastal structures in the transformation of waves from deep water to the reference depth. Obtained wave characteristics at the corresponding reference depth may be inputted as the wave data input in the numerical model. The developed numerical model is sensitive to deep water approach angle that is if deep water approach angle is larger than 67° one-line theory based on smaller approach angle is not satisfied; causing errors in the results. Besides, due to natural geographical and topographic obstacles such as a headland or an island, waves are naturally affected by shoaling, refraction and diffraction. To overcome this problem and to reflect these conditions, reference depth concept is applied where the approach angle is much smaller due to combined effect of diffraction and refraction.

4.4. Wave Diffraction and Combined Refraction-Diffraction

Accurate and realistic prediction of wave transformation is obligatory to obtain realistic predictions of shoreline change in situations of a coastal structure. In

CSIM, Kamphuis's (2000) method is applied together with a modification by Kraus's (1984) method. The basic calculations for breaking wave height and depth of breaking are performed according to Eqns. 3.30 and 3.28, respectively by defining wave breaker index (γ_b) equal to 0.78. During calculation of breaking wave height, iteration is performed, until the breaking wave height converge a certain value with tolerable margin of error (Eqn. 3.30). In order to visualize tolerable margin of error concept, different iteration numbers are introduced to the numerical model and a figure is obtained. The used wave data involves deep water waves with significant wave heights of 1 meter, significant wave periods of 4 seconds and deep water approach angles of 30° . Iteration numbers of 1, 2, 3, 4, 5, 10, 20 and 100 are introduced into the numerical model. At each iteration number, breaking wave heights are obtained and Figure 4.4 is drawn using these data.

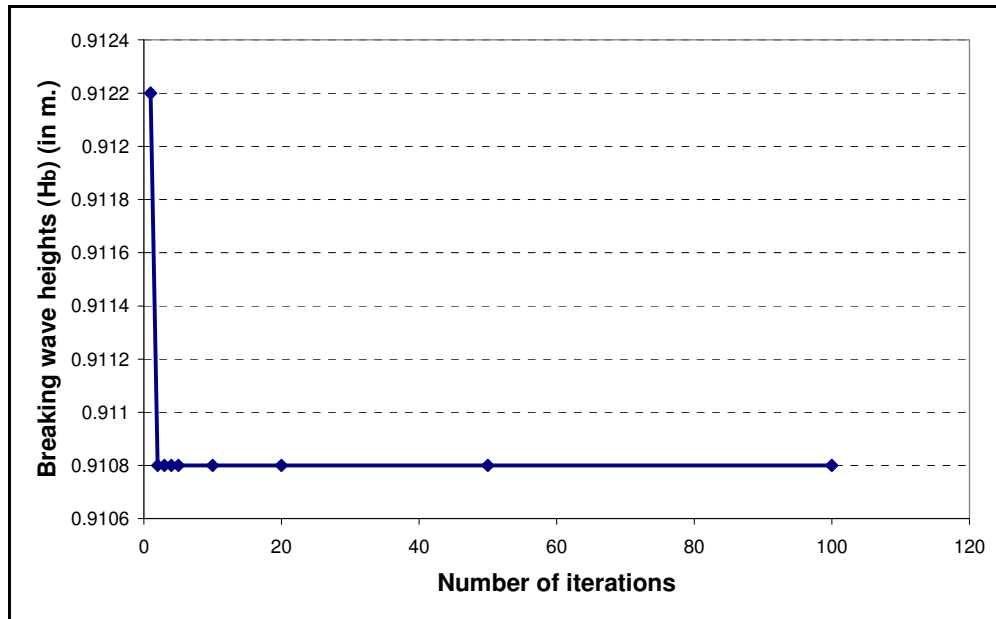


Figure 4.4 Breaking Wave Heights for Each Iteration

As observed in Figure 4.4, after the first iteration, breaking wave height (H_b) converges to a certain value. Therefore, the iteration number, which is normally 10 in the numerical model, CSIM, is enough to obtain a reasonable value.

Following the iteration procedure performed for breaking wave height, using a certain value for breaker index which is 0.78 (CEM, 2003) in the numerical model and the calculated value of breaking wave height, depth of breaking is determined (Eqn. 3.28). One of the important points that need attention is that breaking wave height and depth of breaking is assumed unchanged for each calculation cell alongshore. Unless a structure exists at the shoreline system, same assumption is applicable for breaking wave angles. Subsequently, diffraction coefficients for every location behind a structure are determined by using Kamphuis's equations (3.36(a), (b) and (c)). From now on, diffraction calculations are modified with intrusion of Kraus's method (1984). In CSI, to compute diffraction coefficients in the transition zone of breakwaters, the trend of diffraction coefficient in the shadow zone is linearly extended up to a value of 1.0 beyond sheltered zone. However, in CSIM, for the same region, diffraction coefficients theoretically converge to 1.0 till the end of the shoreline which means that in reality, computed values of diffraction coefficients are less than 1.0. Figure 4.5 and 4.6 which show the diffraction coefficients are obtained one of which is for groins and the other is for offshore breakwaters in order to explain the situation visually.

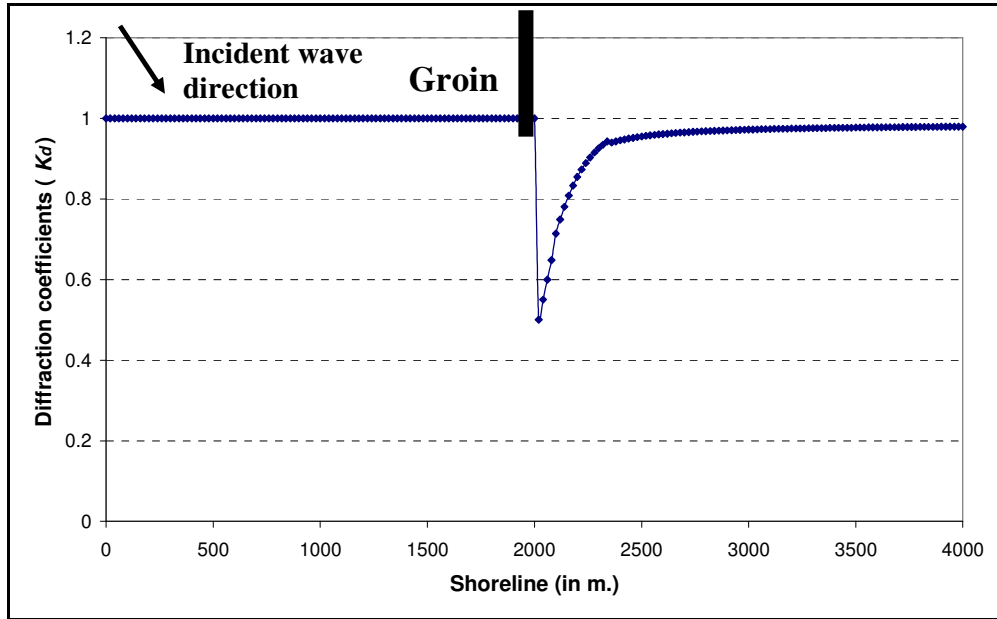


Figure 4.5 Diffraction Coefficients (K_d) in case of a Single Groin

Figure 4.5 is obtained for a 4000 m shoreline with a 200 m groin at the middle of the shoreline (at 2000 m). As seen Figure 4.5, diffraction coefficients get very close values to 1.0 by the end of the shoreline. Thus, this shows that the effect of a single groin placed at a random location on shoreline is observed throughout the downdrift shoreline. This assumption does not lead into a very critical error in shoreline evolution processes.

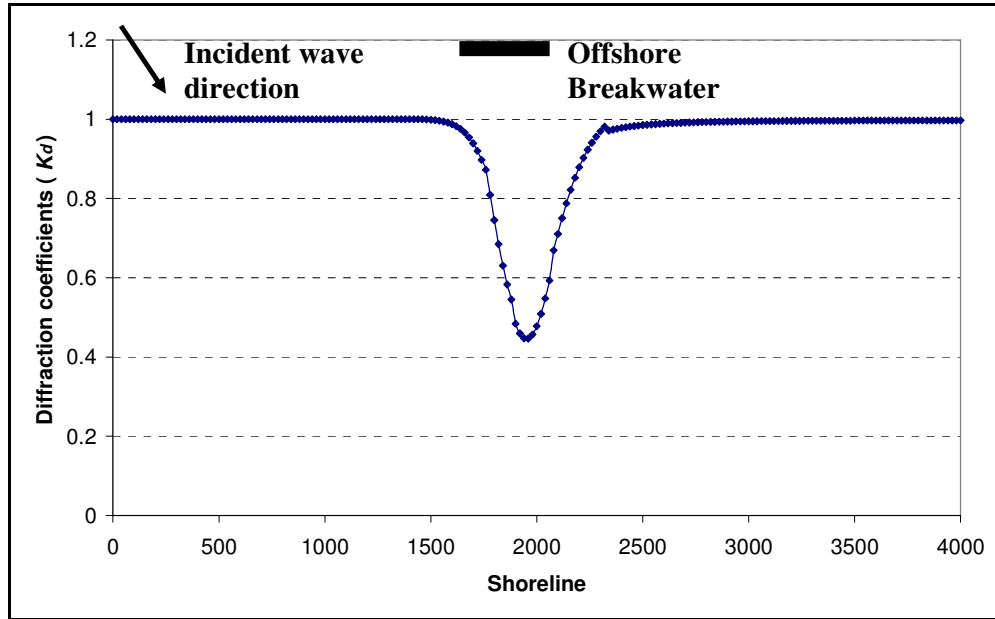


Figure 4.6 Diffraction Coefficients (K_d) in case of an Offshore Breakwater

Just like Figure 4.5, same kind of figure is obtained for a 4000 m shoreline with a 200 m long offshore breakwater which is 200 m away from the shoreline in seaward direction and 1800 m away from the first boundary of shoreline. As observed in Figure 4.6, diffraction coefficients get very close values to 1.0 by the end of the shoreline. Similar results were obtained by Requejo et al. (2003) in case of an offshore breakwater. At several sample simulations that are performed with the developed numerical model it is observed that at the end of shadow zone, diffraction coefficients, K_d get very close to value 0.9.

4.4.1. Wave Diffraction Calculations for a Groin

A single groin acts like a semi-infinite offshore breakwater in case of diffraction calculations. Initially calculated wave breaking parameters, H_b , d_b and α_b in the sheltered zones of structures without taking the diffraction effect are modified according to impacts of diffraction sources. Kamphuis (2000) came up with a

relation (Eqn. 3.36) for random sea waves that is the result of a regression analysis for wave diffraction near structures.

A further modification concerning the diffraction effect of a groin at its sheltered zone is performed on wave breaking height using Eqn. 3.37. From this point on, combined effect of refraction and diffraction is taken into account. Kamphuis (2000) introduces a relationship which reflects the combined refraction and diffraction effect in breaking wave angle inside and outside the shadow zone of a single groin;

$$\alpha_{bd} = \alpha_b K_d^{0.375} \quad 4.12$$

where α_{bd} is the diffracted breaking wave angle.

Kamphuis (2000) denotes that due to diffraction, a further increase in breaking angle should be considered within the shadow zone of a groin;

$$\alpha_{bd} = \alpha_b K_d^{0.375} \left[\frac{2y_A}{l_{gb} [\tan \alpha_i + \tan(0.88\alpha_b)]} \right] \quad 4.13$$

where y_A is the lateral distance between point A, which is in the shadow zone of a groin and a point (G) on the groin, l_{gb} is the distance between tip of the groin to the breaker line, α_b is the undiffracted breaking wave angle and α_i is the incident wave angle at the tip (T₂) of the structure (Figure 4.7). In Figure 4.7, L_g and θ denote the length of groin from the shoreline and the angle between point A and the extension of incident wave direction, respectively.

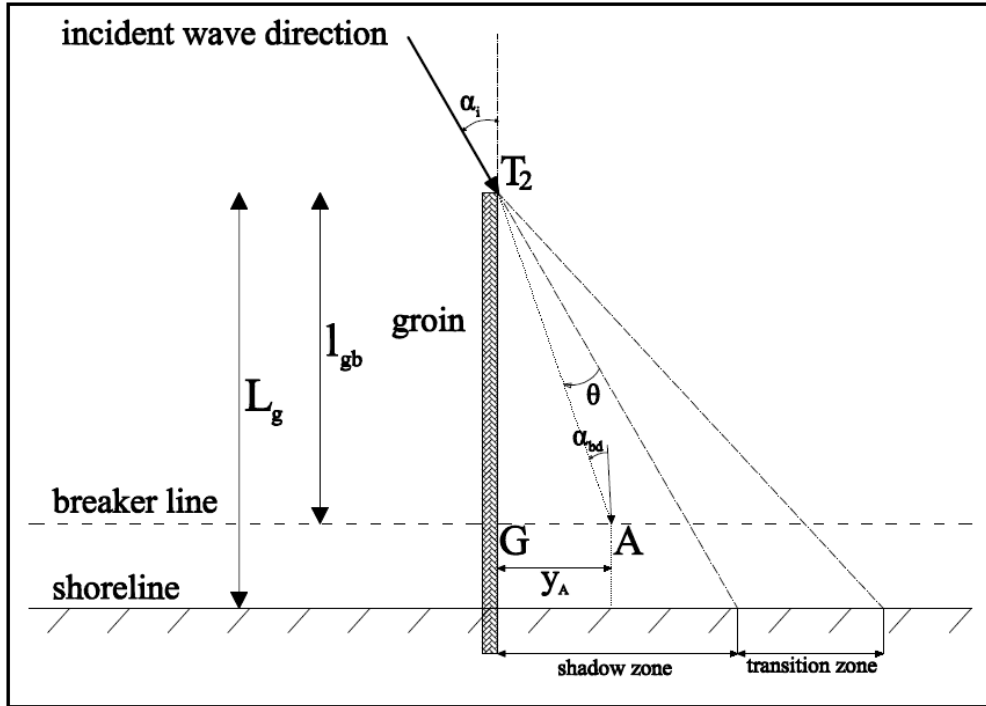


Figure 4.7 Diffraction of Waves at the Sheltered Zone of a Groin (Kamphuis, 2000)

4.4.2. Wave Diffraction Calculations for an Offshore Breakwater

The critical situation for an offshore breakwater is its effect on wave diffraction and transformation processes because of its complexity compared to the groins. In the numerical model, an offshore breakwater which is within the breaker line in landward direction is assumed to have no diffracting effect and hence no shoreline change effect (Şafak, 2006). For an opposite situation, where offshore breakwater is beyond the breaker line, diffraction calculations are based on Kamphuis's (2000) approach and combined effect of diffraction coefficients in case of consecutive offshore breakwaters are based on Vafaei's (1992) approach.

In the numerical model, where offshore breakwaters are beyond the breaker line, the diffraction coefficients computed from left and right tips of the breakwater are called K_{d1} and K_{d2} , respectively (Figure 4.8). Since half of the wave energy is lost

along the line from the tip of the breakwater to the breaker line and wave energy is related to square of wave height, at opposite ends, K_d gets a value 0.71 (Goda, 1985). In addition, in CSI, diffraction coefficients are linearly extended to reach 1.0 at some distance at the end of the transition zone at both sides which is mentioned previously. However in CSIM, just like in groins, for offshore breakwaters, it is assumed that diffraction coefficients do not exactly get the value 1.0 at these regions, but only theoretically converge to value 1.0.

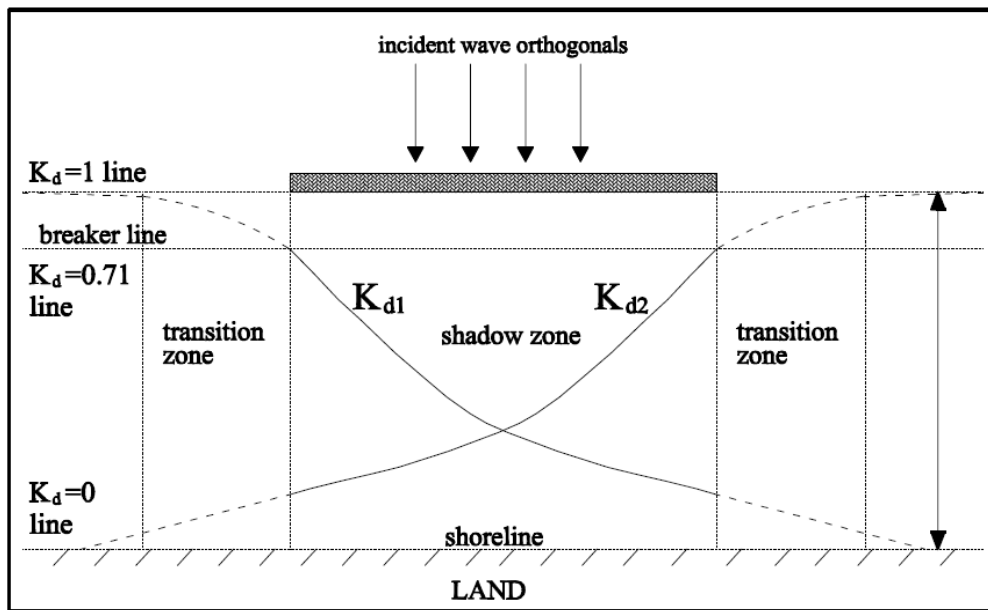


Figure 4.8 Schematic Representations of K_{d1} and K_{d2} (Artagan, 2006)

For offshore breakwaters, Vafaei (1992) initially finds two breaking wave rays from two tips of the breakwater (Figure 4.9) and adds these two wave rays vectorially to identify the breaking wave heights and angles.

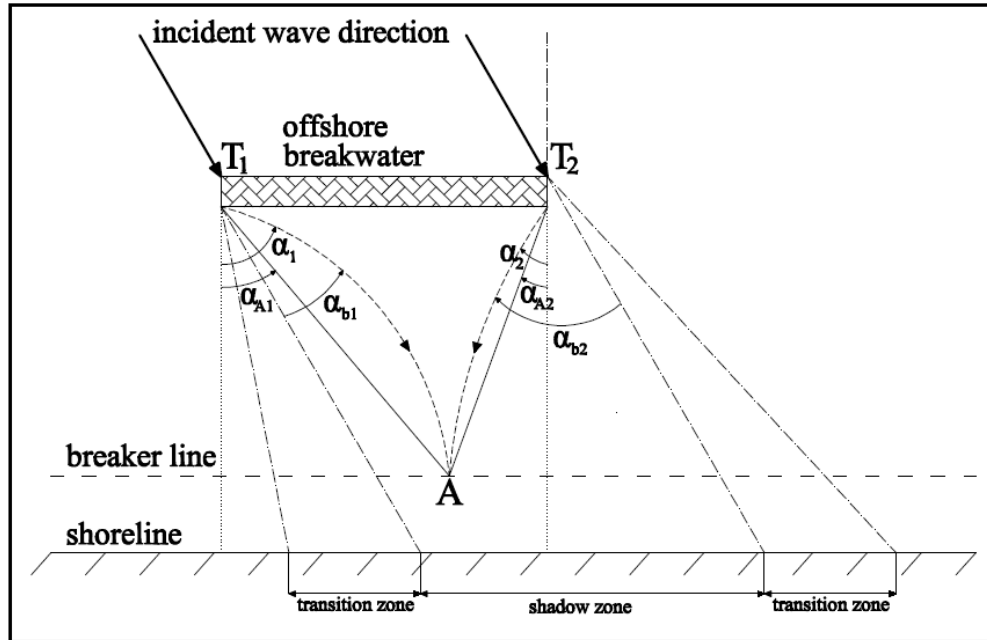


Figure 4.9 Schematic Figure of Proposed Method in CSIM for Wave Diffraction Calculations

In Figure 4.9, A is a point at the sheltered zone of offshore breakwater on the breaker line and T_1 and T_2 are two tips of offshore breakwater. As observed from Figure 4.9, due to the radial change of waves around the tip of the breakwater to form a milder elliptic wave field under the influence of inertia, a transition zone, where waves can change course gradually next to the structure is formed in addition to the effect of shoaling and refraction (Dabees, 2000).

In the vectorial summation of wave rays, H^2 is used instead of H since the energy transfer is proportional to H^2 (Vafaei, 1992) as;

$$E_w = \frac{\rho g H^2}{8} \quad 4.14$$

where E_w is the wave energy and H is the wave height at a particular location. Thus, aforementioned diffraction coefficients, K_{d1} and K_{d2} (Figure 4.10), are divided into their x and y components and these values are added to each other as;

$$K_{dx} = K_{dx1} + K_{dx2} \quad 4.15(a)$$

$$K_{dy} = K_{dy1} + K_{dy2} \quad 4.15(b)$$

where K_{dx1} and K_{dx2} are the x components of diffraction coefficients, K_{d1} and K_{d2} and K_{dy1} and K_{dy2} are the y components of diffraction coefficients of K_{d1} and K_{d2} from both tips of the breakwater. Exact diffraction coefficient in the transaction area of sheltered zones of two consecutive offshore breakwaters or in the shadow zone of a single offshore breakwater is found by taking the square-root of the summation of square of both K_{dx} and K_{dy} (Figure 4.10) values as;

$$K_d = \sqrt{K_{dx}^2 + K_{dy}^2} \quad 4.16$$

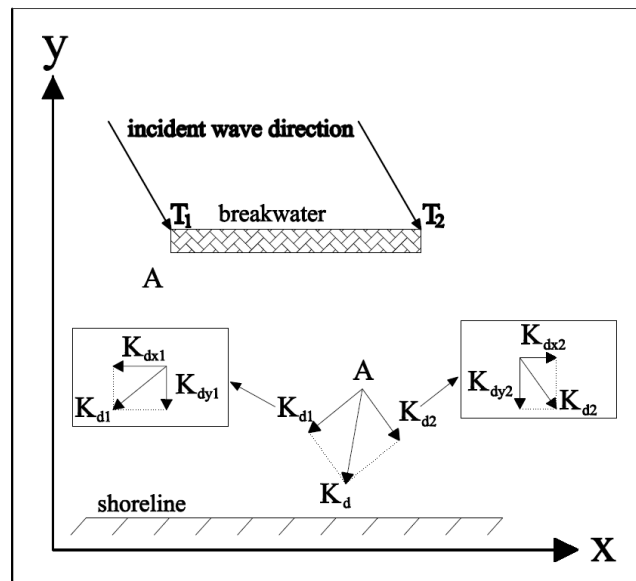


Figure 4.10 Vectorial Summation of Diffraction Coefficients

In case of a permeable offshore breakwater permeability corrections are performed on diffraction coefficient and finally, diffracted breaking wave height is calculated from Eqn. 3.37.

4.5. Longshore Sediment Transport Rate, CERC Formula

As mentioned previously, an option for longshore transport rate equation for the developed numerical model is CERC formula (Eqn. 3.17). The first term in CERC formula (Eqn. 3.17) accounts for longshore sediment transport produced by obliquely incident breaking waves and the second term is used to describe the effect of another generating mechanism for longshore sand transport, the longshore gradient in breaking wave height ($\partial H_b/\partial x$). The contribution arising from the longshore gradient of breaking wave height might be neglected because it is very small compared to the changes occur due to oblique wave incidence in an open-coast situation (CEM, 2003). Hence, by neglecting $\partial H_b/\partial x$ in CERC formula in the numerical model, Eqn. 3.17 is reduced to;

$$Q_l = H_b C_{gb}^2 a_l \sin 2\alpha_{bs} \quad 4.17$$

The application of CERC equation as in Eqn. 4.17 is previously given in the study of Ravens and Sitanggang (2005) where the assumption of constant breaking wave height and constant depth of breaking is mentioned along the shore. Even though this assumption results in some errors in diffraction effects on shoreline change in the vicinity of structures, it remains as a minor problem.

Another modification for CSIM comes in the calculation of longshore sediment transport parameter, a_l (Eqn 3.18). The calibration parameter K_l is assumed as a certain value in GENESIS, and as previously mentioned although several studies have been performed about calibration parameter K_l , there is not a certain agreement on which one is better and applicable in numerical models. Among

these formulas, it is decided that King's (2005) formula for calibration parameter K_I (Eqn 3.21) should be used in the developed numerical model. The reason for this choice is that in King's (2005) studies, the data represents very wide range of D_{50} and shows a clear trend of decreasing transport with increasing grain size. However, one point that needs attention in his studies is that due to wide divergence of the data, Eqn 3.21 should only be used for initial estimates.

4.6. Structures

Coastal structures are designed and implemented to stabilize coastline. Mainly, groins, offshore breakwaters and seawalls are most used types of coastal stabilization structures. Developed numerical model, CSIM, will be applied for groins and offshore breakwaters.

4.6.1. Groins

In the developed numerical model, groins are defined perpendicular to the shoreline. The permeability and offshore length of each groin can be specified at arbitrary locations along the shoreline. As mentioned previously, offshore length of a groin plays an important role in shoreline evolution over time because it is assumed that groins that do not exceed breaker line is not effective in diffraction calculations of breaking waves (Şafak, 2006).

The location of a groin with respect to the coordinates of the shoreline defines the boundary conditions. If the groin is at the boundary of the simulated shoreline, the boundary conditions for the groin is also specified as boundary conditions of the shore and if the groin is within one of the calculation grids, it is accounted for as a constraint (Dabees, 2000).

The influence of a groin on a shore is defined by the ratio of the amount of sand passing that groin and the amount of sand arriving at the updrift side of that groin. Sand movement past a groin is controlled by the combined action of sand moving

around the tip of the groin which is called sand bypassing and sand transmission through or over the groin.

4.6.1.1. Bypassing

For long and impermeable groins, groin intercepts the longshore sediment transportation by acting as a barrier and accretes beach material at its updrift side. Throughout time due to increasing accretion, beach profile moves seaward until a time when the groin can no longer block alongshore transportation of sand. This situation results in movement of sediments around the tip of the groin to the groin's downdrift side (Figure 4.11).

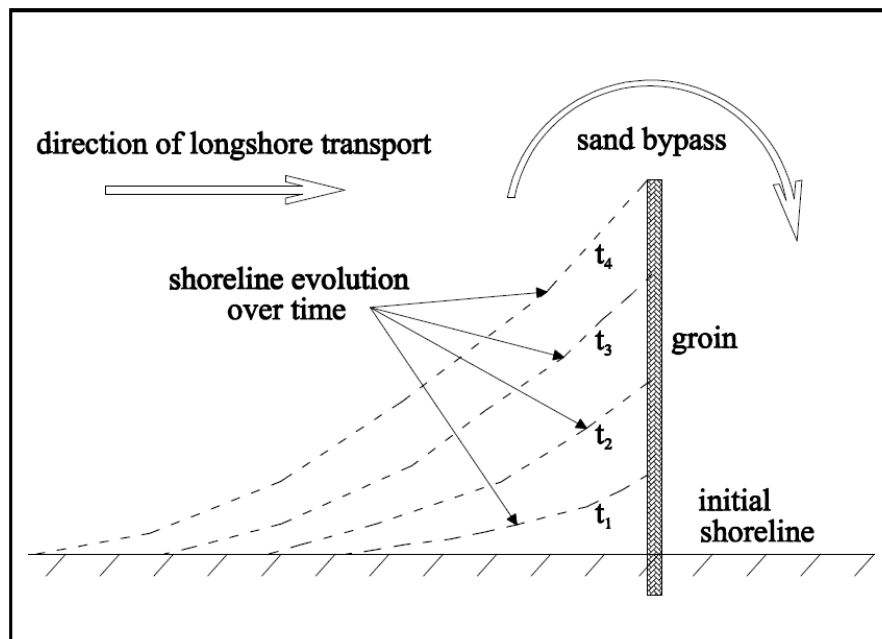


Figure 4.11 Ground Plan of Bypassing Around a Groin

Sediment bypassing may be intercepted or delayed due to cross-shore processes at the region. During a severe storm, some of the accumulated beach material at the updrift side of the groin may be carried into the deep water region and may never

be brought back by longshore or offshore transportation. This undesired condition not only affects the retreated updrift side but also the downdrift side due to the fact that alongshore movement of most of the transported sediment will be stopped by the groin decreasing the sediment amount passing through or over the structure to the downdrift side. Thus, an additional degree of erosion will be observed at the downdrift side of the groin for compensation of the pre-storm shore profile at the updrift side. Another issue is that in nature, when sand bypassing starts around the edge of the groin, some of the bypassed sand accumulates at the seaward end of the groin. However, as this condition is an outcome of cross-shore distribution of sediment transportation, one-line models which exclude the cross-shore transportation can not actualize this condition and all of the bypassed sand is visualized at the downdrift side of the groin.

The critical element that determines the bypassed amount of sediment is the water depth at the seaward tip of the groin, D_g and the limiting depth of longshore transportation, D_{LT} . Assuming a uniform cross-shore distribution of the longshore sediment transport rate, Hanson (1987) implemented a simple relation in which bypassing factor is denominated in terms of a bypassing factor, *BYP*, which is based on the assumption that if the total amount of sand arriving at the updrift side is specified as 1.0, bypassed sediment amount is related to the division of D_g by D_{LT} as;

$$BYP = 1 - D_g / D_{LT} \quad 4.18$$

Bypassing factor takes a value between 0 and 1. If D_g is higher than D_{LT} , bypassing factor is set to 0 in the calculations. Each time step, as water depth at seaward end of each groin may be different as well as the changing shoreline and shore profile, bypassing factor takes a different value at each time step and each groin location.

A more realistic approach for bypassing factor is introduced by considering 2-dimensional (cross-sectional) approach (Figure 4.12) in CSI;

$$BYP = 1 - (D_g / D_{LT})^2 \quad 4.19$$

In this approach as sediment trapping capacity of a groin changes at each time step, an effective length of groin is defined (Figure 4.12);

$$L_e = L_g - y_{acc} \quad 4.20$$

where L_e is the effective length of groin, y_{acc} is the distance of accumulated sediment at the updrift side of the groin and L_g is the length of groin from the shoreline. In CSIM, a modified version of Kamphuis's (2000) bypassing factor formula is used as;

$$BYP = 1 - \frac{L_e D_{LT} - 0.6 A_p L_e^{5/3}}{y_{LT} D_{LT} - 0.6 A_p y_{LT}^{5/3}} \quad 4.21$$

where y_{LT} is the offshore distance of limiting depth of longshore sediment transport and D_{LT} is the limiting depth of longshore sediment transport (Figure 4.12).

Şafak (2006) specifies that since CSI is based on longshore sediment transport and resulting shoreline changes, replacing D_c with D_{LT} and y_c with y_{LT} is necessary in bypassing relation. Similarly, this approach is implemented in the numerical model, CSIM.

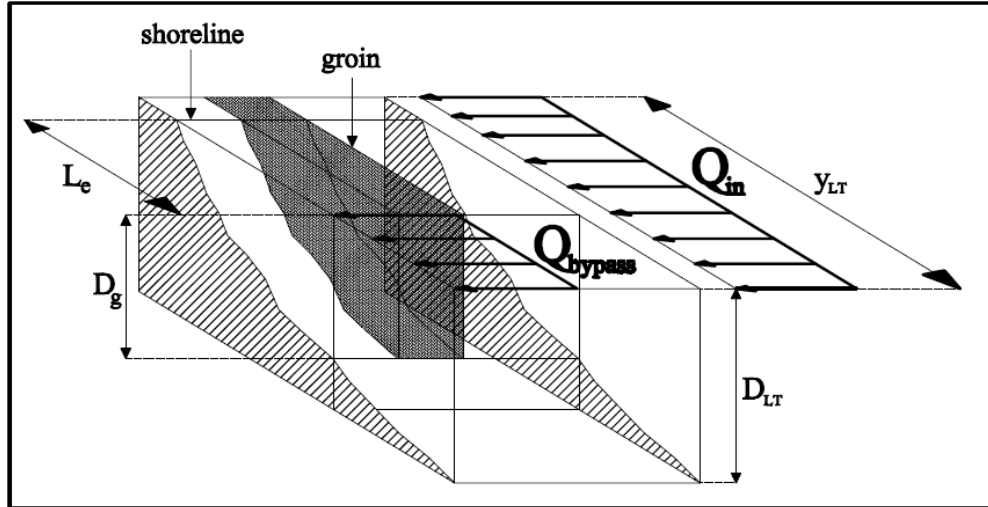


Figure 4.12 Bypassing Approach in the Developed Numerical Model

Moreover, just like in Hanson's (1987) bypassing equation, if effective length of groin is greater than offshore distance of limiting depth of longshore transport, bypassing factor is set to 0. Similarly, if the accumulation at the updrift side of the groin reaches its maximum possible value ($L_e=0$), bypassing factor takes a value of 1.0 meaning that all the sediment is transferred around the tip of the groin to the downdrift side of the groin. This situation implies that the groin loses its functionality. However, this case is only possible if a long term unidirectional flow exists (Şafak, 2006).

In order to observe the response of shoreline when bypassing occurs during the existence of groins, several simulations are performed and presented in Figure 4.13.

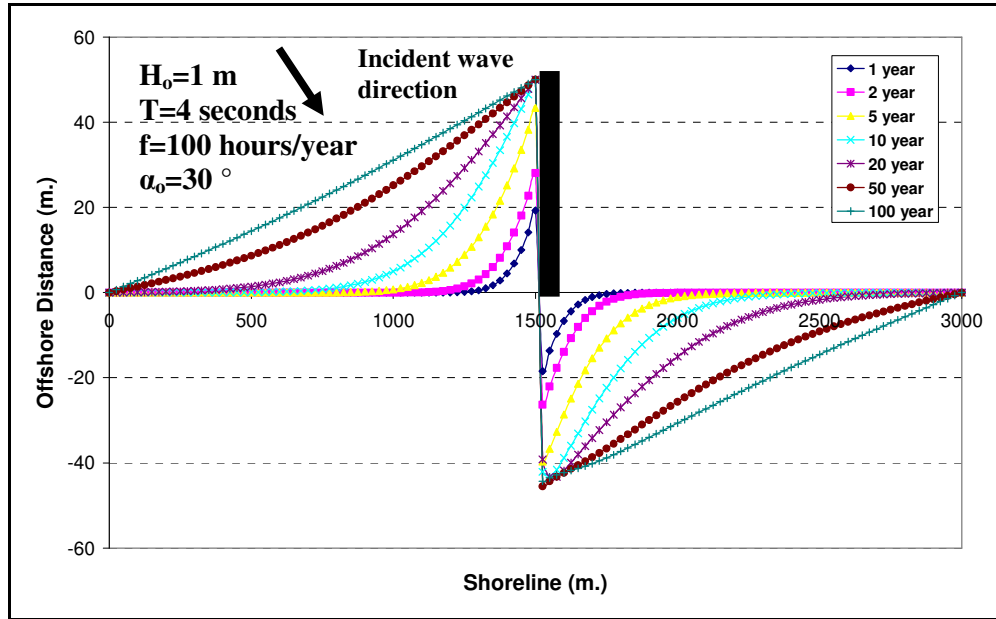


Figure 4.13 Bypassing around an Impermeable Groin at an Initially Straight Shoreline

Figure 4.13 is obtained for an impermeable groin of 50 m length in seaward direction which is at the middle of a 3000 m length shoreline for 1, 2, 5, 10 and 20 year repetitions. The wave data is illustrated in the corresponding figure. As observed from Figure 4.13, at both sides of the groin, erosion and accretion has a trend of increase and after some time, bypassing starts to occur and this trend is decreased at close regions of both sides of the groin. This decrease is due to fulfilled capacity of the groin to accrete at updrift side and erode at downdrift side.

4.6.1.2. Permeability

Groins usually permit some of the sediment to pass to its downdrift side through or over its body. The fraction of sand bypassing that is defined as sand transmission through or over the groin is denoted with a permeability factor, PERM in the numerical model. This transmission may occur due to porosity of the groin material or relative groin height with respect to the wave height or water level at a certain time. As one-line model assumption specifies that longshore

sediment transport is independent of the shoreline orientation, variations of the shoreline location close to the groin are strongly related to the permeability of the groin. Thus, the decline in sand accumulation at the updrift side of the groin is abated by decreasing the longshore sediment transport speeds and as a result decreasing the longshore transport rates at the updrift side of the groin (Hanson, 1987).

In order to check if a groin acts correctly when it is permeable, simulations are performed in CSIM for permeable groins and the results are illustrated in Figure 4.14;

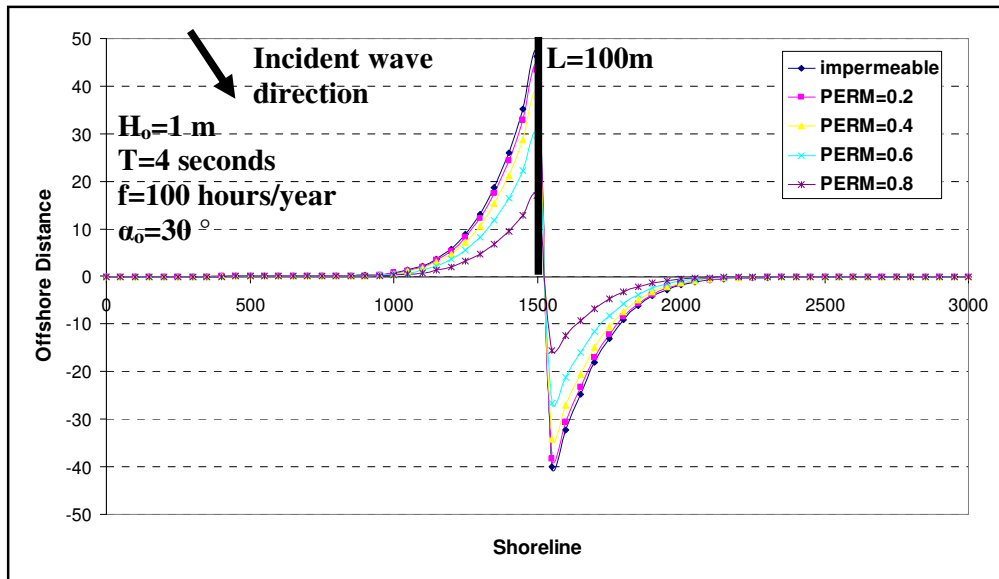


Figure 4.14 Effect of Permeability of a Single Groin (t=5 years)

During the simulation, a groin of 100 m length is placed at the middle of a 3000 m initially straight shoreline and 5 year simulations are performed concerning various permeability ratios for the groin. As seen in Figure 4.14, both accretion and erosion trends tend to decrease as permeability ratio (*PERM*) of the groin increase which is in agreement with the expected situation.

4.6.1.3. Combined Effect of Bypassing and Permeability

The effect of bypassing and permeability is designated together in the numerical model just like in GENESIS (Hanson, 1987), ONELINE (Dabees, 2000) and CSI (Şafak, Artagan, Baykal, 2006) by a single factor, PB;

$$PB = BYP + PERM(1 - BYP) \quad 4.22$$

In the implicit scheme, boundary conditions for a groin should be defined differently in terms of EE_G and FF_G depending on the direction of longshore sediment transport. For a negative transport direction setting $EE_G=PB$ and $FF_G=0$ at the groin location gives;

$$Q_G = PBQ_{G-1} \quad 4.23$$

and for a positive transport direction setting $EE_G=0$ and FF_G to

$$FF_G = \frac{PB(FF_{G-1})}{1 - PB(EE_{G-1})} \quad 4.24$$

following relation is obtained;

$$Q_G = PBQ_{G+1} \quad 4.25$$

where the subscript (G) denotes the longshore sediment transport at the updrift side of the groin, $G-1$ and $G+1$ denote the longshore sediment transport at the downdrift side of the groin respectively, depending on the direction of transport. It is understood from these conditions that the calculation cells at both sides of the groin are treated separately.

These corrections on longshore sediment transport rate, alone are not enough for accurate estimation of shoreline evolution at the updrift side of the groin. As diffraction significantly takes part in the processes at the sheltered zone of a groin, a modification on breaking wave angles and diffraction coefficients is fateful (Dabees, 2000) as;

$$K_{dP} = K_d(1 - PERM) + PERM \quad 4.26$$

$$\alpha_{dP} = \alpha_d(1 - PERM) + \alpha_b PERM \quad 4.27$$

where K_{dP} is the modified diffraction coefficient according to permeability and α_{dP} is the modified breaking wave angle according to permeability. These equations are derived by a rationale that for a totally permeable groin ($PERM=1$), corrections on diffraction results in a solution specifying that no diffraction occurs.

4.6.2. T-Groins

Groins are generally built perpendicular to the shoreline, but in some situations, an addition parallel or angled to the shoreline is designed at the seaward end of the groin (Figure 4.15). These structures are called T-groins or angled T-groins.

In the numerical model offshore distance of the shoreline-parallel part of a T-groin should be same as the length of the shoreline-perpendicular part of the T-groin. On the other hand, the symmetry of the shoreline-parallel part of T-groin with respect to shoreline-perpendicular part of T-groin does not have to be proper, meaning that groins may take an L shape from an aerial view. A new modification is performed on CSI which facilitate the user to define the offshore distances of the two tips of the shoreline-parallel part of the T-groin separately. Therefore, unlike in CSI, the shoreline-parallel part of a T-groin may be entered as an inclined offshore breakwater into the numerical model. Thus, in addition to T and

L shaped groins, angled T and L shaped groins can be specified and visualized in the numerical model is as in Figure 4.15.

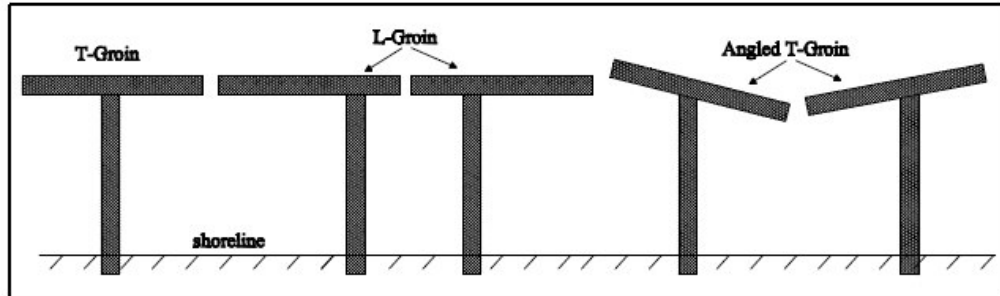


Figure 4.15 Types of Groins that can be Simulated with the Methodology Used for T-Groins

In the numerical model, two parts of the groin, shoreline-parallel and shoreline-perpendicular parts are separately inserted. Shoreline-perpendicular part is entered into the program manually as a normal I-shaped groin and the other part is introduced as an offshore breakwater. The shoreline-perpendicular part of a T-groin behaves as an impermeable groin which separates the two sides of the groin that lay behind the shoreline-parallel part. Therefore, the shoreline-parallel part of a T-groin, as it is entered as an offshore breakwater, works just like an offshore breakwater with a difference in diffraction calculations. That is as at some distance from the tip of the shoreline-parallel part of the T-groin waves encounter an impermeable groin (shoreline-perpendicular part of the T-groin), diffraction calculations and modifications are performed up to this point separately for both sides of the shoreline-perpendicular part of the T-groin (Figure 4.16). All the remaining calculations for an offshore breakwater are same for the shoreline-parallel part of the T-groin.

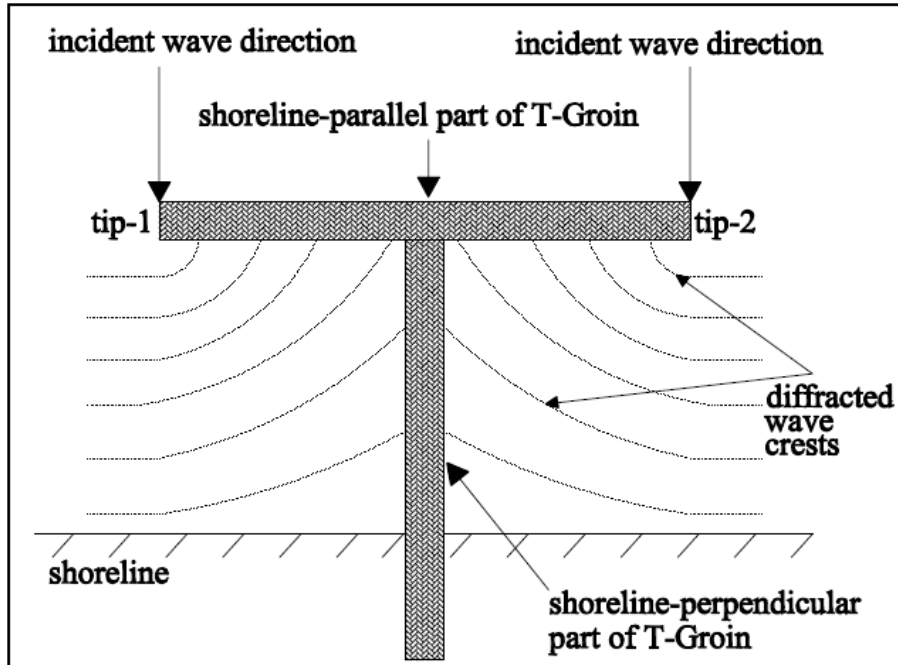


Figure 4.16 Diffraction Condition behind a T-Groin

In order to observe the impact of a T-groin on the shoreline, a sample model test is implemented. By using CSIM, a sample simulation is performed on an initially straight shoreline with a T-groin at the middle of the shoreline. The wave climate data, dimensions of T-groin and the obtained shoreline changes are illustrated in Figure 4.17.

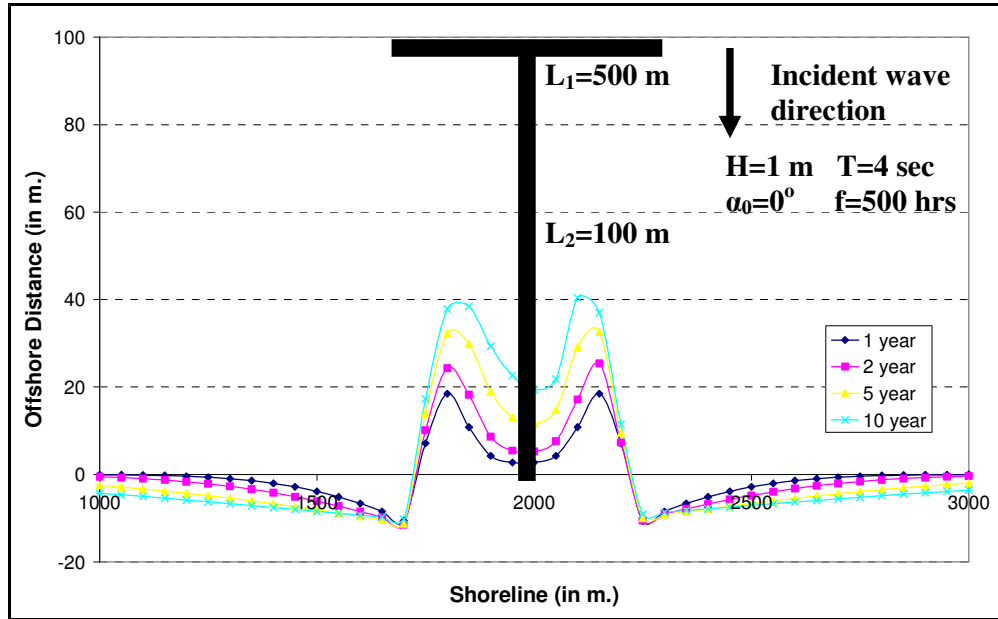


Figure 4.17 Shoreline Evolution in case of a Single T-groin

In Figure 4.17, it is observed that similar amount of accumulation occurs at both sides of shore-perpendicular part of T-groin as deep water incident wave direction is perpendicular to the shoreline. That is wave approach angle is 0° . The accumulation at these sides may vary according to changes in deep water wave approach angle.

4.6.3. Offshore Breakwaters

In the developed numerical model, the orientations of offshore breakwaters with respect to shoreline can be specified variously. In case of a permeable offshore breakwater, permeability corrections are performed on diffraction coefficients and finally, diffracted breaking wave heights are calculated using Eqn. 3.37 as in CSI.

In order to understand the shoreline response to an offshore breakwater, sample simulations are performed with a wave climate data that is composed of waves of 1 m significant wave height, 4 second significant wave period and 30° deep water

wave approach which occurs 100 hours in a year. An initially straight shoreline of 4000 m length is the sample shore and a 200 m offshore breakwater is placed in the middle of the shoreline and 200 m away from the shoreline in seaward direction and results are presented in Figure 4.18.

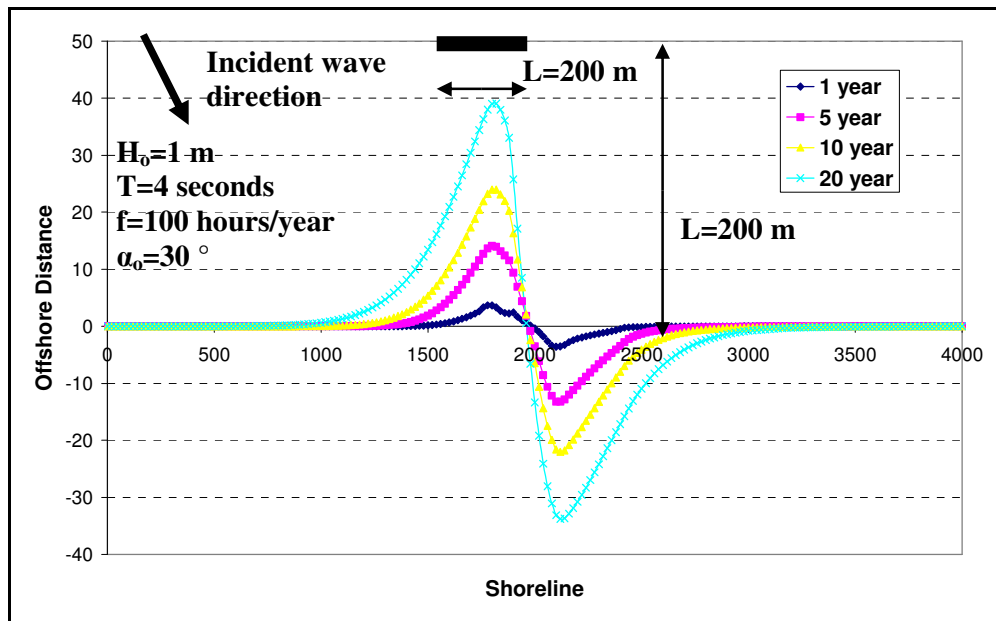


Figure 4.18 Shoreline Evolution of an Initially Straight Shoreline in case of an Offshore Breakwater

CHAPTER 5

A CASE STUDY

In this chapter, the developed numerical model, CSIM is applied as a case study in Bafra Delta, Black Sea coast of Turkey, for verification of the developed numerical model. Additionally, influence of wave data input, annual and seasonal wave data inputs and reference depth concept are discussed.

5.1. Problem at Case Study Area

Bafra Delta is the mouth of Kızılırmak River where it discharges into Black Sea (Figure 5.1). After the construction of several dams on Kızılırmak River, the amount of sediment budget carried to Bafra Delta is reduced which results in erosion up to 30 m per year at the region. A shore protection system was necessary to prevent the erosion at the site. Therefore, 2 Y-shaped groins and 1 I-shaped groin are constructed very close to river mouth (Figure 5.2) (Kökçinar et al., 2005). However, chronic erosion is not prevented totally and only shifted to the eastern part of the previously eroded shore. Hence, a series of additional groins at the eastern part of the previously constructed I-shaped groin and a groin at the western part of Y-shaped groins are added to the existing system in 2003. During these stages, in order to monitor the shoreline evolution, shoreline measurements are taken at several times. The shoreline measurements in April 1999 (Figure 5.2), in January 2003 and in February 2007 (Figure 5.3) are obtained from General Directorate of State Hydraulic Works (DSI).

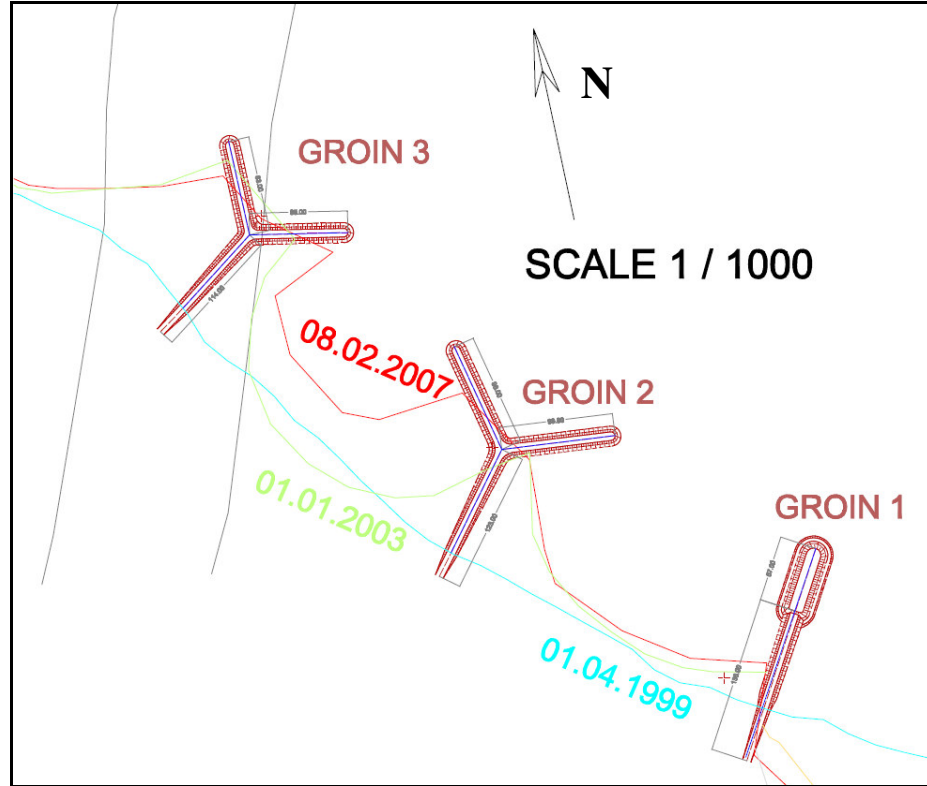


Figure 5.3 Layout of Groins and Measured Shoreline Coordinates in 1999, 2003 and 2007 at Bafra Delta (February, 2007)

5.2. Wave Hindcasting

In order to apply the numerical model to this case study, the wave regime of the region should be obtained. Measured local wind data of Sinop Region which contains the meteorological data of 40 years between 1966 and 2006 is obtained from General Directorate of Meteorological Affairs. The fetch distance studies are performed in order to understand the effective wave approach directions of the region (Şafak, 2006). These directions lay between West-North-West (WNW) to East-South-East (ESE) (Figure 5.4). Additionally, after the analysis of the wind data, it is understood that West (W) direction is also effective at the region.

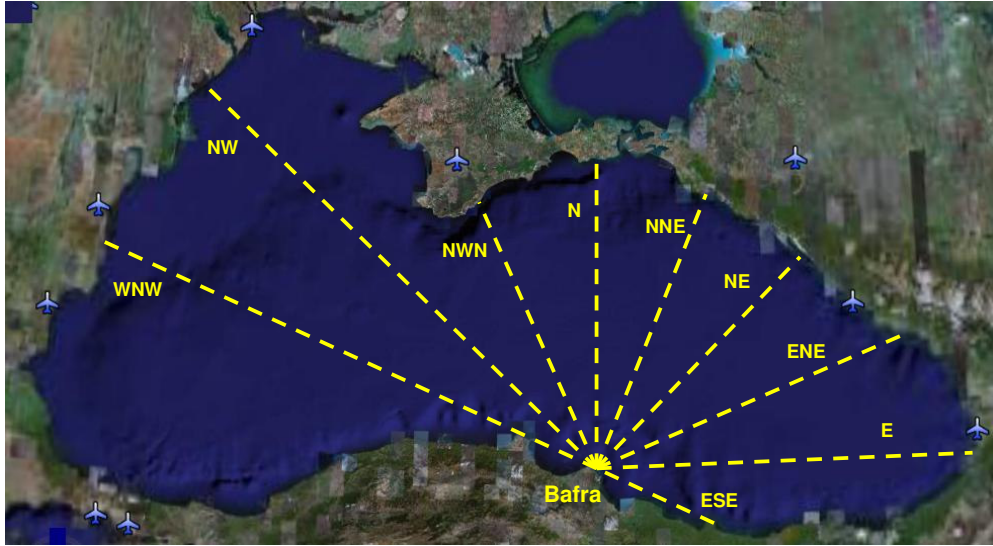


Figure 5.4 Fetch Distances for Bafra Region

During wind data analysis, average wind data sets are converted to independent storms considering that storm condition is achieved if wind velocity is greater than 3 m/sec. These elected storm data and fetch distances for each direction are used to obtain log-linear annual probability equations for each direction (Table 5.1). These annual probability equations are also illustrated in Figure 5.5 and Figure 5.6.

Table 5.1 Effective Fetch Distances and Probability Equations for Effective Wave Directions

Direction	Effective Fetch Distance (km)	Log-Linear Probability Equation
W	388	$H_s = -0.577181 \cdot \ln[Q(>H_s)] + (-0.859472)$
WNW	617	$H_s = -0.558200 \cdot \ln[Q(>H_s)] + (-1.464985)$
NW	502	$H_s = -0.358501 \cdot \ln[Q(>H_s)] + (-0.423128)$
NNW	373	$H_s = -0.452198 \cdot \ln[Q(>H_s)] + (-1.097526)$
N	330	$H_s = -0.718634 \cdot \ln[Q(>H_s)] + (-0.772767)$
NNE	331	$H_s = -0.887583 \cdot \ln[Q(>H_s)] + (-3.119386)$
NE	333	$H_s = -0.872248 \cdot \ln[Q(>H_s)] + (0.108211)$
ENE	382	$H_s = -0.847995 \cdot \ln[Q(>H_s)] + (-0.487093)$
E	349	$H_s = -0.732358 \cdot \ln[Q(>H_s)] + (-0.559060)$
ESE	282	$H_s = -1.103443 \cdot \ln[Q(>H_s)] + (-3.235475)$

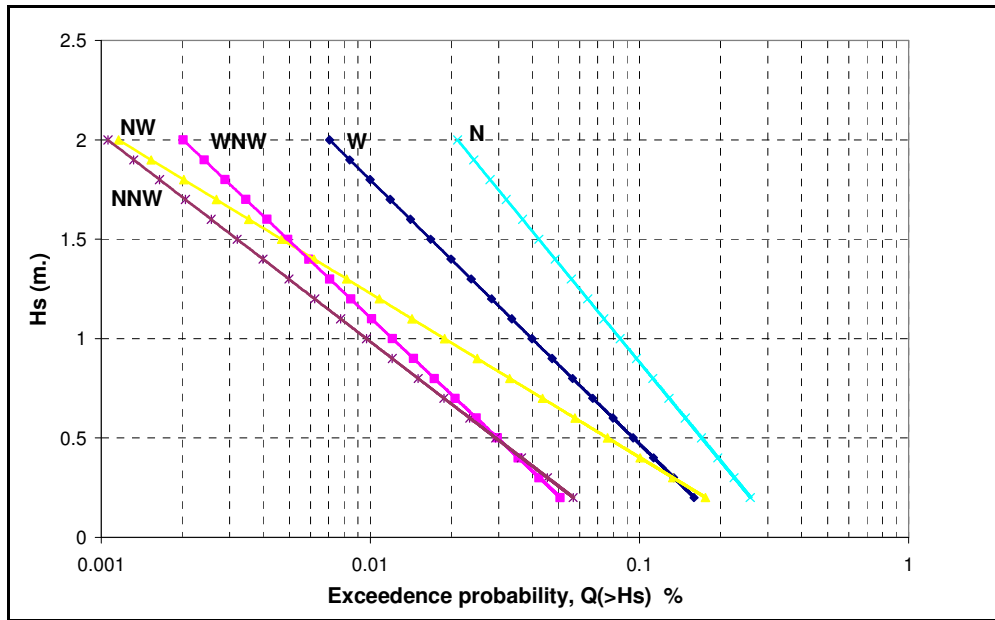


Figure 5.5 Probability Distributions of Deep Water Significant Wave Height for Directions, W to N

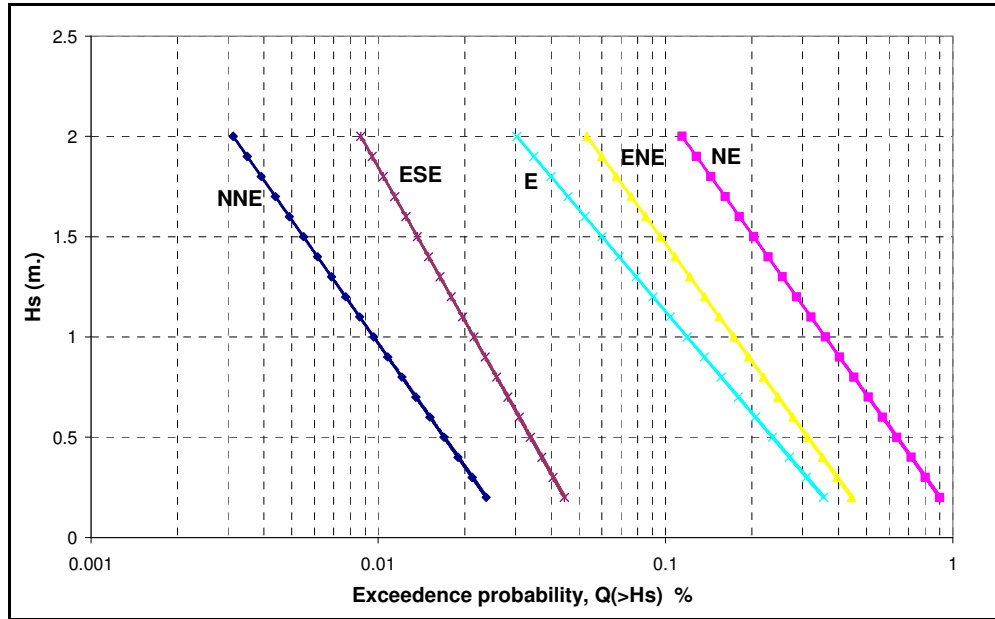


Figure 5.6 Probability Distributions of Deep Water Significant Wave Height for Directions, NNE to ESE

5.3. Model Wave Data

The wave data input is composed of a matrix with 4 columns which represent significant wave height, significant wave period, frequency and deep water approach angle, respectively. If more than one direction is effective, for each direction, wave data that contains above parameters added to the wave data input.

As wave data input represents the wave climate of the case study region, one of the critical points about wave data input is the decision on sequence of wave data input (frequencies, wave heights, wave approach angles) should be introduced to the numerical model. This is crucial issue because the response of the coastal system is strongly non-linear and unpredictable. Şafak's (2006) studies showed that the sequence of wave data input does not affect the shoreline evolution significantly. Therefore, case study simulations with CSIM at Bafra Delta are performed with annual wave data input starting from ESE to W as in Table 5.2.

Table 5.2 Average Annual Deep Water Wave Heights, Corresponding Periods and Annual Exceeding Frequencies at Bafra Delta

Direction	H (m.)	T (sec.)	f (hrs.)
W	1.36	4.63	56.31
WNW	1.35	4.61	2119.41
NW	1.32	4.57	1037.02
NNW	1.21	4.37	781.83
N	1.57	4.98	112.31
NNE	1.06	4.10	313.44
NE	1.05	4.06	97.67
ENE	0.87	3.70	241.18
E	0.95	3.87	95.23
ESE	1.20	4.35	564.82

Wave data input may be composed of annual or seasonal wave data sets. Güler et al. (1998) showed that the difference between shoreline evolution attained by annual and seasonal wave data sets is not significant. In the present case study, in order to understand the effect of these data sets at case study area, seasonal and annual wave data sets are obtained for Bafra Region and simulations are implemented by using these wave data inputs (Appendix B). Additionally, annual and seasonal wave data inputs of waves approaching from reference depth are also illustrated in Appendix (Appendix B).

In the numerical model, waves with higher frequencies are decided to be used which is the case specified by Şafak (2006). Therefore, as previously mentioned the shoreline evolution is determined by more often observed storms rather than severe storms with less frequency which is the assumptions of one-line numerical models. Thus, significant wave heights are determined using;

$$H_o = \frac{\sum(P_i H_i)}{\sum P_i} \quad 5.1$$

where H_i and P_i represent wave height and occurrence probability of waves with height of H_i (Güler et al., 1998).

Moreover, significant wave heights and the relations between significant wave periods and significant wave heights are derived using this method. Finally wave data sets which contain average significant wave heights, significant wave periods and annual occurrence frequencies for each direction are obtained by performing long term wave statistics. These wave data sets are one of the main inputs of the numerical model in the case study. In the application, annual deep water wave data transformed to a reference depth and the corresponding wave data input is given in Table 5.3. The values in Table 5.3 represent the annual deep water significant wave characteristics.

Table 5.3 Average Annual Reference Depth Wave Heights, Corresponding Periods and Annual Exceeding Frequencies at Bafra Delta

Direction	H (m.)	T (sec.)	f (hrs.)
W	0.68	4.63	56.31
WNW	0.86	4.61	2119.41
NW	1.11	4.57	1037.02
NNW	1.14	4.37	781.83
N	1.48	4.98	112.31
NNE	0.96	4.10	313.44
NE	0.92	4.06	97.67
ENE	0.79	3.70	241.18
E	0.85	3.87	95.23
ESE	0.94	4.35	564.82

Along with wave data sets that are composed of ten directions, wave data sets which involve two representative wave directions one of which is defined for W, WNW, NW and NNW directions and the other for N, NNE, NE, ENE, E and ESE directions are implemented in the developed numerical model for comparison of these methods (Table 5.4).

Table 5.4 Average Annual Reference Depth Wave Heights, Corresponding Periods and Annual Exceeding Frequencies for Representative Waves at Bafra Delta

Direction	H (m.)	T (sec.)	f (hrs.)
Representative Wave 1	0.91	4.11	1312.33
Representative Wave 2	0.99	4.56	4106.88

The wave data of representative wave characteristics in Table 5.4 is achieved by performing the following equations;

$$H_r = \frac{\sum H_i f_i}{\sum f_i} \quad 5.1$$

$$T_r = \frac{\sum T_i f_i}{\sum f_i} \quad 5.2$$

$$f_r = \sum f_i \quad 5.3$$

where H_r , T_r and f_r are the representative wave height, representative wave period and representative frequency, respectively and H_i , T_i and f_i are the wave height, wave period and frequency of waves from each direction, respectively.

Case study simulations are performed with 4 year repetition. With the wave data available in Table 5.2, Table 5.3 and Table 5.4, wave data input alternatives are summarized in Table 5.5.

Table 5.5 Applied Wave Data Input Methods at the Case Study for Bafra Delta

Input Method	Wave Directions	Annual / Seasonal Wave Data	Deep Water / Reference Depth
1	Representative Waves	Annual	Deep Water
2	Representative Waves	Seasonal	Deep Water
3	Representative Waves	Annual	Reference Depth
4	Representative Waves	Seasonal	Reference Depth

5.4. Case Study Simulation Results and Discussions

In the case study simulations, Y-groins are given as inclined T-groins concerning that behavior of Y-groins may not be achieved successfully within the numerical model. Besides, as representative waves and all effective waves are supposed to give same evolution results, at the first stage of case study studies, annual and seasonal wave data of representative waves are implemented for simulations at the case study area. All the simulation results are compared with measured field data. For comparison of annual and seasonal wave data input, sample simulations are performed with Inputs 1 and 2 and Inputs 3 and 4, respectively and the obtained results are illustrated in Figure 5.7 and Figure 5.8.

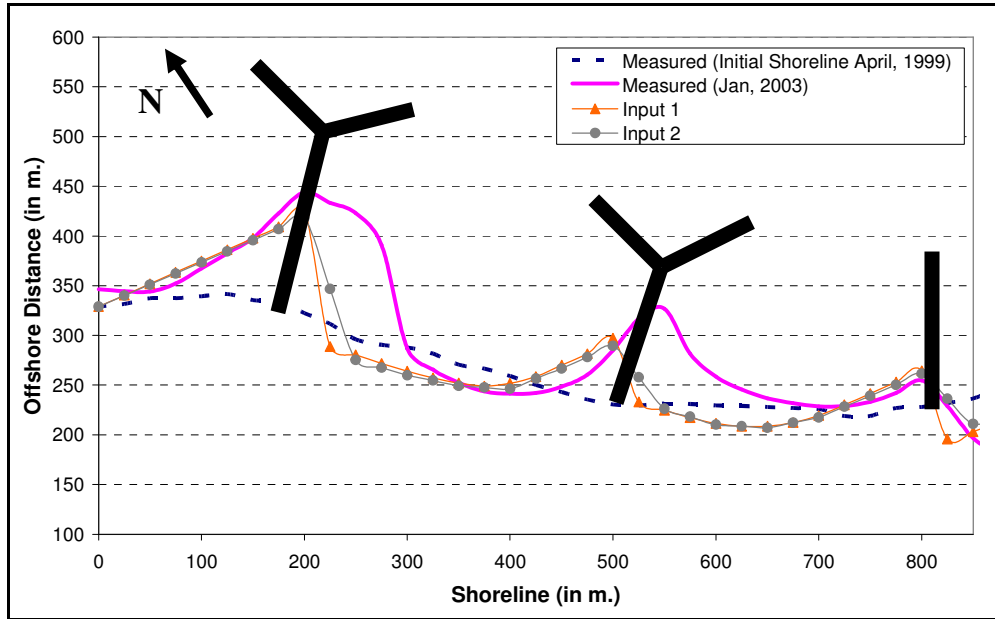


Figure 5.7 4 Year Simulation Results of Shoreline Evolution under Annual and Seasonal Wave Data Input Methods (Input 1 and Input 2)

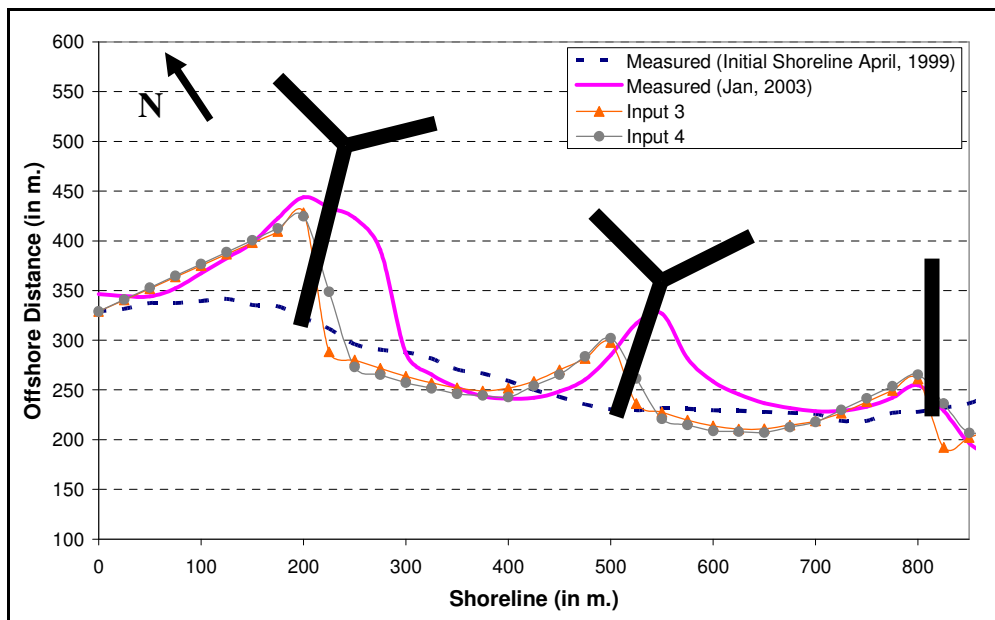


Figure 5.8 4 Year Simulation Results of Shoreline Evolution under Annual and Seasonal Wave Data Input Methods (Input 3 and Input 4)

In Figure 5.7 and Figure 5.8, it is derived that both approaches lead almost the same shoreline change and the trend of shoreline evolution is reached for most of the shoreline especially for the left side of groins where accretion is observed. Therefore, it is understood that it does not change the shoreline evolution whether to implement annual or seasonal wave data inputs.

In order to understand the effect of waves approaching from a reference depth and waves approaching from deep water, sample simulations are performed with all wave data inputs that are mentioned previously. Figure 5.9 and Figure 5.10 are obtained with the results of simulations that are performed with Inputs 1 and 3 and Inputs 2 and 4, respectively.

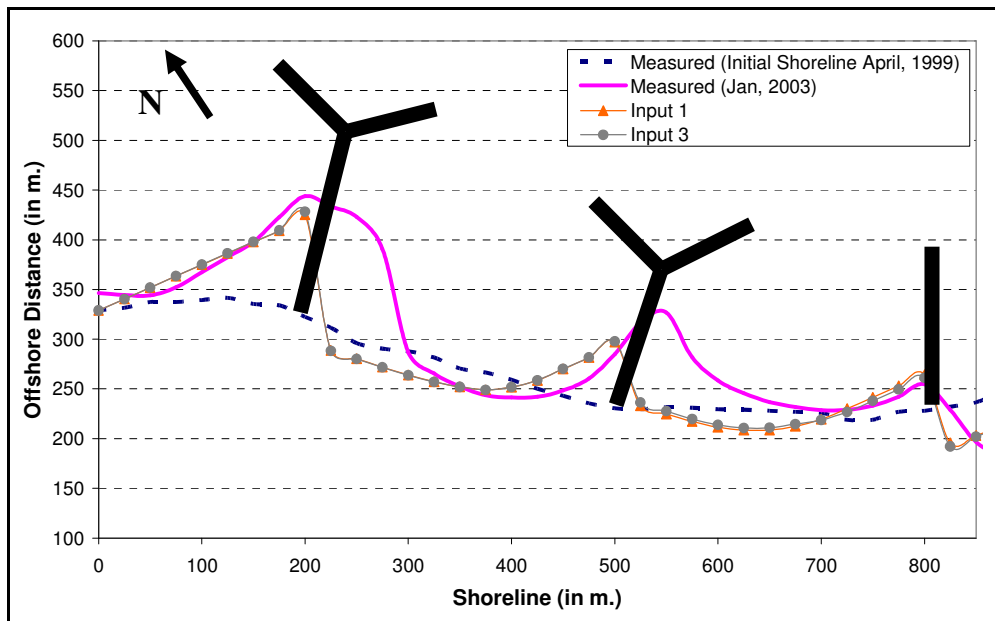


Figure 5.9 4 Year Simulation Results of Shoreline Evolution under Wave Data Input Methods of Deep Water and Reference Depth (Input 1 and Input 3)

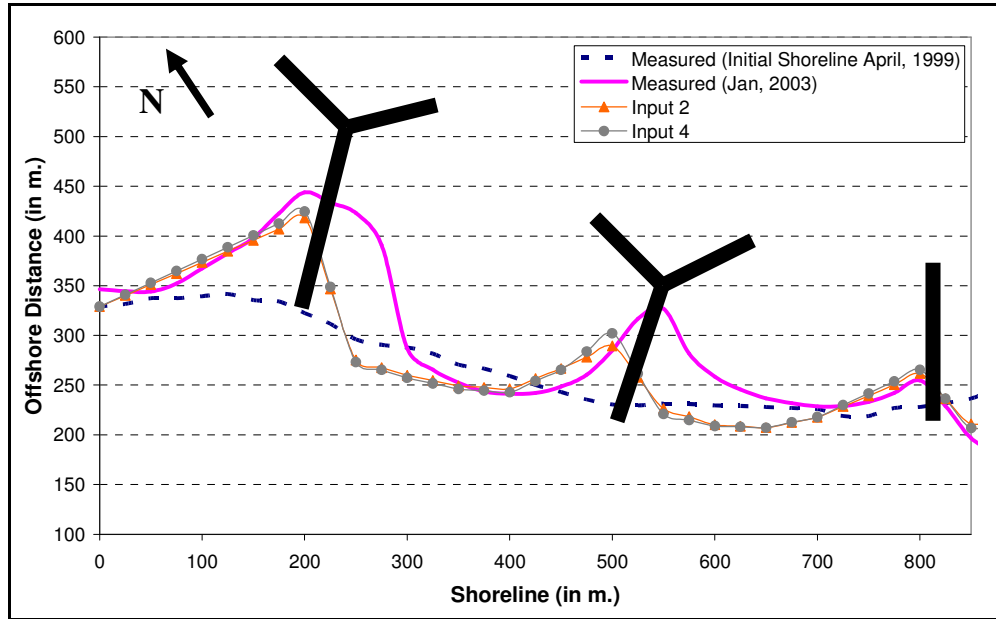


Figure 5.10 4 Year Simulation Results of Shoreline Evolution under Deep Water and Reference Depth Wave Data Input Methods (Input 2 and Input 4)

As observed from Figure 5.9 and 5.10, the outcomes of 4 year simulations that are performed with inputs 1 and 3 and inputs 2 and 4 are very similar to each other. Moreover, the trend of shoreline change is achieved in these simulations especially for locations where accretion occurs due to groins. Therefore, it may be concluded that using annual or seasonal wave data inputs do not affect the shoreline evolution processes significantly.

Obtained shoreline evolution results with all wave data input methods are shown in Figure 5.11.

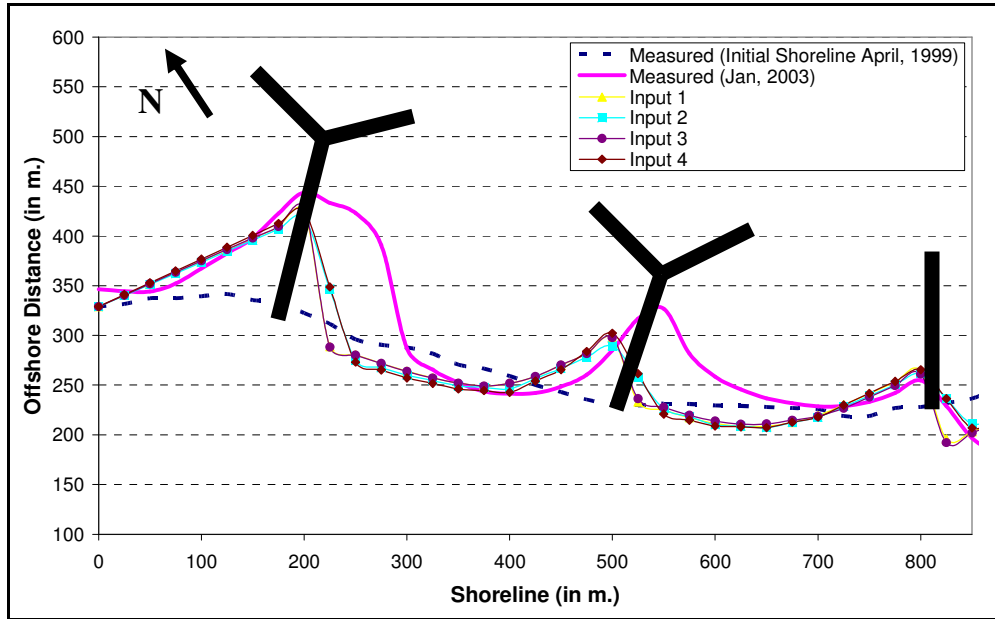


Figure 5.11 4 Year Simulation Results of Shoreline Evolution under All Wave Data Input Methods

It may be derived from Figure 5.11 that performing simulations with waves approaching from deep water or reference depth or using annual and seasonal wave data sets do not change the shoreline evolution results significantly. It is observed from Figure 5.11 that simulation performed with all wave data inputs give almost the same result for most of the shore while preserving the shoreline evolution trend for most of the shoreline when compared to the measured field data. However, at several locations at the shoreline, amount of accretion is not attained especially for both sides of second Y-groin and between two Y-groins. That is due to the complexity of the shoreline and too closely constructed structures which complicate the diffraction coefficient calculations and hence shoreline evolution processes and the slight difference in behaviors of inclined T-groins which is implemented in the case study simulations and Y-groins which is the actual groin types at the case study area.

At final stage, simulation results of explicit numerical model, CSI and implicit numerical model, CSIM are illustrated in Figure 5.12. Both simulations with CSI and CSIM are performed with input method 1 which is chosen arbitrarily.

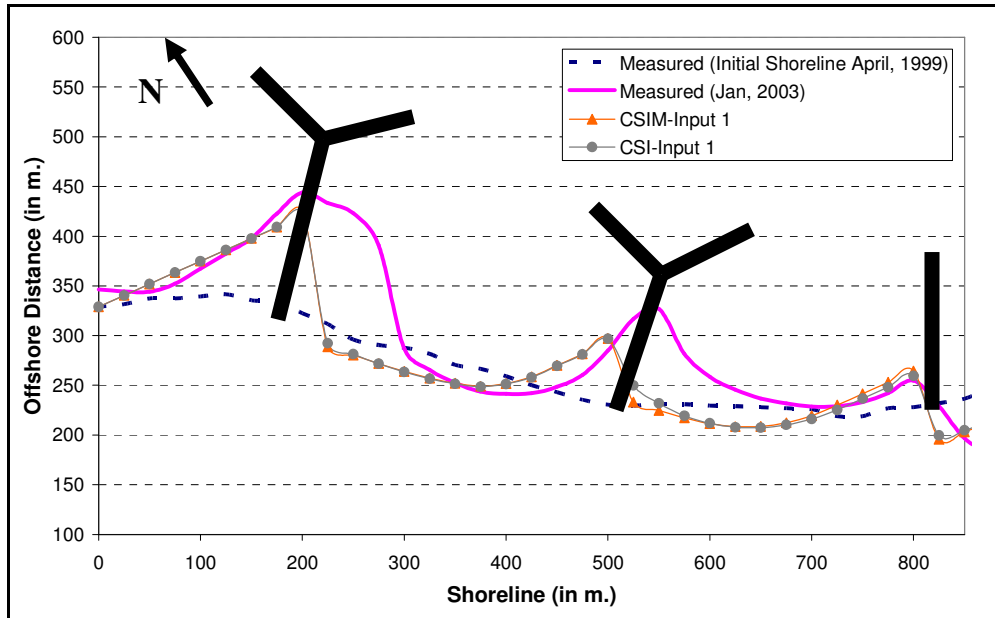


Figure 5.12 4 Year Simulation Results of Shoreline Evolution of CSI and CSIM with Input 1

It is seen in Figure 5.12 that CSI and CSIM compute similar shoreline evolution results even though CSI is an explicit numerical model in which Kamphuis's longshore transport rate equation is utilized and CSIM is an implicit numerical model in which CERC equation is used. As a result of all comparisons that are performed with aforementioned wave data input methods it is emerged that implementing reference depth wave data inputs and deep water wave data inputs or using annual and seasonal wave data inputs in the numerical model do not change the shoreline results significantly. Besides, all simulations that are performed with all wave data input methods lead close shoreline evolution results for accretion at the left side of groins. At several locations, shoreline trend is

achieved but the accumulation amount remained very low compared to the measured field data. This is due to the slight difference in behavior of Y-groins and T-groins, assumptions in the numerical model, small errors in the measured field data and difficulty in definition and simulation of longshore transportation processes at shores where structures are constructed too closely.

CHAPTER 6

CONCLUSION

The aim of this study was to contribute to understanding nearshore processes and provide better ways of simulating the relation between coastal structures and nearshore processes and to fill the blanks of remaining unknowns in longshore sediment transportation concept. For this purpose, an implicit one-line numerical model is developed by modifying the basis of the explicit numerical model, CSI (Şafak, 2006, Artagan, 2006 and Baykal, 2006). These modifications are;

- changes in diffraction calculations at the sheltered zones of groins and offshore breakwaters
- implementing new sediment scale parameter equations (A_p)
- definition of inclined T-groins and L-groins
- new diffraction coefficient calculation approaches which are for offshore breakwaters using vectorial summation of the diffraction coefficients at their sheltered zones and as for T-groins calculating the shoreline changes separately at two sides of the structure by defining the shore-perpendicular part as a boundary

Longshore sediment transport rate, CERC equation is utilized within the developed numerical model. In the development of the model, breaking wave height changes along the shoreline ($\partial H_b / \partial x$) in CERC equation is neglected based on the assumption that it is small and less effective on determination of longshore transport rate compared to breaking wave angles (Hanson and Kraus, 1989).

Execution times and stability ratios of the numerical model are compared with the execution times and stability ratios obtained by CSI, and it is seen that the implicit numerical model is faster than the explicit numerical model and the stability numbers are comparable with CSI.

In the numerical model simulations all wave data inputs are prepared according to representative wave directions. Using representative wave directions in seasonal and annual wave data sets is appropriate for practical purposes. Besides, in the numerical model, reference depth concept is implemented where wave data sets are transformed to a chosen reference depth within the model wave data. As representative wave data, annual and seasonal waves are implemented as input data and it is found that there is no significant difference in results.

Sample simulations are performed by implementing different shaped groins such as I-shaped groins, T-groins and offshore breakwaters to an initially straight shoreline. T-groins which cause complicated nearshore processes especially at both sides of shore-perpendicular part of T-groins are difficult to implement in the numerical model.

Finally, in order to verify the numerical model's applicability, a case study at Bafra Delta is performed. Before the application of case study simulations, local wind data is analyzed and wave climate of the region is obtained for numerical model simulations. By obtaining two representative waves for the wave data, using annual and seasonal wave data, deep water wave data and wave data for the chosen reference depth which is 5 meters for the case study area, several sample simulations are performed and these input methods are compared with each other and with the measured field data. Consequently, it is seen that, numerical model results are in good agreement qualitatively with the measured field data for all wave data input methods.

For future studies, even though permeability is not a popular study area for groins, the combined effect of permeability and bypassing of groins should be studied in

detail especially for verification of the numerical model results with laboratory measurements in order to successfully adapt their impacts in the numerical models.

Moreover, even though many modifications are performed in the numerical model, case study simulations show that numerical model has some difficulties in various conditions such as lack of achieving parabolic formations between two groins. In case of closely constructed groins, simulating parabol like shoreline formations would not be achieved yet due to the complicated pattern of diffraction and breaking within the overlapped shadow regions of the structures. This situation should be handled with the future studies. In addition, tombolo formations behind offshore breakwaters remain as an unsolved problem. Future studies may be performed on these conditions.

One-line numerical models are the first step in a long journey which leads to building up of a two-line numerical model and finally to the development of n-line numerical model. In case of shores which are strongly affected by cross-shore sediment transportation and by severe storms with less occurrence probabilities, shoreline change models must be upgraded to take into consideration especially cross-shore sediment transport.

In conclusion, coastal erosion is a major problem along the coasts especially in case of human interference by constructing coastal structures. To protect the eroded coastal areas, hard structures were used in the past as the most common remedial measures. However, with the new concept of “work with nature”, the applicability and effectiveness of nature-friendly measures such as beach nourishment, geotextile tubes and gabion units are introduced. Moreover, before decision of constructing any hard structure is given, a detailed and thorough study is absolutely necessary in order to understand the consequences after installation and if necessary, numerical models and laboratory experiments should be implemented in order to predict the possible long term shoreline changes. Together with giving the utmost care on the preservation of nature, concerning the

optimum solution to the problem, availability of the resources at the region and monitoring the shoreline changes periodically in order to take any possible future measures at necessary times, the aforementioned steps are crucial in order to come up with successful measures to shoreline problems. Consequently, numerical models can be used as a tool to simulate the probable shoreline changes reflecting the coast-structure interaction.

REFERENCES

- Artagan, S.S., (2006), “A One-Line Numerical Model for Shoreline Evolution under the Interaction of Wind Waves and Offshore Breakwaters”, M.S. Thesis, METU, Ankara, Turkey
- Bakker, W.T., (1969), “The Dynamics of a Coast with a Groyne System”, Proceedings of 11th Coastal Engineering Conference, ASCE, pp. 492-517.
- Bakker, W.T., Klein Breteler, E.H.J., and Roos, A., (1970), “The Dynamics of a Coast with a Groyne System”, Proceedings of the 11th Conference on Coastal Engineering, ASCE, pp. 1001-1020.
- Baykal, C., (2006), “Numerical Modeling of Wave Diffraction in One-Dimensional Shoreline Change Model”, M.S. Thesis, METU, Ankara, Turkey
- Bruun, P. (1954), “Coast Erosion and the Development of Beach Profiles”, TM-44, US Army Corps of Engineers, Beach Erosion Board
- CEM (Coastal Engineering Manual), (2003), U.S. Army Corps of Engineers, Coastal Engineering Research Center, U.S. Government Printing Office
- Cooper, J.A.G., and Pilkey, O.H., (2004), “Alternatives to the Mathematical Modeling of Beaches”, Journal of Coastal Research, Volume 20, No. 3, pp. 641-644.
- Crank, J., (1975), “The Mathematics of Diffusion”, 2nd edition, Clarendon Press, Oxford, England

Dabees, M.A., (2000), "Efficient Modeling of Beach Evolution", PhD Thesis, Queen's University, Canada, 174 pp

Dean, R.G., (1977), "Equilibrium Beach Profiles: U.S. Atlantic and Gulf Coasts", Department of Civil Engineering, Ocean Engineering Report No. 12, University of Delaware, Newark, Delaware.

Dean, R.G., and Yoo, C.H., (1992), "Beach-Nourishment Performance Predictions", Journal of Waterway, Port, Coastal and Ocean Engineering, Volume 118, No.6, pp. 567-585.

Del Valle, R., Medina, R., and Losada, M.A., (1993), "Dependence of Coefficient K on Grain Size", Technical Note No. 3062, Journal of Waterway, Port, Coastal and Ocean Engineering, Vol. 119, No. 5, pp. 567-574.

Goda, Y., (1985), "Random Seas and Design of Maritime Structures", University of Tokyo Press.

Güler, I., Ergin, A., and Yalçiner, A.C., (1998), "The Effect of the Use of Wave Data for the Numerical Solution of Shoreline Evolution", Journal of Coastal Research, Special Issue No. 26, pp. 195-200

Hallermeier, R.J., (1978), "Uses of a Calculated Limit Depth to Beach Erosion", Proceedings of the 16th Coastal Engineering Conference, American Society of Civil Engineers, New York, NY, pp. 1493-1512.

Hanson, H., (1987), "GENESIS: A Generalized Shoreline Change Numerical Model for Engineering Use", Ph.D. Thesis, University of Lund, Lund, Sweden

Hanson, H., and Kraus, N.C., (1986), "Forecast of Shoreline Change Behind Multiple Coastal Structures", Journal of Coastal Research, Vol. 5, No. 1, pp. 1-27.

Hanson, H., and Kraus, N.C., (1989), "GENESIS: Generalized Model for Simulating Shoreline Change", Technical Report CERC-89-19, Report 2 of a Series, Workbook and User's Manual, U.S. Army Corps of Engineers, Waterways Experiment Station, Vicksburg, MS, USA.

Hanson, H., and Kraus, N.C., (1993), "Optimization of Beach Fill Transitions", Beach Nourishment Engineering and Management Considerations-Proceedings of Coastal Zone '93, pp. 103-117, ASCE, New York

Hanson, H., and Larson, M., (1987), "Comparison of Analytic and Numerical Solutions of the One-Line Model of Shoreline Change", Proceedings of Coastal Sediments '87, ASCE, pp. 500-514.

Hulsbergen, C.H., Bakker, W.T., and van Bochove, G., (1976), "Experimental Verification of Groyne Theory", Proceedings of the 15th Conference on Coastal Engineering, ASCE, 1976, pp. 1439-1458.

Kamphuis, J.W., (1991), "Alongshore Sediment Transport Rate", Journal of Waterway, Port, Coastal and Ocean Engineering, ASCE, Volume 117, pp. 624-640.

Kamphuis, J.W., (2000), "Introduction to Coastal Engineering and Management", World Scientific, Singapore-New Jersey-London-Canada

King, D.B., (2005), "Influence of Grain Size on Sediment Transport Rates with Emphasis on the Total Longshore Rate", U.S. Army Corps of Engineers, 24 pp.

Komar, P.D., (1977), "Beach Sand Transport: Distribution and Total Drift", Journal of Waterway, Port, Coastal and Ocean Engineering Division, American Society of Civil Engineers, Vol. 103, pp. 225-239.

Komar, P.D., (1988), “Environmental Controls on Littoral Sand Transport”, Proceedings of 21st Coastal Engineering Conference, ASCE, pp. 1238-1252.

Komar, P.D., and Inman, D.L., (1970), “Longshore Sand Transport on Beaches”, Journal of Geophysical Research, Vol. 75, No. 30, pp. 5914-5927.

Kökpınar, M.A., Darama, Y., and Güler, I., (2007), “Physical and Numerical Modeling of Shoreline Evolution of the Kızılırmak River Mouth, Turkey”, Journal of Coastal Research, Volume 21

Kraus, N.C., (1983), “Applications of Shoreline Prediction Model”, Proceedings of Coastal Structures 83, American Society of Civil Engineers, pp. 632-645.

Kraus, N.C., (1984), “Estimate of Breaking Wave Height Behind Structures”, Journal of Waterway, Port, Coastal, and Ocean Engineering”, ASCE, Vol. 110, No. 2, pp.276-282.

Kraus, N.C., Isobe, M., Igarashi, H., Sasaki, T.O., and Horikawa, K., (1982), “Field Experiments on Longshore Transport in the Surf Zone”, Proceedings of 18th International Conference on Coastal Engineering, ASCE, New York, pp. 969-988.

Kraus, N.C., and Harikai, S., (1983), “Numerical Model of the Shoreline Change at Oarai Beach”, Coastal Engineering, Vol. 7, No. 1, pp. 1-28.

Kraus, N.C., Hanson, H., and Harikai, S., (1985), “Shoreline Change at Oarai Beach – Past, Present and Future”, Proceedings of 19th Coastal Engineering Conference, ASCE, pp. 2107-2123.

Kraus, N.C., Hanson, H., Scheffner, N.W., Chou, L.W., Cialone, M.A., Smith, J.M., and Hardy, T.A., (1986), “Coastal Processes at Sea Bright to Ocean

Township, New Jersey”, Unpublished Draft Report, US Army Engineer, Waterways Experiment Station, Coastal Engineering Research Center

Kriebel, D.L., and Dean, R.G., (1985), “Numerical Simulation of Time-Dependent Beach and Dune Erosion”, Coastal Engineering, Vol. 9, pp. 221-245.

Larson, M., Hanson, H., and Kraus, N.C., (1987), “Analytical Solutions of the One-Line Model of Shoreline Change”, Technical Report CERC-87, U.S. Army of Engineer Waterways Experiment Station, Coastal Engineering Research Center.

Le Mehaute, B., and Soldate, M., (1978), “Mathematical Modeling of Shoreline Evolution”, Tetra Tech Report No. TC-831, Tetra Tech, Inc., Pasadena, CA.

Le Mehaute, B. and Soldate, M., (1980), “A Numerical Model for Predicting Shoreline Changes”, Miscellaneous Report 80-6, U.S. Army Corps of Engineers, Fort Belvoir, Coastal Engineering Research Center, 72 pp.

Mimura, N., Shimizu, T., and Horikawa, K., (1983), “Laboratory Study on the Influence of Detached Breakwater on Coastal Change”, Proceedings of Coastal Structures '83, ASCE, pp. 740-752.

Munk, W.H., (1949), “The Solitary Wave Theory and its Application to Surf Problems”, Symposium on Gravity Waves, Circular No. 521, National Bureau of Standards, Washington D.C., pp. 376-462.

Ozasa, H., and Brampton, A.H., (1980), “Models for Predicting the Shoreline Evolution of Beaches Backed by Seawalls”, Report, Hydraulics Research Station, Wallingford.

Pelnard-Considere, R., (1956), "Essai de Theorie de l'Evolution des Forms de Rivage en Plage de Sable et de Galets", 4th Journees de l'Hydraulique, Les Energies de la Mer, Question III, Rapport No. 1, pp. 289-298.

Perlin, M., (1979), "Predicting Beach Planforms in the Lee of a Breakwater", Proceedings of Coastal Structures '79, ASCE, pp. 792-808.

Perlin, M. and Dean R.G., (1978), "Prediction of Beach Planforms with Littoral Controls", Proceedings of 16th Coastal Engineering Conference, ASCE, pp. 1818-1838.

Phillips, M.R., and Jones, A.L., (2005), "Erosion and Tourism Infrastructure in the Coastal Zone: Problems, Consequences and Management", Tourism Management, Vol.27, pp. 527-524.

Price, W.A., Tomlinson, D.W., and Willis, D.H., (1973), "Predicting Changes in the Plan Shape of Beaches", Proceedings of 13th Coastal Engineering Conference, ASCE, pp. 1321-1329.

Ravens, T.M., and Sitanggang, K.I., (2005), "Numerical Modeling and Analysis of Shoreline Change on Galveston Island", Journal of Coastal Research, Volume 22, No. 0, pp. 160-171.

Requejo, S., Gonzalez, M., and Medina, R., (2003), "Breaking Wave Characteristics Behind a Breakwater", Coastal Sediments 2003

Roelvink, J.A., and Broker, I., (1993), "Cross-shore Profile Models", Coastal Engineering, Volume 21, pp. 163-191

Shore Protection Manual (SPM), (1984), U.S. Government Printing Office, Washington D.C.

SOPAC, Pacific Islands Applied Geoscience Commission, South Pacific Sea Level and Climate Monitoring Project, (1991)

Swart, D.H., (1976), "Predictive Equations Regarding Coastal Transports", Proceedings of 15th Coastal Engineering Conference, ASCS, pp. 1113-1132

Şafak, I., (2006), "Numerical Modeling of Longshore Sediment Transport", M.S. Thesis, METU, Ankara, Turkey

Thieler, E.R., Pilkey, O.H., Young, R.S., Bush, D.M., and Chai, F., (2000), "The Use of Mathematical Models to Predict Beach Behavior for U.S. Coastal Engineering: A Critical Review", Journal of Coastal Research, Volume 16, No.1, pp. 48-70.

Vafaei, A.R., (1992), "Mathematical Modeling of Shoreline Evolution in the Vicinity of Coastal Structures", M.S. Thesis, METU, Ankara, Turkey

Willis, D.H., (1977), "Evaluation of Alongshore Transport Models", Proceedings of Coastal Sediments '77, ASCE, pp. 350-365.

APPENDIX A

FLOWCHART OF THE DEVELOPED NUMERICAL MODEL

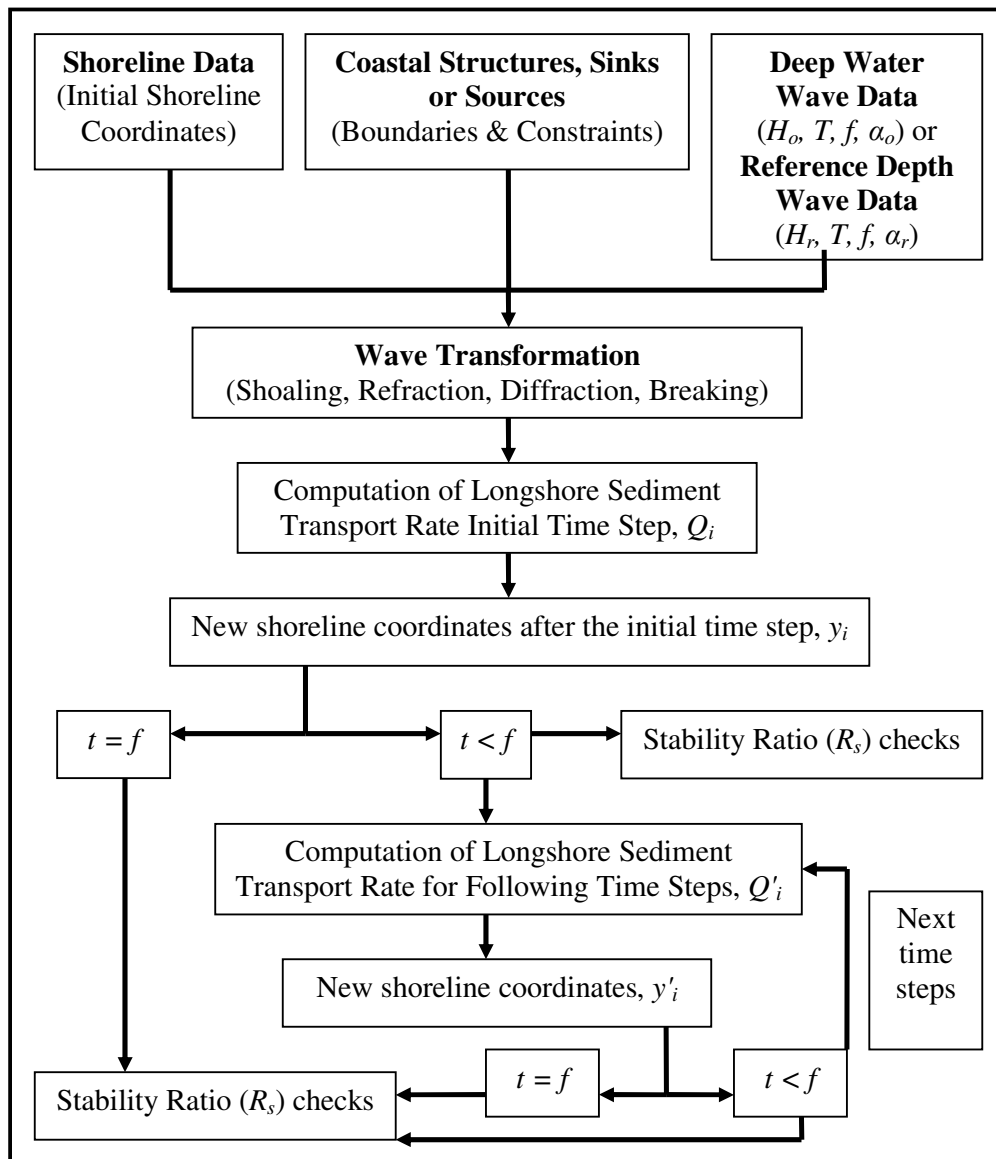


Figure A.1 Flowchart of the Developed Numerical Model

APPENDIX B

SHORELINE AND WAVE DATA OF CASE STUDY SIMULATIONS

Table B.1 Annual Deep Water Representative Wave Data of Case Study Simulations

H_o	T	f	α_o
1.113744	4.180229	1424.638	-35.7905
1.313544	4.553112	3994.571	63.5605

Table B.2 Annual Representative Wave Data of Case Study Simulations at Reference Depth

H_o	T	f	α_o
0.907598	4.111615	1312.331	-46.0864
0.988912	4.564841	4106.878	47.53754

Table B.3 Seasonal Deep Water Representative Wave Data of Case Study Simulations

H_o	T	f	α_o
1.118449	4.193457	279.06	-51.3635
1.128343	4.210764	1290.631	62.09176
0.935619	3.84031	414.962	-48.2784
1.182572	4.31735	1287.947	61.83367
0.939609	3.848371	615.294	-53.7924
1.255943	4.451157	1273.899	61.4542
1.185744	4.318983	283.416	-43.9959
1.416022	4.726982	1089.14	63.2801
1.118449	4.193457	279.06	-51.3635
1.128343	4.210764	1290.631	62.09176
0.935619	3.84031	414.962	-48.2784
1.182572	4.31735	1287.947	61.83367
0.939609	3.848371	615.294	-53.7924
1.255943	4.451157	1273.899	61.4542
1.185744	4.318983	283.416	-43.9959
1.416022	4.726982	1089.14	63.2801
1.118449	4.193457	279.06	-51.3635
1.128343	4.210764	1290.631	62.09176
0.935619	3.84031	414.962	-48.2784
1.182572	4.31735	1287.947	61.83367
0.939609	3.848371	615.294	-53.7924
1.255943	4.451157	1273.899	61.4542
1.185744	4.318983	283.416	-43.9959
1.416022	4.726982	1089.14	63.2801
1.118449	4.193457	279.06	-51.3635
1.128343	4.210764	1290.631	62.09176
0.935619	3.84031	414.962	-48.2784
1.182572	4.31735	1287.947	61.83367
0.939609	3.848371	615.294	-53.7924
1.255943	4.451157	1273.899	61.4542
1.185744	4.318983	283.416	-43.9959
1.416022	4.726982	1089.14	63.2801
1.118449	4.193457	279.06	-51.3635
1.128343	4.210764	1290.631	62.09176
0.935619	3.84031	414.962	-48.2784
1.182572	4.31735	1287.947	61.83367
0.939609	3.848371	615.294	-53.7924
1.255943	4.451157	1273.899	61.4542
1.185744	4.318983	283.416	-43.9959
1.416022	4.726982	1089.14	63.2801
1.118449	4.193457	279.06	-51.3635
1.128343	4.210764	1290.631	62.09176

0.935619	3.84031	414.962	-48.2784
1.182572	4.31735	1287.947	61.83367
0.939609	3.848371	615.294	-53.7924
1.255943	4.451157	1273.899	61.4542
1.185744	4.318983	283.416	-43.9959
1.416022	4.726982	1089.14	63.2801
1.118449	4.193457	279.06	-51.3635
1.128343	4.210764	1290.631	62.09176
0.935619	3.84031	414.962	-48.2784
1.182572	4.31735	1287.947	61.83367
0.939609	3.848371	615.294	-53.7924
1.255943	4.451157	1273.899	61.4542

Table B.4 Seasonal Representative Wave Data of Case Study Simulations at Reference Depth

H_o	T	f	α_o
0.803466	4.193457	279.06	-58.0581
0.995381	4.210764	1290.631	47.26821
0.696759	3.84031	414.962	-53.7979
1.034917	4.31735	1287.947	47.57994
0.690658	3.848371	615.294	-60.4891
1.098356	4.451157	1273.899	46.91544
0.903063	4.318983	283.416	-49.2717
1.244476	4.726982	1089.14	47.42026
0.803466	4.193457	279.06	-58.0581
0.995381	4.210764	1290.631	47.26821
0.696759	3.84031	414.962	-53.7979
1.034917	4.31735	1287.947	47.57994
0.690658	3.848371	615.294	-60.4891
1.098356	4.451157	1273.899	46.91544
0.903063	4.318983	283.416	-49.2717
1.244476	4.726982	1089.14	47.42026
0.803466	4.193457	279.06	-58.0581
0.995381	4.210764	1290.631	47.26821
0.696759	3.84031	414.962	-53.7979
1.034917	4.31735	1287.947	47.57994
0.690658	3.848371	615.294	-60.4891
1.098356	4.451157	1273.899	46.91544
0.903063	4.318983	283.416	-49.2717
1.244476	4.726982	1089.14	47.42026
0.803466	4.193457	279.06	-58.0581
0.995381	4.210764	1290.631	47.26821

0.696759	3.84031	414.962	-53.7979
1.034917	4.31735	1287.947	47.57994
0.690658	3.848371	615.294	-60.4891
1.098356	4.451157	1273.899	46.91544
0.903063	4.318983	283.416	-49.2717
1.244476	4.726982	1089.14	47.42026
0.803466	4.193457	279.06	-58.0581
0.995381	4.210764	1290.631	47.26821
0.696759	3.84031	414.962	-53.7979
1.034917	4.31735	1287.947	47.57994
0.690658	3.848371	615.294	-60.4891
1.098356	4.451157	1273.899	46.91544
0.903063	4.318983	283.416	-49.2717
1.244476	4.726982	1089.14	47.42026
0.803466	4.193457	279.06	-58.0581
0.995381	4.210764	1290.631	47.26821
0.696759	3.84031	414.962	-53.7979
1.034917	4.31735	1287.947	47.57994
0.690658	3.848371	615.294	-60.4891
1.098356	4.451157	1273.899	46.91544
0.903063	4.318983	283.416	-49.2717
1.244476	4.726982	1089.14	47.42026
0.803466	4.193457	279.06	-58.0581
0.995381	4.210764	1290.631	47.26821
0.696759	3.84031	414.962	-53.7979
1.034917	4.31735	1287.947	47.57994
0.690658	3.848371	615.294	-60.4891
1.098356	4.451157	1273.899	46.91544

Table B.5 Initial Shoreline Data of Case Study Simulations

Shoreline Coordinate in x-axis	Shoreline Coordinate in y-axis
0	329
25	331.5
50	337.5
75	337.5
100	339.5
125	341.5
150	335.5
175	334
200	322.5
225	311.5
250	296
275	290.5
300	288
325	281.5
350	270.5
375	266.5
400	259
425	250
450	243
475	235.5
500	230.5
525	229.5
550	231.5
575	231
600	229.5
625	229
650	228
675	227
700	226
725	219
750	219
775	227
800	228
825	232
850	236.5
875	246.5
900	245.5
925	247.5
950	253
975	259
1000	265

APPENDIX C

INPUTS AND OUTPUTS OF CASE STUDY AND SAMPLE SIMULATIONS

Case Study Simulation Inputs and Outputs

Initial shoreline:

[1]:Initially straight shoreline

[2]:Read from file

2

Enter the alongshore distance increment, dx, in m. :

25

Enter time increment, dt, in hours:

0.5

Enter the median grain size diameter, D50, in m.:

0.00023

Enter beach berm height above still water level, B, in m.:

2

Enter the number of sources/sinks:

0

Enter the number of seawalls:

0

Enter the number of tapered beach fills:

0

Enter the number of offshore breakwaters:

2

Enter the distance of offshore breakwater 1 from left:

175

Enter the width (horizontal along x-axis) of offshore breakwater 1:

150

Enter the distance of tip-1 of offshore breakwater 1:

126

Enter the distance of tip-2 of offshore breakwater 1:

151

Enter the permeability coefficient of offshore breakwater 1 :

0

Enter the distance of offshore breakwater 2 from left:

450

Enter the width (horizontal along x-axis) of offshore breakwater 2:

150

Enter the distance of tip-1 of offshore breakwater 2:

145

Enter the distance of tip-2 of offshore breakwater 2:

154

Enter the permeability coefficient of offshore breakwater 2 :

0

Enter the number of groins:

3

Enter the distance of groin 1 from left:

225

Enter the length of groin 1:

139

Enter the permeability of groin 1:

0

[1]:Diffracting Groin

[2]:Non-Diffracting Groin

2

Enter the distance of groin 2 from left:

525

Enter the length of groin 2:

157

Enter the permeability of groin 2:

0

[1]:Diffracting Groin

[2]:Non-Diffracting Groin

2

Enter the distance of groin 3 from left:

800

Enter the length of groin 3:

150

Enter the permeability of groin 3:

0

[1]:Diffracting Groin

[2]:Non-Diffracting Groin

1

Enter the number of repetitions:

4

Enter the reference depth of wave data:

50

The data that is given above includes the beach profile data, shoreline data and structure input data that are implemented in the developed numerical model during case study simulations. If the inserted data is not logical or not in limits, a warning sign appears on the screen and the program asks for replacement of a new and logical data instead of the wrong data as;

Enter the distance of groin 2 from left:

10000

Correct the location of groin 2 and execute the program again.

Enter the distance of groin 2 from left:

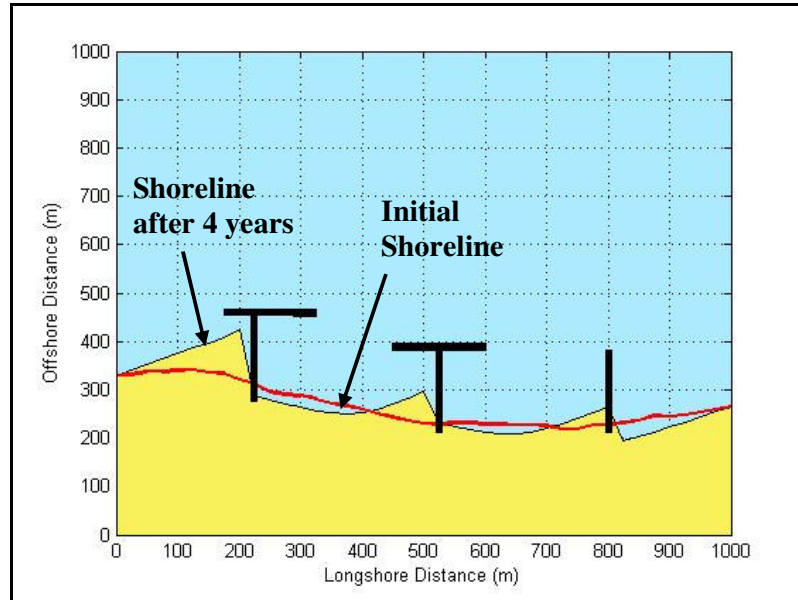


Figure C.1 4 Year Case Study Simulation Results of Shoreline Evolution under Annual Deep Water Wave Data Input

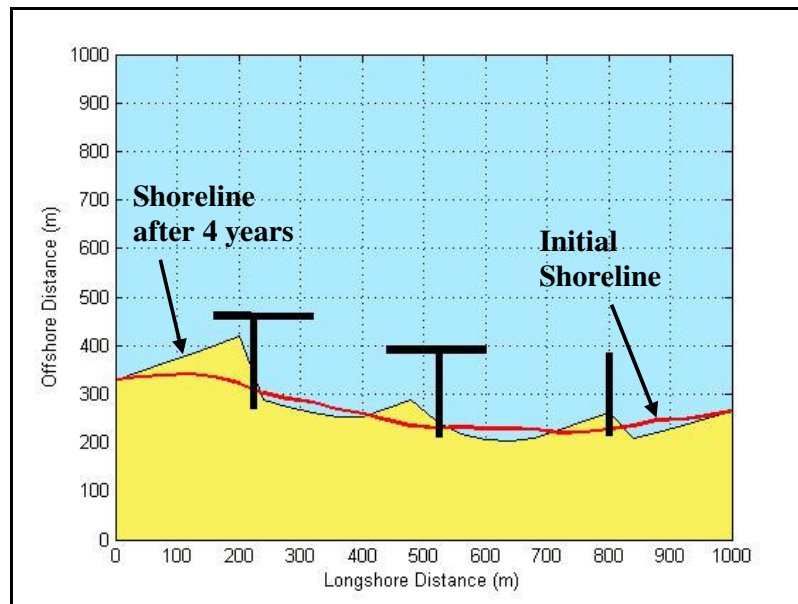


Figure C.2 4 Year Case Study Simulation Results of Shoreline Evolution under Seasonal Deep Water Wave Data Input

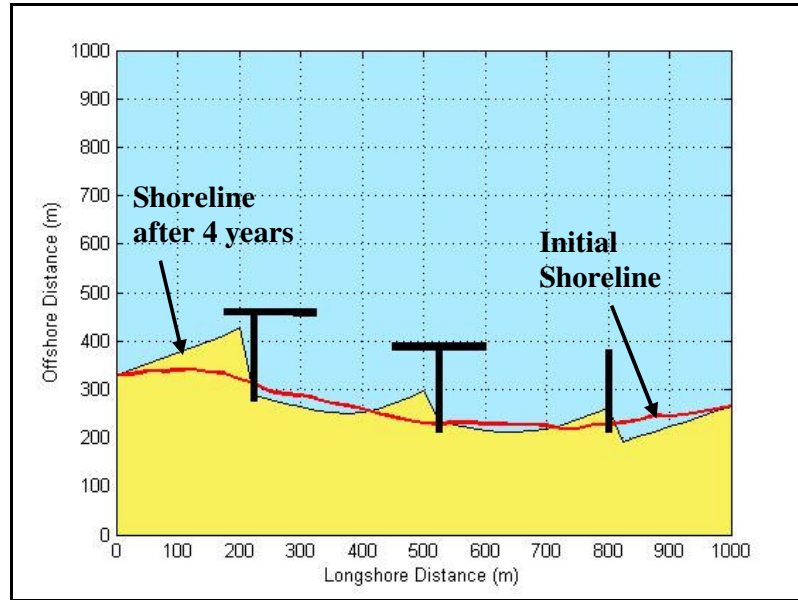


Figure C.3 4 Year Case Study Simulation Results of Shoreline Evolution under Annual Reference Depth Wave Data Input

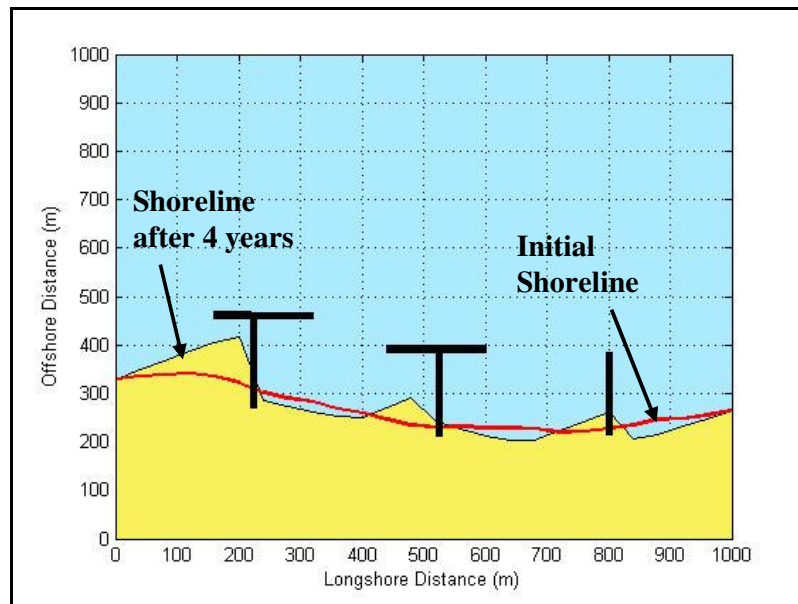


Figure C.4 4 Year Case Study Simulation Results of Shoreline Evolution under Seasonal Reference Depth Wave Data Input

Sample Simulation Inputs and Outputs

Table C.1 Annual Deep Water Representative Wave Data of Sample Simulations

H_o	T	f	α_o
1	4	100	30

The following sample simulations are performed at an initially straight shoreline of 1000 m. length, 25 m. longshore increment, dx and 0.5 hour time increment, dt .

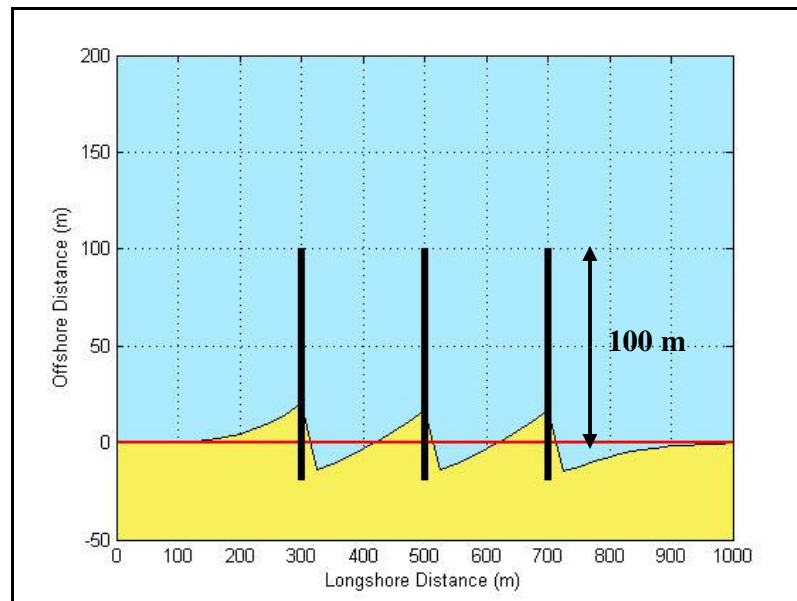


Figure C.5 Sample Simulation 1

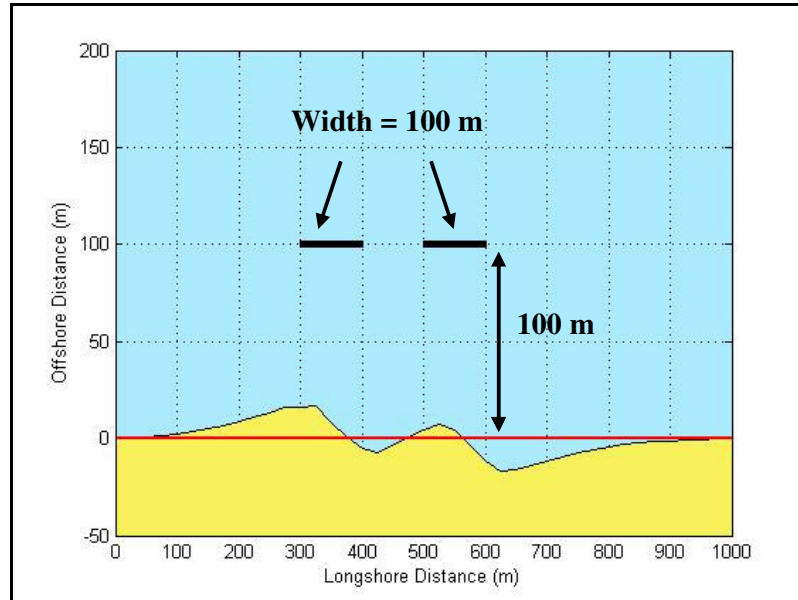


Figure C.6 Sample Simulation 2

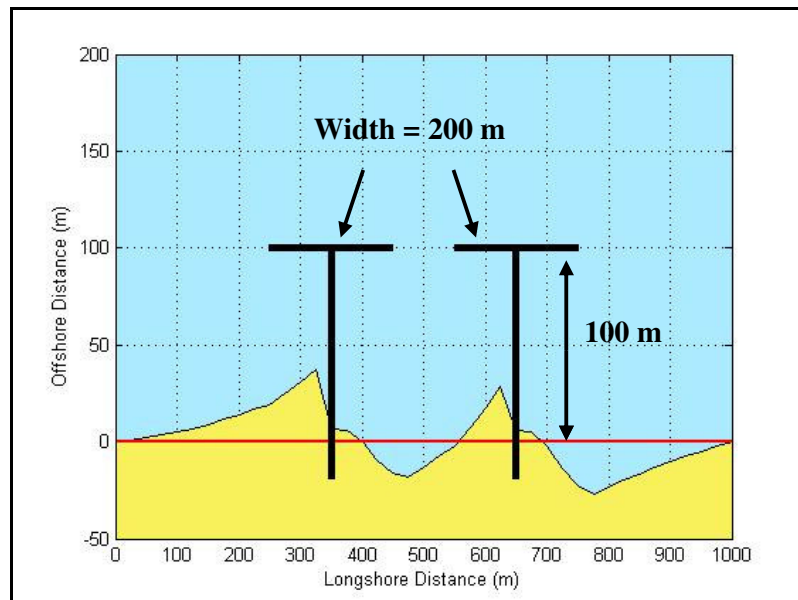


Figure C.7 Sample Simulation 3